NORMAL AND DISEASED CIRCUITRY IN THE CEREBELLAR AND CEREBRAL CORTEX

A THESIS
SUBMITTED TO THE FACULTY OF
UNIVERSITY OF MINNESOTA
BY

SAMUEL WILLIAM CRAMER

IN PARTIAL FULFILLMENT OF THE REQUIREMENTS
FOR THE DEGREE OF
DOCTOR OF PHILOSOPHY

DR. TIMOTHY EBNER

SEPTEMBER, 2014

Acknowledgements

There are many individuals that have contributed to my scientific journey. Unfortunately, I cannot name everyone but I would like to collectively thank you. There are those that were particularly instrumental to my journey and deserve special thanks.

John Paton, Susan Shurson, and Nicholas Berg—thank you your help navigating the logistics of academic scheduling and requirements along the way.

Dr. James Ashe—thank you for your guidance as Director of Graduate Studies and for your support of my fellowship application.

Thesis Committee members—Drs. Paul Mermelstein, Paulo Kofuji and Harry Orr—thank you for your guidance and thoughtful suggestions during the evolution of this work.

Dr. Harry Orr and Jillian Frisch, Brennon O'Callaghan, and Lisa Duvick—thank you for your patience and assistance in helping me with the Western blot experiments.

Dr. Yasushi Nakagawa—thank you for providing the space, materials, and expertise for performing immunohistochemistry and for your support of my fellowship application.

I would like to thank the members of the Ebner laboratory for all of their contributions:

Gang Chen—thank you for teaching me the basics of optical imaging, data processing, and electrophysiology as well as all of your help troubleshooting problems. Above all, thank you for providing me with an introduction to basic research.

Wangcai Gao—thank you for patiently teaching me how to perform Ca^{2+} optical imaging. In particular I would like to thank you for allowing me to continue the project you initiated investigating the role of parallel fibers. Your technical and experimental ideas were invaluable.

Xinming Wang—thank you for the many hours you spent teaching me how to perform single unit Purkinje cell recordings.

Justin Barnes—thank you for teaching me the optical imaging surgical preparation as well as for the coffee and lunch breaks.

Claudia Hendrix—thank you for teaching me a few of the basics of proper statistical analysis.

Russell Carter—thank you for your thoughts on experimental design and analytical approaches.

Michael McPhee—thank you for all of your work to make the laboratory run smoothly and for all of the hours spent preparing perfectly arranged figures and posters.

Kris Bettin and Lauren Skalicky—thank you for your help with manuscript editing and preparation as well as help navigating the various regulatory bodies.

Angela Hewitt and Martha Streng—thank you for commenting on experiments and analyses.

Laurentiu Popa—thank you for all the interesting conversations (science related and otherwise) as well as your invaluable computational contributions that always took the analysis to the next level.

Dr. Tim Ebner—thank you for providing me with the early introduction to basic research that sparked my interest in pursuing the MD/PhD training path. I appreciate all of the support and training you have provided to me over the years.

Dedication

I would like to dedicate this thesis to my family who has continually provided support throughout my training and in particular to my parents for fostering my inquisitive nature from an early age.

Above all, I dedicate this work to my beloved wife Julianne who has steadfastly lent encouragement and grounding during the ups and downs along the way. You are the best.

Abstract

The cerebellum is a major motor control structure with a highly ordered circuity. The parallel fibers (PFs) are a dominant element of the cerebellar circuitry. Parallel fibers are the bifurcated axons of the granule cells (GCs) that project across the surface of the cerebellar cortex and synapse on the major output neuron, the Purkinje cell (PC). However, the role of PFs in the cerebellum has long been controversial and a matter of intense debate. Early studies inspired the "beam" hypothesis whereby GC activation results in PF driven, post-synaptic excitation of beams of PCs. However, the "radial" hypothesis postulates that the ascending limb of the GC axon provides the dominant input to PCs and generates patch-like PC responses. To address the beam versus patch controversy and PF function in the cerebellar cortex, this thesis used optical imaging and single PCs recordings in the mouse cerebellar cortex, both in normal mice and in a murine model of a P/Q-type Ca^{2+} channelopathy. The results provide the first demonstration of beam-like activation of PCs in the cerebellar cortex to peripheral input in normal mice. Furthermore, the pattern of PC responses depends on extracellular glutamate and its local regulation by excitatory amino acid transporters. The findings account for the contradictions of previous studies, clarifying why the responses in some regions of the cerebellar cortex are patch-like and other beam-like.

Altered GC-PF-PC synaptic transmission is hypothesized to produce cerebellar motor dysfunction. This thesis tests this hypothesis in the tottering (*tg/tg*) mouse that has mutation in the gene that codes for the α_{1A} pore-forming subunit of the P/Q-type voltage

gated Ca^{2+} channel and is a model for human episodic ataxia type 2 (EA2). This channel is highly expressed on both GCs and PCs. Further, both EA2 patients and *tg/tg* mice have cerebellar ataxia. The thesis shows that the GC-PF-PC synaptic transmission is reduced in the *tg/tg* mouse and a main pharmacological therapy for EA2, 4-aminopyridine, rescues the deficits. The results strongly implicate decreased GC-PF-PC function in the baseline ataxia.

Both EA2 patients and *tg/tg* mice have non-episodic neurologic dysfunction, such as the cerebellar ataxia, but also episodic dysfunction. The episodic abnormalities involve the cerebral cortex, including epilepsy, migraine headaches and cognitive dysfunction. The final component of the thesis examined whether episodic abnormalities are present in the cerebral cortex of the *tg/tg* mouse. Optical imaging and single cell recording results demonstrate highly abnormal excitability changes throughout the cerebral cortex of *tg/tg* mice consisting of transient low frequency oscillations (LFOs) very high power. The LFOs are mediated, at least in part, by neuronal activity. Unexpectedly, the LFOs are driven by reducing excitatory inputs to the cerebral cortex. Furthermore, the high power LFOs are decreased markedly by acetazolamide and 4-aminopyridine, the primary treatments for EA2, demonstrating disease relevance. The LFOs in the *tg/tg* mouse represent an abnormal state involving decreased excitatory synaptic transmission and may underlie non-cerebellar symptoms that characterize P/Q-type Ca^{2+} channelopathies.

Table of Contents

List of Figures

Chapter II. Re-evaluation of the beam and radial hypothesis of parallel fiber action in the cerebellar cortex

Chapter III. *In vivo* optical imaging demonstrates altered cerebellar circuitry in the *tottering* mouse

Chapter IV. Abnormal excitability and episodic low frequency oscillations in the cerebral cortex of the *tottering* mouse

CHAPTER I: BACKGROUND

Introduction

In this first chapter I will begin by providing a brief overview of the cellular organization and circuitry of the cerebellum. I will then provide background for the first aim of my thesis that examined the role of parallel fibers (PFs) in the cerebellar cortex. I also introduce the subject of the final two aims, the mutant *tottering* (*tg/tg*) mouse. I provide context for the investigation of how abnormalities in PF-Purkinje cell excitation might contribute to the gait ataxia exhibited by this mouse as well as for the question of whether abnormal episodic activity occurs in the cerebral cortex of the *tg/tg* mouse.

Cytoarchitecture and cortical circuitry of the cerebellum

The lattice cytoarchitecture of the cerebellar cortex, comprised of just seven different neuronal cell types, is beautifully deceiving, as this outwardly simple arrangement obscures the underlying complexity of the cerebellum. Detailed histological descriptions of the cerebellar cortex may be found elsewhere (Eccles et al., 1967;Palay and Chan-Palay, 1974;Mugnaini, 1972) and, therefore, only a brief overview is provided here. The cerebellar cortex is divided into three layers from superficial to deep: the molecular layer, the Purkinje cell layer and the granular layer. The molecular layer contains the PF axons of granule cells (GCs), stellate and basket cell interneurons, as well as the dendritic arbors of the principle neuron of the cerebellar cortex—the Purkinje cell

(PC). The PC layer is largely a monolayer of PC somata but also contains the interspersed somata of Bergmann and candelabrum glia (Sillitoe and Joyner, 2007). The granular layer is comprised primarily by the most numerous neuronal cell types in the brain, the GC. Golgi, Lugaro and unipolar brush cells (all inhibitory interneurons) are also found in the granular layer. The three layers of the cerebellar cortex overlay the white matter tracts that contain the afferent (climbing fiber and mossy fiber axons) and efferent (PC axons) cerebellar projections.

The cerebellar cortex receives excitatory glutamatergic input from mossy fibers and climbing fibers. The majority of afferent input to the cerebellar cortex is conveyed by the mossy fibers. Mossy fibers receive input from a combination of peripheral sensory nerves and numerous central structures. The specific inputs received by individual mossy fibers differ depending on the cerebellar cortical zone that they project to. Projections to the vestibulocerebellum arise from the vestibular nuclei while spinocerebellar pathways project to the vermis. Mossy fiber tracts conveying peripheral sensory information from the spinocerebellar tracts and from the motor cortex *via* the pontine nuclei project to the intermediate zone of the cerebellar cortex (Eccles et al., 1967;Llinas, 1981). The lateral zone of the cerebellar cortex receives mossy fiber projections arising from the basal pontine nuclei which provide information from nearly all cerebral cortical regions, but especially from premotor, supplementary motor areas, sensorimotor, parietal association, and visual cortices (Allen and Tsukahara, 1974;Glickstein et al., 1985).

As the sole output, PCs are the fundamental computational unit of the cerebellar cortex. Morphologically, PCs are one of the most recognizable neuronal cell types in the brain due to their massive and elaborate, planer dendritic arbors that extend into the molecular layer in perpendicular alignment to the folia and PFs. PCs are GABAergic inhibitory neurons (Ito et al., 1970) that massively converge (~25:1) on their targets in the deep cerebellar nuclei (DCN) and the vestibular nuclei (Caddy and Biscoe, 1979;Harvey and Napper, 1991;Heckroth and Abbott, 1994).

The output of the cerebellum is generated by the DCN and the vestibular nuclei. Somatotopic representations of the body are found in each of the nuclei (Allen et al., 1977;Allen et al., 1978;Asanuma et al., 1983d;Asanuma et al., 1983a;Asanuma et al., 1983b;Asanuma et al., 1983c;Thach et al., 1992) and the nuclei influence motor control over the ipsilateral musculature. Cerebellar output is conveyed to essentially all CNS motor areas including the spinal cord, the vestibular, reticular, and red nuclei, the superior colliculus, and, *via* the thalamus, the primary motor and premotor cortices, and the prefrontal cortex. In the quiescent state, DCN neurons maintain a consistent firing rate of 40-50 Hz (Fortier et al., 1989;Thach, 1978).

Basic electrophysiological properties of the PC

Neurons of the inferior olivary nucleus, located in the brainstem, project climbing fibers across the midline into the contralateral cerebellar cortex (Eccles et al., 1967). As

the climbing fibers enter the cerebellar cortex, they branch in the parasagittal plane and contact approximately 10 PCs with each PC receiving input from a single climbing fiber. A climbing fiber makes extensive synaptic connections with its target PCs (~1000s) such that climbing fiber activation strongly depolarizes the PC (ECCLES et al., 1964;Schmolesky et al., 2002). The action potential produced in the PC by the climbing fiber input is known as a complex spike which is a unique, prolonged depolarization consisting of a single action potential followed by a series of smaller spikelets (Eccles et al., 1966b;ECCLES et al., 1964;Eccles et al., 1967). The spontaneous complex spike rate in PCs is typically quite low and averages ~1 Hz (Armstrong and Rawson, 1979;Keating and Thach, 1995;Thach, 1968).

The other type of action potential exhibited by PCs is the simple spike (SS) and is characterized by the traditional action potential waveform. The average spontaneous SS rate in PCs is ~ 50 Hz but may reach a maximal rate of ~250 Hz (Eccles et al., 1966a;Thach, 1968;Thach, Jr., 1967;Bell and Grimm, 1969). PCs intrinsically fire action potentials, even in the absence of synaptic input (Raman and Bean, 1999;Hausser and Clark, 1997;Hausser et al., 2004). The intrinsic SS firing exhibited by PCs is driven by a unique resurgent Na^+ current (Raman and Bean, 1997). Therefore, SS firing in PCs reflects the net total of the intrinsic PC activity plus the sum of their synaptic inputs.

Parasagittal organization of the cerebellum

Beyond the traditional histological description of the cerebellar cortex, anatomical and immunohistochemical examination reveals a further layer of complexity. Cerebellar patterns have been described based on molecular expression domains and by patterns of connectivity. For example, both classical anatomical techniques and gene expression studies led to the subdivision of the cerebellar cortex into transverse zones that divide the cerebellum along the anteroposterior axis (Voogd and Ruigrok, 1997;Ozol et al., 1999). The anterior zone encompasses vermian lobules I-V and the hemispheric simplex lobule in the mouse; the central zone VI-VII, Crus I and Crus II; the posterior zone VIII-IX, paramedian and cupula; and the nodular zone X, flocculus and paraflocculus (Apps and Hawkes, 2009;Larouche and Hawkes, 2006).

Parasagitally aligned stripes demarcated by the expression of molecular markers further subdivide the transverse zones. Zebrin II is the most extensively studied of these markers (Brochu et al., 1990) and, since the initial discovery, has been determined to be the glycolytic enzyme aldolase C (Ahn et al., 1994;Hawkes and Herrup, 1995). Zebrin II stripes are symmetrically distributed across the midline, highly consistent between individuals (Brochu et al., 1990;Hawkes et al., 1985;Hawkes and Leclerc, 1987;Fujita et al., 2014), and found in a variety of mammalian species (Sillitoe et al., 2005). PCs that express zebrin II (zebrin II+) comprise stripes of a few hundred to a few thousand PCs and alternate between zones in which all PCs are zebrin II+ (e.g., the central and nodular zones) and zones with alternating stripes of zebrin II+ and zebrin II negative (zebrin II-)

PCs (e.g., the anterior and posterior zones) (Larouche and Hawkes, 2006;Apps and Hawkes, 2009).

A number of other molecules are co-expressed with zebrin II including: zebrin I (Hawkes et al., 1985;Hawkes and Leclerc, 1987), sphingosine kinase 1a (Terada et al., 2004), phospholipase Cβ3 (Sarna et al., 2006), excitatory amino-acid transporter 4 (EAAT4) (Dehnes et al., 1998), metabotropic glutamate receptor 1α (mGluR1α) (Mateos et al., 2001), integrin β1 (Murase and Hayashi, 1996), protein kinase Cδ (Chen and Hillman, 1993;Barmack et al., 2000), and the $GABA_{B2}$ receptor (Chung et al., 2007). There are also molecular markers of zebrin II- PCs including phospholipase Cβ4 (Sarna et al., 2006), NMDA receptor (NR2C subunit) (Karavanova et al., 2007), and neuroplastin (Marzban et al., 2003). Importantly, many of these molecules are involved with synaptic transmission and intracellular signaling pathways, suggesting that excitability differs in zebrin II+ versus zebrin II- zones.

The parasagittal organization in the cerebellar cortex extends beyond the molecular phenotype of PCs. Molecular layer inhibitory interneurons (basket and stellate cells) are also organized in parasagittal zones (Szentagothai, 1965). Furthermore, the dendritic arbor of Golgi cells does not cross PC stripe boundaries (Sillitoe et al., 2008). Physiological studies have also determined that the inhibitory fields of the molecular layer interneurons are confined to zebrin II+ stripes and exert their action within this

parasagittal arrangement (Ekerot and Jorntell, 2001;Ekerot and Jorntell, 2003;Jorntell and Ekerot, 2002;Gao et al., 2006;Dizon and Khodakhah, 2011).

The climbing fiber projections from the inferior olive and the PC projections to the DCN are organized in parasagittal zones (Brodal and Kawamura, 1980;Voogd and Ruigrok, 2004;Buisseret-Delmas and Angaut, 1993;Voogd and Bigare, 1980). Mossy fibers terminate in the granule layer, exhibiting a reproducible, partially overlapping relationship with the overlying PC zebrin II+ zones (Wu et al., 1999;Ji and Hawkes, 1994;Voogd et al., 2003;Pijpers et al., 2006;Yaginuma and Matsushita, 1987;Voogd, 1969). Mapping of the mossy fibers and climbing fibers within a single parasagittal zone of PCs has demonstrated a high degree of overlap between the two inputs (Voogd et al., 2003;Pijpers et al., 2006;Garwicz et al., 1998). Physiological studies have provided further evidence for the convergence of mossy fibers and climbing fiber inputs within the same PC zone (Odeh et al., 2005). However, for both mossy fibers and climbing fibers there is not a perfect alignment between their terminals and zebrin II+ or zebrin II- PCs (Sugihara and Shinoda, 2004;Voogd et al., 2003).

The parasagittal compartmentalization extends to the cerebellar output, the DCN. DCN neurons receive inhibitory projections from PCs as well as collateral excitatory inputs from climbing fibers as they project to the cerebellar cortex (Shinoda et al., 1987;Sugihara, 2011). Tract tracing studies show that PCs located within the same zebrin II parasagittal zone, in adjacent or separate lobules, project to a restricted region

within the DCN (Sugihara et al., 2009;Voogd and Ruigrok, 2004;Pijpers et al., 2005;Apps and Garwicz, 2000). Futhermore, climbing fiber collaterals and axons from the PCs innervated by the same climbing fibers converge to the same area within the DCN (Sugihara et al., 2009). Despite the evidence that the parasagittal organization observed in the cerebellar cortex is maintained in the DCN output neurons, the functional consequences of this are not understood.

Functional differences in parasagittal zones

Excitability and information processing differs across parasagittal zones. For example, the proteins involved in glutamatergic neurotransmission are differentially expressed in parasagittal stripes of PCs. The mGluR1b splice variant is found on zebrin II- PCs (Mateos et al., 2000). While, as mentioned above, EAAT4 and protein kinase Cδ are expressed in zebrin II+ PCs (Chen and Hillman, 1993;Barmack et al., 2000). The parasagittal expression pattern of EAAT4 produces regional differences in the susceptibility of the PF-PC synapse to long term depression (Gao et al., 2003;Wadiche and Jahr, 2005) .

Parasagittal zones also differ in the expression of long latency patches. Patches of elevated activity are evoked by high frequency PF stimulation. The patches appear along the PC beam evoked by PF stimulation at latencies of ~25 s (Wang et al., 2011), are mGluR1 dependent and are restricted to zebrin II+ PC zones. Furthermore, the patches

require intracellular Ca^{2+} release *via* PLCβ and ryanodine receptors (RyR). The patches also exhibit robust, mGluR1 dependent, long-term potentiation to high-frequency PF stimulation, another example of synaptic plasticity that differs among the PC zones (Wang et al., 2011;Wang et al., 2009). A possible mechanism is suggested by the observation that both mGluR1 receptors and the downstream signaling pathway in PCs are organized in parasagittal zones (Hartmann and Konnerth, 2009). As mentioned, the PLCβ3 isoform is found on zebrin II+ PCs while the PLCβ4 isoform and the mGluR1b splice variant are found on PCs in zebrin II- zones (Hartmann and Konnerth, 2009;Apps and Hawkes, 2009). The mGluR1b variant couples poorly to the PLC signaling pathway compared to the mGluR1a variant. Therefore, differences in signaling potency may underlie the expression and the unique properties of the long-latency patches (Wang et al., 2011).

Another example of functional differences in parasagittal zones is the amount of glutamate released per climbing fiber action potential. In cerebellar slice preparation the climbing fibers projecting to zebrin II+ zones release more glutamate per action potential than climbing fibers projecting to zebrin II- PC zones (Paukert et al., 2010). Enhanced glutamate release by climbing fibers in the zebrin II+ zones produces a longer-duration excitatory post-synaptic current, prolonging the complex spikes in zebrin II+ PCs. Longer duration complex spike produce greater amplitude long-term depression (Yang and Lisberger, 2014), therefore the prolonged complex spikes in zebrin II+ PCs likely

increases the susceptibility and/or the duration of plasticity at the climbing fiber-PC synapse in the zebrin II+ zones.

Finally, the PC zebrin II phenotype in the parasagittal zones influences susceptibility to cell death. PC death resulting from genetic neurodegeneration or toxicity often preferentially occurs in zebrin II+ or Zebrin II- PC zones (depending on the specific degenerative disease process or the toxin) rather than being randomly distributed across PCs in the cerebellar cortex (Sawada et al., 2009;Leclerc et al., 1992;Welsh et al., 2002;Sarna et al., 2003;Fletcher et al., 2001;Angner et al., 2000;Balaban and Severs, 1991;Balaban et al., 1988). Overall, one subpopulation of PCs does not appear to be more sensitive to genetic or toxic insult than the other (Sarna and Hawkes, 2003). In conclusion, the patterned loss of PCs may occur because the insult is localized to parasagittal zones or because all of the PCs receive the same level of insult but some PC populations are more susceptible to the particular injury.

In summary, parasagittal PC zones exhibit differences in response to PF and CF input, including in excitability and synaptic plasticity as well as susceptibility to cell death. Though the extent is unknown, these parasigittal differences add another layer of complexity to the basic computations performed by the cerebellar cortex.

The role of PFs in the cerebellar cortex

The cerebellar molecular layer is dominated by PF axons project mediolaterally across the cerebellar cortical surface (Palay and Chan-Palay, 1974;Haines et al., 1982;Voogd, 1967). The length of the PFs is species dependent, for example being 3-4 mm in the cat (Brand et al., 1976) and 1-2 mm in the mouse (Huang et al., 2006a). PFs make 100,000 - 200,000, glutamatergic synapses on PC dendrites. Given their massive numbers and striking medio-lateral geometry, PFs are widely thought to play a central role in the computations performed by the cerebellar cortex. Multiple theories have been proposed to explain the functional role of PFs in cerebellar cortical processing. One of the early theories is the "beam" hypothesis which postulates that MF activation of a cluster of GCs results in beam-like excitation of PCs (Eccles et al., 1967). Proponents of the beam hypothesis suggested that the PFs provide for spatial-temporal transformations, such that propagation of action potentials along the PFs sequentially activates PCs at precisely timed intervals (Braitenberg and Atwood, 1958;Braitenberg, 1961;Braitenberg et al., 1997). Consequently, the distance traveled by the action potentials would be coded by the timing of the PC responses. The PFs have also been hypothesized to coordinate the movements of different body parts across PC parasagittal zones (Thach et al., 1992). In the Marr-Albus theory, the PF-PC synapse is the plastic element and posited to be central to the cerebellum's role in motor learning (Marr, 1969;Albus, 1971;Ito, 2002;Ito, 2006;Hansel et al., 2001). Given that individual PFs synapse on 100's of PCs and form the axonal element of the most abundant neuron type in the mammalian brain, understanding PF function is essential to understanding cerebellar cortical function.

Under the beam hypothesis, PFs serve a central role equal to their striking anatomical prominence in the cerebellar cortex. However, the beam hypothesis remains highly controversial. Simultaneous recordings of PCs separated by more than 100 μm in the medio-lateral direction have uncovered only scant evidence for temporal synchrony in their simple spike discharge (Ebner and Bloedel, 1981;Heck et al., 2007;Shin and De Schutter E., 2006;Bell and Grimm, 1969;Bosman et al., 2010;Garwicz and Andersson, 1992). Mapping of the responses to peripheral inputs reveal short-latency patches of PC activation, but little evidence for beam-like PC activation (Bower and Woolston, 1983;Santamaria et al., 2007;Shambes et al., 1978a;Cohen and Yarom, 1998;Rokni et al., 2007;Gao et al., 2006;Rokni et al., 2008).

The radial hypothesis is based on the radial organization of the PCs that receive synapses from the GC axon as it ascends to the molecular layer and synapses on PCs (Gundappa-Sulur et al., 1999;Lu et al., 2009;Napper and Harvey, 1988;Llinas, 1982). The radial hypothesis postulates that the ascending axon of GCs provides the dominant input to PCs and that PCs located laterally are only weakly, if at all, activated by the PFs (Gundappa-Sulur et al., 1999;Rokni et al., 2007;Rokni et al., 2008;Santamaria et al., 2002;Santamaria and Bower, 2005;Llinas, 1982). The synaptic connections made along the ascending limb have been argued to be stronger, have a higher number of connections on a PC, and result in more synchronous activation of PCs than that provided by PF synapses (Llinas, 1982;Sims and Hartell, 2006;Sims and Hartell, 2005;Isope and Barbour, 2002;Rokni et al., 2008). Modeling studies found almost no role for the PFs in

modulating PC simple spike discharge, suggesting instead that PFs provide a level of background tone (Santamaria et al., 2002;Santamaria et al., 2007;Santamaria and Bower, 2005).

An alternative hypothesis holds that the two segments of the GC axon serve different functional roles with the ascending limb providing an innate PC input while the PF limb provides a plastic or acquired PC input (Rokni et al., 2008). This view is based on the observation that the synapses between the granule cell ascending axon and PCs do not appear to exhibit plasticity (Sims and Hartell, 2006). In contrast, plasticity at the PF-PC synapse is a well established phenomenon (Jörntell and Ekerot, 2002;Wang et al., 2011;Gao et al., 2003;Ito and Kano, 1982;Lev-Ram et al., 2002;Salin et al., 1996).

However, despite there being more experimental support for the radial hypothesis than the beam hypothesis, major concerns also exist with the radial hypothesis. Ascending limb synapses provide only 3 - 6% of the total synapses on a PC (Napper and Harvey, 1988;Lu et al., 2009;Huang et al., 2006b), and not the 20% claimed in one study (Gundappa-Sulur et al., 1999). In the cerebellar slice, the strength of the synapses between the ascending axon and PCs and between PFs and PCs are equivalent and PFs activate PCs for at least several hundred μm along the PFs (Isope and Barbour, 2002;Walter and Khodakhah, 2009).

A variant of the radial hypothesis proposes that GABAergic inhibition generated by cerebellar interneurons prevents beam-like activation by PFs (Bower, 2002;Santamaria et al., 2007;Santamaria et al., 2002). Experimental support remains equivocal (Rokni et al., 2007;Santamaria et al., 2007). However, the response to PF activation can be highly modulated by local conditions, including locally elevated extracellular glutamate transients resulting from climbing fiber discharge (Dzubay and Jahr, 1999), PF-PC synaptic spillover(Carter and Regehr, 2000) and retrograde release of glutamate from PCs (Levenes et al., 2001;Crepel, 2007;Shin et al., 2008;Duguid et al., 2007). Increased glutamate both facilitates PF-PC synaptic transmission by temporary suppression of stellate cell inhibition (Carter and Regehr, 2000) as well as inhibits PF-PC synaptic transmission, (Levenes et al., 2001;Crepel, 2007) leading to the hypothesis that the response patterns in the cerebellar cortex are controlled at least in part, by excitatory amino acid transporters (EAATs).

EAATs provide the primary means for glutamate re-uptake following excitatory transmission mediated glutamate release. Therefore, the EAATs control the amplitude and duration of excitatory post-synaptic currents (Takahashi et al., 1995;Takayasu et al., 2004), limit receptor desensitization, as well as ensure a high signal-to-noise ratio for glutamatergic synaptic transmission (Barbour et al., 1994;Marcaggi and Attwell, 2005). In the cerebellar cortex, four distinct EAAT4 isoforms (EAAT1-4) are expressed in the molecular layer (Takayasu et al., 2009). EAAT1 and EAAT2 are expressed on the surface membranes of Bergmann glial processes that surround the peri-synaptic spaces on

dendtritic spines of PCs (Chaudhry et al., 1995;Lehre and Danbolt, 1998). At the PF-PC synapse, EAAT1 and EAAT2 re-uptake ~80% of synaptic glutamate while the remaining ~20% is taken up by the peri-synaptically localized, PC specific transporter EAAT4 (Dehnes et al., 1998;Tanaka et al., 1997;Otis et al., 2004). Despite not being the primary transporter responsible for glutamate uptake at the PF-PC synapse, EAAT4 is notable due to its non-uniform expression by PCs across the cerebellar cortex (as mentioned above)(Dehnes et al., 1998;Gincel et al., 2007) which influences parasagittal zone PC excitability.

Given that the PFs are a striking element of the cerebellum and that their functional significance to the cerebellar circuitry has been controversial, the first aim of this thesis investigated the role of PF in PC activation. Specifically, using optical imaging to re-evaluate the beam versus radial hypothesis and map the spatial patterns of cerebellar activation *in vivo*. In addition, the aim tested the hypothesis that molecular layer inhibition modifies the granule cell-PF-PC response and investigated the role of parasagittal zonal differences in cerebellar activation to GC-PF input.

Episodic ataxia type 2 and the mutant *tottering* mouse

The hallmark of episodic neurological dysfunction, including channelopathies, is that neurons and neural circuits transiently enter an abnormal excitability state resulting in an acute and self-limiting attack (Ryan and Ptacek, 2010;Kullmann, 2010). One

family of the Ca^{2+} channelopathies is caused by autosomal dominant mutations of the *CACNA1A* gene that encodes the α_{1A}, pore-forming subunit of the human $Ca_v2.1$ (P/Q-type) voltage gated Ca^{2+} channel (Ophoff et al., 1996;Kramer et al., 1995). Clinical manifestations of *CACNA1A* mutations include episodic ataxia type 2 (EA2), familial hemiplegic migraine type 1 (FHM1), spinocerebellar ataxia type 6, or a combination of the three (Jen et al., 2004;Jen et al., 2007;Baloh et al., 1997;Rajakulendran et al., 2010). The spectrum of symptoms and severity of disease depends on the specific mutation. Over 80 mutations of the *CACNA1A* that give rise to EA2 have been identified (Rajakulendran et al., 2012). Mutations that result in EA2 are predicted or have been shown to cause a loss or decrease of P/Q-type Ca^{2+} channel function (Wappl et al., 2002;Spacey et al., 2004;Jen et al., 2004;Pietrobon, 2010). EA2 is characterized by paroxysmal attacks of cerebellar dysfunction including limb and gait ataxia, and nystagmus: episodes persist for hours to days. EA2 patients may also display paroxysmal dystonic symptoms (Spacey, 1993). Between episodes, patients exhibit progressive or (less commonly) static cerebellar dysfunction, including ataxia, and regional cerebellar atrophy (Baloh et al., 1997;Jen et al., 2007;Denier et al., 1999).

The *tottering* (*tg/tg*) mouse contains a recessive missense mutation in *Cacna1a*, ortholog of the human gene *CACNA1A*, resulting in a substitution of leucine for proline in the pore-forming region of the P/Q-type Ca^{2+} channel (Fletcher et al., 1996). In the *tg/tg* mouse there is a 30-40% reduction in P/Q-type Ca^{2+} current in PCs with little change in the kinetics of the channel (Wakamori et al., 1998). The phenotype of the *tg/tg*

mouse is characterized by paroxysmal dystonia, mild ataxia, and absence seizures, between dystonic episodes. The *tg/tg* mouse is the most widely used model of the human *CACNA1A* disorder EA2.

The P/Q-type Ca^{2+} channels are found in presynaptic terminals, soma, and dendrites of neurons (Mintz et al., 1992;Fletcher et al., 1996;Westenbroek et al., 1995). Importantly, P/Q-type Ca^{2+} channels are heavily expressed in the cerebellum, particularly in PCs and GCs (Mintz et al., 1992;Fletcher et al., 1996;Westenbroek et al., 1995). Due to efficient coupling with protein mediators of exocytosis, P/Q-type Ca^{2+} channels play a centrol role in action potential dependent neurotransmitter release (Pietrobon, 2010;Catterall, 1998). P/Q-type Ca^{2+} channels exhibit a great deal of functional variation that results from a multitude of alternative splice forms (Wykes et al., 2007;Kanumilli et al., 2006;Chaudhuri et al., 2004;Soong et al., 2002;Sandoz et al., 2001;Bourinet et al., 1999). Further variation of the P/Q-type Ca^{2+} channel results from a combination with various auxiliary subunits (Sandoz et al., 2001;De et al., 1994;Bichet et al., 2000;Hobom et al., 2000;Walker and De, 1998). These factors produce the wide spectrum of properties exhibited by the P/Q-type Ca^{2+} channels expressed throughout the brain and spinal cord (Mermelstein et al., 1999;Luvisetto et al., 2004). Despite being expressed by neurons throughout the CNS, P/Q-type Ca^{2+} channels are not functionally expressed by glia (Latour et al., 2003;D'Ascenzo et al., 2004).

In the cerebellum of the adult animal, P/Q-type Ca^{2+} channels are instrumental in synaptic transmission at most synapses including the excitatory, glutamatergic PF-PC and climbing fiber-PC synapses (Mintz et al., 1995) as well as inhibitory GABAergic synapses between PCs and their targets in the DCN (Iwasaki et al., 2000;Forti et al., 2000;Stephens et al., 2001). Consequently, any alteration in P/Q-type Ca^{2+} channel function could fundamentally alter synaptic transmission throughout the cerebellum and altered synaptic release has been hypothesized to underlie cerebellar dysfunction in the *tg/tg* mouse (Matsushita et al., 2002;Zhou et al., 2003). However, the deficits in synaptic transmission in the cerebellar cortex of *tg/tg* mice are not as pronounced as might be expected. There are no obvious deficits in climbing fiber-PC or PC-DCN synaptic transmission (Matsushita et al., 2002;Hoebeek et al., 2008). While some studies have described a reduction in PF-PC synaptic transmission (Matsushita et al., 2002;Chen et al., 2009), another investigation found PF-PC synaptic transmission intact (Zhou et al., 2003). Paired-pulse facilitation, a common functional measure of pre-synaptic release, is intact suggesting that PF-PC synaptic release is normal (Matsushita et al., 2002). An increase in N-type Ca^{2+} channels on the PFs partially compensates for the reduction in P/Q-type Ca^{2+} channel function (Zhou et al., 2003). At the hippocampus and neuromuscular junction, the loss of P/Q-type Ca^{2+} channels is completely compensated for by increase in N-type or R-type Ca^{2+} channels on the presynaptic terminals (Caddick et al., 1999;Qian and Noebels, 2000;Kaja et al., 2007b). Together these findings suggest that changes in pre-synaptic release are not the sole cause of dysfunction.

In addition to serving a central role in synaptic transmission throughout the CNS, P/Q-type Ca^{2+} channels account for approximately 70-80% of the total Ca^{2+} current in PCs (Usowicz et al., 1992;Mintz et al., 1992) and are fundamental to the spontaneous, intrinsic firing of PCs. The distribution of P/Q-type Ca^{2+} channels on PCs exhibits a spatial gradient of expression from relatively low levels at the PC soma to ~2.5 fold higher levels at the apical dendrites (Indriati et al., 2013). Within the plasma membrane, P/Q-type Ca^{2+} channels are positioned in close proximity to Ca^{2+} activated K^+ channels (K_{Ca}) (Indriati et al., 2013). The close association of P/Q-type Ca^{2+} channels with K_{Ca} channels (both the SK and BK varieties) produces a functional coupling (Womack and Khodakhah, 2002;Womack and Khodakhah, 2003;Womack et al., 2009;Indriati et al., 2013). A reduction in P/Q-type Ca^{2+} current, as occurs in the *tg/tg* mutation, increases the firing rate and irregularity of PC simple spike discharge. Similarly, blockade of P/Q-type Ca^{2+} channels in WT mice also results in irregular PC simple spike firing (Hoebeek et al., 2005;Walter et al., 2006).

In the *tg/tg* mouse, abnormal Ca^{2+} dynamics extends beyond reduced P/Q-type Ca^{2+} channel function. For example, in the cerebellum there is increased expression of L-type Ca^{2+} channels in PCs but not in GCs or DCN neurons (Campbell and Hess, 1999;Erickson et al., 2007). Other CNS areas, except the nucleus of the brachium of the inferior colliculus, do not exhibit significant expression increases in L-type Ca^{2+} channels in the *tg/tg* mouse.

The morphological and immunohistochemical changes in the *tg/tg* mouse are subtle. The gross weight of the *tg/tg* mouse brain is approximately the same as that of WT mice (Noebels and Sidman, 1979;Syapin, 1982). Many of the *tg/tg* mouse CNS abnormalities are found in the cerebellum. For example, the weight of the cerebellum is reduced (Syapin, 1982) as well as the cerebellar volume, the thickness of the molecular layer, and the dimensions of the PC soma (Isaacs and Abbott, 1995). Loss of PCs does not appear to occur before about 1 year of age (Levitt, 1988;Isaacs and Abbott, 1995;Sawada et al., 2009). However, though prior to overt cell death, PCs exhibit abnormal axonal swellings (Rhyu et al., 1999), irregular microtubules, and an increase in cytoplasmic organelles (Meier and MacPike, 1971). Furthermore, *tg/tg* mouse PFs contain enlarged varicosities and form multiple synapses on single PC dendritic spines (Rhyu et al., 1999). Examination of *tg/tg* mouse PC terminals at their synapse on DCN neurons shows vacuolar enlargement of the axons and an increased number of mitochondria but no difference in density of axon-terminals or in the number of synapses (Hoebeek et al., 2008).

Noradrenergic projections from the locus coeruleus are increased to all brain regions (Levitt and Noebels, 1981) as are norepinephrine levels (Levitt and Noebels, 1981;Levitt et al., 1987) as well as increased tyrosine hydroxylase (TH) staining in the cerebellum (Hess and Wilson, 1991;Fletcher et al., 1996;Austin et al., 1992). The increased TH expression is spatially restricted to the soma and dendritic arbor of PCs but is distributed throughout the cerebellum. This TH expression profile contrasts with that of normal mice in which the expression in PCs is transient, with a small fraction of PCs

retaining TH expression into adulthood. Interestingly, the increased TH expression in the *tg/tg* mouse occurs in a similar parasagittal banding pattern as zebrin II, though zebrin II staining is unchanged (Hawkes and Herrup, 1995;Fletcher et al., 1996;Abbott et al., 1996). Both the mRNA and protein levels of neuronal nitric oxide synthase (nNOS) are elevated in the immature and adult *tg/tg* mouse cerebellum (Rhyu et al., 2003;Frank-Cannon et al., 2007).

$GABA_A$ receptor changes are notable in the adult *tg/tg* mouse. There is a decrease in $GABA_A$ receptor function in the cerebral cortex and changes in subunit composition and agonist binding properties that may contribute to the absence epilepsy (Tehrani and Barnes, Jr., 1990;Tehrani and Barnes, Jr., 1995). There is a reduction in the number of $GABA_A$ receptors in the cerebellar granular layer largely due to a reduction in the expression of α6 and γ2 subunits (Kaja et al., 2007a). Although the *tg/tg* mouse does exhibit some histological and histochemical abnormalities, they are not remarkable enough to explain the totality of the *tg/tg* mutant phenotype.

Mutant tottering mouse model of cerebellar ataxia

Ataxia is a term applied to the uncoordinated movements resulting from damage of sensory systems or the cerebellum (Diener and Dichgans, 1992;Morton and Bastian, 2004;Bastian, 1997). In humans, cerebellar dysfunction may manifest *via* a multitude of signs and symptoms including limb and gait ataxia, nystagmus, oscillopsia, cognitive

impairment, locomotor dyscoordination, dysarthria, postural instability, and decreased reaction speed (Massaquoi, 2012;Marsden and Harris, 2011;Holmes, 1917;Holmes, 1939;Dow and Moruzzi, 1958). In contrast, the range of motor abnormalities that may manifest as a result of cerebellar dysfunction in the mouse is somewhat more limited. Therefore, in mouse models of cerebellar disease that exhibit impaired motor control, the term ataxia is used to primarily describe the motor abnormalities that manifest as an uncoordinated, wobbly gait (Ribar et al., 2000;Armbrust et al., 2014;Todorov et al., 2012;Glynn et al., 2005).

The cerebellar ataxia exhibited by the *tg/tg* mouse is relatively mild, as the impairment primarily involves the hindlimbs and tail. The animals also display uncoordinated head movements, have difficulty swimming, and cannot turn as well as WT mice (Green and Sidman, 1962;Syapin, 1982). In addition, *tg/tg* mice have deficient balance and do not perform well on the rotarod test (Syapin, 1982;Walter et al., 2006;Alvina and Khodakhah, 2010b;Alvina and Khodakhah, 2010a) and exhibit decreased walking velocities (Scholle et al., 2010). The *tg/tg* mouse also has eye movement deficits including basal upward deviation of the eyes, reduced gain of both the vestibulo-ocular and optokinetic reflex as well as reduced vestibulo-ocular reflex plasticity (Hoebeek et al., 2005;Stahl et al., 2006;Stahl and Thumser, 2013).

One proposed hypothesis attributes the ataxia of the *tg/tg* mouse to increased variability in the simple spike firing of PCs, termed “loss of the precision of pacemaking”

(Walter et al., 2006;Alvina and Khodakhah, 2010b;Alvina and Khodakhah, 2010a). Loss of pacemaking is also hypothesized to underlie impaired sensorimotor processing in the flocculus of the *tg/tg* mouse, leading to eye movement deficits (Hoebeek et al., 2005). While it is established that *tg/tg* PCs exhibit increased variability in simple spike firing relative to WT mice, the role of the increased irregularity in the abnormal motor behavior is controversial (Glasauer et al., 2011;Stahl and Thumser, 2013). Also, the pacemaking hypothesis is primarily based on intrinsic simple spike firing (i.e., with synaptic inputs blocked) measured *in vitro* (Walter et al., 2006;Alvina and Khodakhah, 2010b;Alvina and Khodakhah, 2010a). However, *in vivo*, the simple spike firing of PCs is known for extraordinary variability (Thach, 1968;Chadderton et al., 2004;Ebner and Bloedel, 1981;Yartsev et al., 2009).

An alternative hypothesis proposes that impaired synaptic transmission in the cerebellar cortex may underlie the ataxia in the *tg/tg* mouse. P/Q-type Ca^{2+} channels play an essential role in synaptic transmitter release at the PF-PC and climbing fiber-PC synapses (Mintz et al., 1995). PF-PC synaptic transmission is reduced in the *tg/tg* mouse (Chen et al., 2009;Matsushita et al., 2002). Furthermore, in *tg/tg* mice synaptic transmission is altered in the cerebral cortex (Ayata et al., 2000;Tehrani et al., 1997;Sasaki et al., 2006) and at the neuromuscular junction (Plomp et al., 2000). Therefore, decreased PC responsiveness to PF input has been hypothesized to underlie cerebellar dysfunction in the *tg/tg* mouse, and possibly in EA2 (Matsushita et al., 2002).

To gain a better understating of the mechanisms underlying the baseline ataxia, the second aim of my thesis examines components of the cerebellar cortical circuitry in the mutant *tg/tg* mouse. Using *in vivo* flavoprotein and Ca^{2+} optical imaging as well as single PC extracellular recordings, I test the hypothesis that deficits are present in the GC-PF-PC circuit in the *tg/tg* mouse that are proposed to contribute to the baseline ataxia in this reduction-of-function model of EA2.

Episodic neurological disorders and low frequency oscillations in the tottering mouse

As mentioned above, the *tg/tg* mouse is the most widely used animal model of EA2. The episodic components of the *tg/tg* mouse phenotype include dystonia and absence seizures. The absence seizures are behaviorally characterized by abrupt movement arrest, twitching whiskers, and fixed stare. Electroencephalographic recordings (EEG) show bilateral, synchronous 6-7 per second cortical spike and wave polyspike discharges that occur simultaneously with the cessation of movement (Kaplan et al., 1979;Syapin, 1982;Noebels and Sidman, 1979;Heller et al., 1983). The *tg/tg* mouse exhibits frequent absence seizures, with ictal episodes occurring ≥ 30 times per hour with each episode lasting 0.3-10 seconds (Noebels and Sidman, 1979;Kostopoulos et al., 1987).

The other episodic trait exhibited by the *tg/tg* mouse is generalized dystonia which characteristically begins in the animal's posterior, with the first manifestation

being extension of the hindlimbs. As the attack evolves, the trunk musculature becomes involved, leading to an arched back. At the peak of the attack, the animal loses the ability to ambulate as the majority of its agonist and antagonist muscle groups undergo rhythmic contractions, including the facial muscles. A notable feature of the episodic dystonia is the progressive and stereotypic manner in which attacks evolve. As the dystonic period subsides, the rhythmic muscle contractions cease in the same order as the attack began. Attacks occur spontaneously 1-2 times per day and during the 30-60 min episodes the animal remains conscious (Green and Sidman, 1962;Campbell and Hess, 1998). As in EA2 patients (Jen et al., 2007;Baloh et al., 1997), physiological or psychological stress (e.g., restraint or entry into a novel environment), caffeine, and ethanol trigger the motor attacks in the *tg/tg* mouse (Fureman et al., 2002;Campbell and Hess, 1998).

The episodic motor attacks are a distinct phenotypic element from the absence epilepsy exhibited by the *tg/tg* mouse. EEG recordings during episodes of dystonia do not show any correlated epileptiform activity, though the characteristic absence seizure activity independently occurs during attacks (Kaplan et al., 1979). Furthermore, the absence seizures are ameliorated by antiepileptic drugs while the dystonic episodes are not (Noebels and Sidman, 1979;Kaplan et al., 1979;Fureman et al., 2002). Finally, lesioning the locus coeruleus reduces absence seizures but not the episodic dystonia (Noebels, 1984;Campbell et al., 1999).

Previous studies have well established that the cerebellum and PCs are necessary for the expression of the motor attacks. For example, dystonic attacks result in immediate early gene expression (c-fos) in the cerebellum, including PCs, GCs, the inferior olivary nucleus, and the DCN (Campbell et al., 1999;Raike et al., 2012;Raike et al., 2013). Expression of the *tg/tg* mutation on a PC degeneration mouse line background demonstrates that loss of PCs coincides with the loss of attacks (Campbell et al., 1999). Furthermore, lesions of the anterior cerebellum reduce the duration and frequency of dystonic episodes (Abbott et al., 1996), selective PC loss (Raike et al., 2012), and cerebellar ablation causes complete attack cessation (Neychev et al., 2008). As described above, the *tg/tg* mouse is largely free of gross CNS abnormalities, implying that the deficits are due to the abnormal functioning of neurons, synapses, and/or circuits.

To explain the dramatic motor phenotype exhibited by the *tg/tg* mouse one would expect highly aberrant activity in motor areas throughout the CNS, including the cerebellum. The Ebner laboratory has described abnormal low frequency oscillations (LFOs, 0.04-2 Hz) in the cerebellar cortex of the *tg/tg* mouse using flavoprotein optical imaging *in vivo* (Chen et al., 2009). The oscillations are transient, propagate and are evoked by caffeine. The LFOs spontaneously increase in amplitude in a region, spread to neighboring regions and then subside over a period of 30-120 min. The vast majority of PCs as well as other cerebellar cortical neurons exhibit oscillatory firing patterns at the same low frequencies. Cerebellar and muscle activity become highly coherent during a motor attack. The LFOs appear to be intrinsically generated in the cerebellar cortex as

blocking glutamatergic inputs does not affect the oscillations (Chen et al., 2009). Removal of Ca^{2+} from the bathing solution significantly reduces both the power and area of the LFOs in the cerebellar cortex. Similarly, blocking L-type Ca^{2+} channels reduces the oscillations while L-type Ca^{2+} channel agonists facilitate them, demonstrating the central role L-type Ca^{2+} channels play in generating the oscillations. Furthermore, PF stimulation fails to evoke or modify the LFOs. In awake *tg/tg* mice, caffeine triggers attacks and accentuates the LFOs. This led to the hypothesis that the LFOs transiently disrupt cerebellar cortical function and provide the neural substrate for episodic dystonia (Chen et al., 2009).

Dysfunctional PC firing likely causes the LFOs that, in turn, drive the episodic dystonia in the *tg/tg* mouse. Evidence directly implicating PCs in the LFOs and the episodic dystonia is that L-type Ca^{2+} channels in the cerebellum are selectively upregulated in *tg/tg* PCs (Campbell and Hess, 1998). L-type Ca^{2+} channel agonists evoke the LFOs (Chen et al., 2009) and antagonists prevent the dystonia (Campbell and Hess, 1999). In PCs, Ca^{2+} influx via L-type Ca^{2+} channels initiates the release of intracellular Ca^{2+} stores *via* ryanadine receptor (RyR) activation and/or inositol-triphosphate receptor activation, which in turn initiates oscillations in the PC membrane potential (Kano et al., 1995). Furthermore, RyR antagonists significantly reduce the frequency of attacks (Raike et al., 2013). Finally, in immature PCs, L-type Ca^{2+} channels are the dominant Ca^{2+} channel type and PCs exhibit LFOs similar to those in *tg/tg* mice (Liljelund et al., 2000). Therefore, the changes in the ratio of P/Q-type to L-type Ca^{2+} channels likely

push the PCs toward an aberrant excitability state represented by the LFOs. Triggers initiate the oscillations in PCs and disrupt the normal processing of information in the cerebellar cortex. The LFOs propagate to neighboring regions in the cerebellum and transmit abnormal signals downstream that drive the dystonic movements.

The LFO hypothesis is consistent with a number of studies investigating the role of cerebellar dysfunction in dystonia. In addition to the *tg/tg* mouse, cerebellar dysfunction in other spontaneous mutant mice and rats is known to produce dystonic syndromes (Neychev et al., 2011). Previous work has demonstrated hyper-excitation of the cerebellar cortex *via* glutamatergic agonists (Pizoli et al., 2002;Fan et al., 2012) or direct electrical stimulation (Raike et al., 2012) is sufficient to produce dystonia. Building upon this previous work, while utilizing the high degree of cell type specific stimulation afforded by optogenetics, recent studies have further demonstrated that the synchronous modulation of large populations of PCs is sufficient to cause muscle contractions and movement (Witter et al., 2013;Heiney et al., 2014).

Triggers of episodic neurological dysfunction in EA2 and the tottering mouse

Attacks in EA2 patients and in *tg/tg* mice are initiated by shared triggers. In *tg/tg* mice, PCs are necessary for the generation of attacks (Campbell et al., 1999;Erickson et al., 2007), and depend on L-type Ca^{2+} channels (Campbell and Hess, 1999) to compensate for the decreased P/Q-type Ca^{2+} current. The departure from the normal PC

Ca^{2+} channel expression profile suggests that intracellular Ca^{2+} homeostasis in PCs is fundamental to the attack mechanism. Xanthines, caffeine and theophylline, evoke dystonic attacks in *tg/tg* mice (Fureman et al., 2002). Caffeine causes the release of intracellular Ca^{2+} *via* RyR activation in PCs but not the PF axons of cerebellar GCs (Kano et al., 1995;Carter et al., 2002). The final common pathway of attack triggers is the activation of RyRs, causing mobilization of internal Ca^{2+} stores from the endoplasmic reticulum (Fureman et al., 2002;Fureman and Hess, 2005;Chen et al., 2009;Raike et al., 2013).

Physiological and psychological stressors are powerful attack triggers. Introduction to novel environments and physical restraint reliably evoke dystonic attacks in *tg/tg* mice (Kaplan et al., 1979;Syapin, 1983;Campbell and Hess, 1998). Noradrenergic neurotransmission and the locus coeruleus are widely implicated in mediating the stress response (Sved et al., 2002;Berridge, 2008). Neurons in the locus coeruleus increase firing in response to stress (Abercrombie and Jacobs, 1987). Noradrenergic projections throughout the CNS, including the cerebellar cortex, originate in the locus coeruleus (Olson and Fuxe, 1971;Pickel et al., 1974). Direct electrical stimulation of the locus coeruleus produces prolonged inhibition of PC firing (Hoffer et al., 1973;Woodward et al., 1979). The effects of noradrenergic signaling in the cerebellar cortex are difficult to dissect because norepinephrine produces both excitatory and inhibitory responses in neurons depending on the specific adrenergic receptor and cell type involved (Kondo and Marty, 1997;Saitow et al., 2000;Hirono and Obata, 2006). The

α-adrenergic receptors are expressed by cerebellar interneurons and Bergmann glia (Kulik et al., 1999;Hirono and Obata, 2006). The frequency of dystonic attacks is reduced by blocking α-adrenergic receptors but the severity and duration of attacks is not altered (Fureman and Hess, 2005). In contrast, pharmacological manipulation of β-adrenergic receptors, though found on PCs and molecular layer inhibitory interneurons, has no apparent effect on the attacks (Kondo and Marty, 1997;Hirono and Obata, 2006). Lesions of the locus coeruleus, the source of adrenergic input to the cerebellar cortex, do not affect the episodic dystonia (Noebels, 1984;Campbell et al., 1999), implying that noradrenergic hyperinnervation does not underlie stress mediated triggering of episodic dystonia. Given the complex interplay of molecular signaling pathways and CNS circuitry, it is unsurprising that the mechanism(s) of psychological and physiological attack triggers remain to be determined.

Episodic neurological dysfunction beyond the cerebellum

In both EA2 patients and *tg/tg* mice the primary focus has been on the cerebellar manifestations. However, P/Q-type Ca^{2+} channels are found in presynaptic terminals, soma, and dendrites of neurons throughout the CNS (Mintz et al., 1992;Fletcher et al., 1996;Westenbroek et al., 1995). Consequently, alteration in P/Q-type Ca^{2+} channel function is likely to produce abnormal neuronal activity throughout the CNS including the cerebral cortex. As described above, EA2 patients exhibit non-cerebellar symptoms including migraine, epilepsy, episodic weakness, and cognitive impairment (Jen et al., 2001;Jouvenceau et al., 2001;Van and Szliwowski, 1996;Baloh et al.,

1997;Rajakulendran et al., 2012). EA2 patients also have abnormal EEG findings (Baloh, 2012) and elevated cerebral cortical excitability (Helmich et al., 2010). These symptoms and findings all suggest abnormalities in cerebral cortical function.

Similarly, the *tg/tg* mouse manifests cerebral cortical dysfunction including absence seizures with rhythmic polyspike EEG bursts (Noebels and Sidman, 1979;Kostopoulos et al., 1987). Other cerebral cortical abnormalities include reduced glutamate and GABA release (Ayata et al., 2000), impaired $GABA_A$ receptor mediated inhibition (Tehrani and Barnes, Jr., 1995;Tehrani et al., 1997), decreased muscurinic acetylcholine receptor density (Liles et al., 1986), and increased noradrenergic projections (2-3 fold) from the locus ceruleus (Levitt and Noebels, 1981). The basal cAMP levels are elevated in the cerebral cortex of the *tg/tg* mouse (Tehrani and Barnes, Jr., 1995).

Finally, evidence suggests that CNS structures outside of the cerebellum contribute to attacks of episodic dystonia. First, the attacks evolve in a highly reproducible and stereotypical progression reminiscent of a "Jacksonian march" (Jackson, 1870;Charcot J.M. and Pitres A., 1877), implying the systematic spread of abnormal neural activity across a region of the brain with a highly organized somatotopy, such as the motor cortex. The cerebellum is not known to contain a similar somatotopic organization (Shambes et al., 1978b;Shambes et al., 1978a;Kassel et al., 1984;Bower and Woolston, 1983;Rowland and Jaeger, 2005;Allen et al., 1977;Allen et al., 1978). Second,

a *Cacna1a* mouse line that expresses one mutant P/Q-type Ca^{2+} channel *tg* allele and one null allele throughout the CNS (Tottering^{haplo} mice) exhibits heightened sensitivity to attack triggers compared to the Tottering$^{PC\text{-}haplo}$ mouse that expresses one *tg* allele and one null allele in PCs but is otherwise heterozygous at the P/Q-type Ca^{2+} channel gene locus (Raike et al., 2013). The difference in trigger sensitivity between these two mouse lines suggests that structures outside the cerebellum contribute to the motor attack.

Previously, we described episodic, LFOs in the cerebellar cortex of *tg/tg* mice that are coupled to the dystonic attacks (Chen et al., 2009). Based on the evidence described above, the third aim of my thesis tests whether similar LFOs occur in the cerebral cortex of the *tg/tg* mouse.

CHAPTER II: RE-EVALUATION OF THE BEAM AND RADIAL HYPOTHESIS OF PARALLEL FIBER ACTION IN THE CEREBELLAR CORTEX

Introduction

Parallel fibers make 100,000 - 200,000, excitatory glutamatergic synapses on the dendritic trees of PCs (Eccles et al., 1967). In spite of their massive numbers and striking medio-lateral geometry, there are two markedly different views of the role of PFs in cerebellar cortical function. The classic "beam" hypothesis postulates that mossy fiber (MF) activation of GCs results in beam-like excitation of PCs (Braitenberg and Atwood, 1958;Braitenberg, 1961). In support of this hypothesis, MF input evokes field potentials in the molecular layer well outside of the MF termination area (Garwicz and Andersson, 1992), whisker stimulation co-modulates transversely located PCs (Bosman et al., 2010), and the presence of synchrony in the simple spike firing during natural inputs (De Zeeuw et al., 1997). However, the beam hypothesis is controversial as others reported that peripheral or MF inputs evoke only patches of PC or molecular layer activity (Bower and Woolston, 1983;Santamaria et al., 2007;Cohen and Yarom, 1998;Rokni et al., 2007). Others found little temporal synchrony in the simple spike discharge of PCs separated transversely by more than 100 μm (Ebner and Bloedel, 1981;Heck et al., 2007;Shin and De Schutter E., 2006;Bell and Grimm, 1969).

The alternative hypothesis is based on the radial organization of GC axons as they ascend to the molecular layer and make synaptic contacts on PCs (Gundappa-Sulur et al.,

1999;Lu et al., 2009;Napper and Harvey, 1988;Llinas, 1982;Santamaria et al., 2002;Santamaria and Bower, 2005). This "radial" hypothesis postulates that GC ascending axons provide the dominant input to PCs and that PCs located laterally are very weakly activated by PFs. Compared to PF synapses, the synaptic connections made along the ascending limb are argued to be stronger, have a higher number of connections on a PC, and result in more synchronous activation of PCs (Llinas, 1982;Sims and Hartell, 2005;Isope and Barbour, 2002). Modeling studies found little role for PFs in modulating PC simple spike discharge, suggesting instead PFs provide background tone (Santamaria et al., 2007;Santamaria and Bower, 2005).

There are major concerns with the radial hypothesis. The ascending limb provides only 3 - 6% of the total synapses on a PC (Napper and Harvey, 1988;Lu et al., 2009;Huang et al., 2006b). In the cerebellar slice, synaptic strength between ascending GC axons and PCs, and between PFs and PCs is equivalent, and PFs activate PCs for several hundred μms (Isope and Barbour, 2002;Walter and Khodakhah, 2009). A variant of the radial hypothesis proposes that GABAergic, molecular layer inhibition prevents beam-like activation by PFs (Santamaria et al., 2007;Santamaria et al., 2002).

The present study re-evaluated the beam versus radial hypothesis, using optical imaging to map spatial patterns of activation *in vivo.* The results show beam-like activation in response to MF, GC, and peripheral stimulation. Furthermore, GABAergic inhibition does not prevent beam-like responses. Instead, the non-uniform distribution of

EAAT4 on PCs (Nagao et al., 1997;Dehnes et al., 1998) and regulation of extracellular glutamate concentration may contribute to the pattern of PC activation.

Methods

Animal preparation

Both FVB (Charles River Laboratories, Wilmington MA) and EAAT4 reporter mice on a C57BL/6 background were used for experiments in this study (Gincel et al., 2007). For both lines, mice of either sex were used. All animal experimentation was approved by and conducted in conformity with the Institutional Animal Care and Use Committee of the University of Minnesota. Detailed descriptions of the preparation of animals for optical imaging have been described in previous publications (Gao et al., 2006;Reinert et al., 2004) and are only described briefly. Adult mice ages 3-8 months were anesthetized by an initial intramuscular injection of 2 mg/kg acepromazine followed by an intraperitoneal injection of 2 mg/kg urethane and supplemented with 1.5 mg/kg urethane as needed. Animals were placed in a stereotaxic frame, mechanically ventilated and their body temperature feedback regulated. Depth of anesthesia was monitored via electrocardiogram and testing for responses to somatosensory stimuli. A craniotomy exposed Crus I and II and then a watertight acrylic chamber was constructed around the exposed folia and filled with Ringer's solution gassed with 95% O_2 and 5% CO_2.

Drug administration

Bicuculline [1(s), 9(R)-(-)-bicuculline methochloride], GABAzine (SR-95531), glycine (L-glycine), and NMDA (N-Methyl-D-aspartic acid) were purchased from Sigma (St. Louis, MO). TBOA (DL-*threo*-β-benzyloxyaspartic acid), DNQX (6,7-dinitroquinoxaline-2,3-dione), LY 367385 [(*S*)-(+)-α-amino-4-carboxy-2-methylbenzeneacetic acid], and APV (D-(-)-2-amino-5-phosphonopentanoic acid) were purchased from Tocris Bioscience (Bristol, UK). All drugs were dissolved in normal Ringer's solution and applied to the cerebellar surface by replacing the solution in the optical chamber except for DNQX/APV and NMDA/glycine which were microinjected into the cerebellar cortex.

Simulation, microinjection, lesioning, and electrophysiological techniques

A paralyene-coated tungsten microelectrode (2-5 MΩ, Fredrick Haer Co., Bowdoin, ME) was used to activate MF afferents in the cerebellar white matter (WM). Typical parameters for MF stimulation consisted of six pulses of 100-150 μA, 100-200 μs at 100 Hz. PF stimulation consisted of ten pulses of 100-125 μA, 100 μsec at 100 Hz. Peripheral responses were evoked via bipolar stimulation with two electrodes placed ~1 mm apart either surrounding the ipsilateral C3 vibrissa follicle or in the medial and lateral walking pads on the ventral aspect of the forepaw using 20 V, 300 μs pulses at 10 Hz for 10 s (Gao et al., 2006) or 10-20 V, 300 μs pulses at 100 Hz for 50-100 ms, respectively.

Microinjections of NMDA/glycine or DNQX/APV into the cerebellar cortex were performed by lowering a glass micropipette (1-5 MΩ) beneath the cerebellar surface and triggering single ejection pulses (75-100 kPa, 100-400 ms) using a pico-injection system (PLI-100; Medical Systems, Greenville, NY). The injection parameters were set to deliver as small a volume as possible over a brief duration. The volume of the injection was calculated by collecting an image of the droplet produced upon injection. The image allowed the diameter of the droplet to be measured and the volume (assumed to be spherical) calculated.

In some experiments lesions were generated in the molecular layer. After evoking a beam with PF stimulation, a tungsten microelectrode was used to produce electrolytic lesions across the beam. Typically, lesions were made at 3-5 locations (50 μA, 1 s) to just span the width of the beam. After generating the lesions, the response to PF stimulation was evoked to assess the effectiveness and extent of the lesion, followed by histological verification (see below).

Single unit extracellular recordings of cerebellar neurons used glass-coated, platinum iridium microelectrodes (1-2 MΩ Alpha Omega, Nazareth, Israel) and conventional electrophysiological techniques (Chen et al., 2009). Recordings were restricted to the molecular layer where PCs were identified by the presence of spontaneous simple spikes and complex spikes (Gao et al., 2006). All other neurons were

classified as unidentified cerebellar neurons. Recordings were digitized at 32 KHz and stored online for offline analysis.

Optical imaging

The anesthetized animal in the stereotaxic frame was placed on an x-y stage mounted on a modified Nikon (Tokyo, Japan) epifluorescence microscope fitted with a 4X objective. Images of Crus I and Crus II were acquired with a Quantix cooled charge coupled device camera with 12 bit digitization (Roper Scientific, Tucson, AZ). A 100 W mercury-xenon lamp (Hamamatsu Photonics, Shizouka, Japan) with direct current (DC) controlled power supply (Opti Quip, Highland Mills, NY) was used as the light source. Images were binned 2 X 2 to yield images of 256 X 256 pixels with a resolution of ~ 10 X 10 μm per pixel.

Ca^{2+} imaging was performed by first loading the Ca^{2+} dye via a series of microinjections into the imaging field. The solution consisted of 10 mM Oregon Green 488 BAPTA-1/AM (Invitrogen, Carlsbad, CA) dissolved in DMSO plus 20% Pluronic F-127 solution (Invitrogen) and diluted 20 times in normal Ringer's solution (Stosiek et al., 2003;Sullivan et al., 2005;Gao et al., 2006). A glass micropipette (resistance 1-5 MΩ) was filled with the dye solution and lowered to a depth of ~150-300 μm in the cerebellar cortex. Injections were made in approximately 15 locations to uniformly stain the folium of interest and the preparation was then incubated for 30 min to allow the Ca^{2+} dye to equilibrate. Images were captured using a custom Ca^{2+} filter set with excitation at 490-

510 nm, a long-pass dichroic mirror of 515 nm, and emission at 520-530 nm. Flavoprotein autofluorescence imaging used a bandpass excitation filter (455 ± 35 nm), a dichroic mirror (500 nm), and a >515 nm long-pass emission filter (Gao et al., 2006;Reinert et al., 2004).

Optical imaging data analysis

A series of Ca^{2+} or flavoprotein images consisting of 40-310, 200 ms frames (5 frames/sec) was acquired. Difference images were then generated by subtracting the average of nine control frames (control average) from each control and experimental frame. These difference images were then divided by the control average, yielding images in which the intensity of each pixel reflects the ΔF/F change in fluorescence relative to the control average.

As shown in Figures 1 and 2, MF stimulation and microinjection of NMDA/glycine resulted in beam-like responses with a centrally located increase in Ca^{2+} fluorescence. Quantification aimed to capture both aspects of the responses. Therefore, regions of interest (ROIs) were placed on the beam-like responses medial and lateral to the stimulation/microinjection (Beam component). A rectangular region (area of 2500 μm^2) centered over the stimulation/microinjection site (Center component) was also measured. This approach was also applied to the beam-like response evoked in Crus II by vibrissal stimulation in the presence of TBOA and to the beam responses evoked by direct PF stimulation (Fig. 10). The Center ROI was placed on the patch-like region

evoked in the absence of TBOA, and the beam regions placed on the areas of increased fluorescence that extended medially and laterally from the patch in the presence of TBOA. The average ΔF/F response corresponding to peak activation (3 frames) was determined for each ROI and averaged for each series.

For peripheral, WM, and GC stimuli, we used the following method to quantify the length of the evoked responses parallel to the long axis of the folium, referred to as mediolateral axis (ML), and along the perpendicular axis, referred to as rostrocaudal axis, (RC). The dimensions of the evoked responses were measured by first generating images of the significant evoked responses by first low-pass filtering (3 X 3) the ΔF/F image, and then determining the mean and SD of a control region. The pixels above or below this mean ± 2 SD were pseudocolored, aligned, and superimposed on an image of the folia using a custom program written in Matlab (MathWorks, Natick, MA). Based on this thresholding, a 100 X 100 μm grid was overlaid on the response region and the response dimensions were then measured along the RC and the ML axes of the folium. The ML and RC lengths were determined for each 100 μm section of the grid and the ratio of the average ML and RC lengths (ML/RC) was computed.

The quantification of the beam-like response in Crus I followed a similar procedure as that described for the NMDA/glycine microinjection and MF stimulation experiments. However, multiple ROIs were defined corresponding to the medial and lateral portion of the beam-like response. The region of the folium where the molecular

layer was lesioned was omitted from analyses (see example ROIs in Fig. 5). This procedure was repeated post lesion in order to compare the peripherally evoked ΔF/F response on-beam before and after the PF disruption.

Example images displayed in Figures 1, 2, and 3 were constructed by averaging 4-32 trials pixel by pixel and then averaging the 5-10 frames encompassing the maximum of the response of interest. Resultant images were scaled to ± 1.5% ΔF/F for grayscale display using Metamorph (Molecular Devices, Downington, PA).

To quantify the spatial relationship between the peripherally evoked optical responses and the distribution of EAAT4, an ROI for the region with the response was identified by thresholding the ΔF/F response to define the portion of the folia exhibiting the peak evoked fluorescence. The ΔF/F along the ROI was determined for both the Ca^{2+} indicator responses and the background fluorescence, which are related to the EAAT4 expression level, across the folium. The correlation coefficient (ρ) between these two ΔF/F spatial profiles was computed.

Electrophysiology analysis

Analysis of single unit recordings consisted of constructing peri-stimulus time histograms (1 ms bins) of spike firing 10 ms prior to stimulus onset and 40 ms post-stimulus using Spike 2 (Cambridge Electronic Design Limited, Cambridge, England). The number of trials ranged from 100-200. Cells were counted as responding to the

stimulus if ≥ 3 consecutive post-stimulus bins contained firing rates greater or less than the pre-stimulus baseline mean ± 2 SDs. The latency of the response was defined as the bin with the first significant increase or decrease (onset) and the end of the response (offset) was the bin at which the firing no longer differed significantly from baseline. The duration of the response was defined as the time between onset and the offset. Response amplitude was defined as the average change in firing during the response compared to mean baseline firing. Percent change in firing from baseline was used to normalize for different firing rates among neurons.

Histology

Post experiment, animals were transcardially perfused with 1% phosphate buffered saline followed by 4% paraformaldehyde in phosphate buffer (pH = 7.4). Brains were then extracted, post-fixed in paraformaldehyde for 2 hours and cryoprotected in 30% sucrose. Cryosectioning of the cerebellum was performed to obtain 40 μm thick, coronal sections that were thionine stained for lesion identification.

Statistical analysis

The statistical analysis was performed using SAS (SAS Institute, Cary, NC). The effects of various drugs, pre-and post-lesion responses, and on versus off patch single-unit response latency were statistically evaluated using a paired Student's *t* test. ΔF/F responses evoked by microinjection of NMDA/glycine at various depths below the cerebellar cortex were statistically evaluated with ANOVA (within-subject design with

repeated measures) followed by Bonferroni *post hoc* test ($P < 0.01$). In the text and figures all values are reported as means ± SD. When describing the results of an experiment, "n" refers to the number of animals used.

Results

WM stimulation evokes a beam-like response

The initial *in vivo* experiment used Ca^{2+} imaging to examine the spatial distribution of cerebellar cortical activation in response to MF input. To directly activate MFs, a microelectrode aligned approximately perpendicular to the surface of Crus II was lowered to a depth of 450-500 μm and stimuli were delivered to the WM. Note that in the FVB mouse the molecular layer, PC layer and granular layer combined are ~440 μm thick (Oz et al., 2011;Serinagaoglu et al., 2007). The example response reveals beam-like activation of the cerebellar cortex along the entire folium with a centrally located, patch-like response above the stimulation site (Fig. 1A). Similar responses were observed in each mouse tested (n = 7), consistent with activation of a group of GCs by MF afferents that in turn leads to PF activation of PCs. The results also are consistent with a strong local activation above the site of WM stimulation that likely includes excitation of PCs by ascending GC axons (Cohen and Yarom, 1998;Llinas, 1982;Isope et al., 2002;Walter et al., 2009).

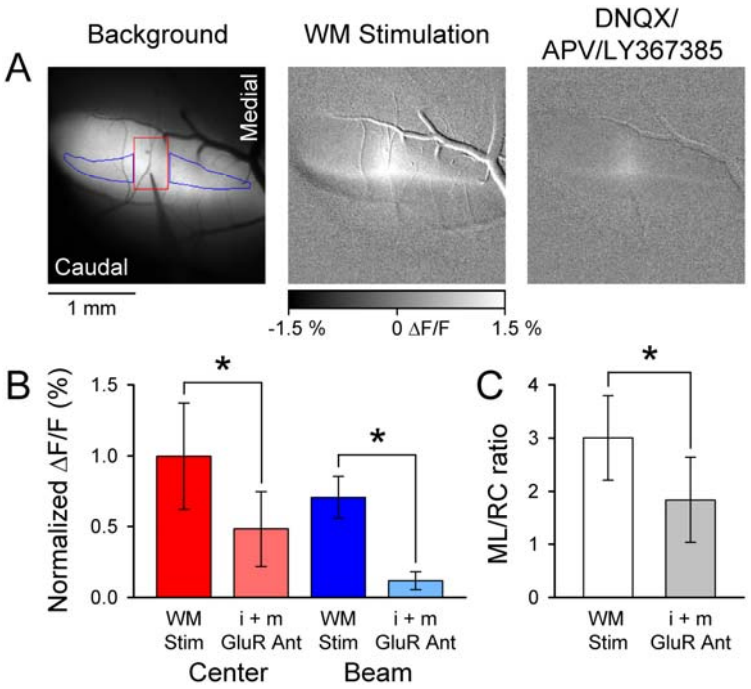

Figure 1. WM stimulation evokes beam-like responses. **A** Left is background fluorescence image of Crus II after injection of Oregon Green. Also shown is electrode placement within the folium and ROIs used to quantify the Center (red) and Beam (blue) components of the fluorescence response. Microelectrode was lowered to a depth of 500 µm below the surface. Middle image shows the beam-like Ca^{2+} response to WM stimulation (200 µA, 100 µs pulses at 100 Hz for 100 ms). Right image shows the beam response is largely blocked by i+mGluR antagonists (100 µM DNQX, 250 µM APV, and 200 µM LY367385). **B** Summary data (mean ± SD, n = 4 mice) for the Center and Beam response components before and after block by GluR antagonists (* = $p < 0.05$ for this and all figures). **C** Summary ML/RC data for WM stimulation (open bar) and after (filled gray bar) application of i+mGluR antagonists (n = 4 mice).

To determine the pre- versus postsynaptic nature of the response, a cocktail of ionotropic and metabotropic glutamate receptor (i+mGluR) antagonists (100 µM DNQX, 200 µM LY 367385, and 250 µM APV to antagonize AMPA, mGluR1, and NMDA receptors, respectively) was added to the optical chamber Ringers. The example images show a large reduction in the response in the presence of the i+mGluR antagonists (Fig. 1A). Although both the Center and Beam components were reduced significantly compared to baseline (Center $t_3 = 87.31$, $P < 0.0001$ and Beam $t_3 = 9.31$, $P = 0.0026$, Fig.

1B), the Beam component had the larger decrease (83 ± 16%). This finding demonstrates that the beam-like response is primarily post-synaptic. A small beam-like response remains that likely represents a less than 100% block of synaptic transmission. In the presence of i+mGluR antagonists, 51 ± 45% of the Center response remains. Both direct activation of CF afferents (pre-synaptic component) and antidromic activation of PCs likely contribute to the remaining response. In fact, the Center response has a parasagittal shape consistent with the projection pattern of the CF afferents (Sasaki et al., 1989;Chen et al., 1996). To quantify the geometry of the response evoked by WM stimulation, we measured the length of the response along the ML and RC axes of the folium and determined the ratio of the ML/RC axes. The ML/RC ratio is also used in subsequent experiments in order to compare the geometry of the responses evoked by different stimuli. The ML/RC ratio for WM stimulation was 3.00 ± 0.79 (Fig. 1C). Upon application of i+mGluR antagonists, the ratio decreased significantly to 1.84 ± 0.80 (t_3 = 7.42, P = 0.0051, Fig. 1C). Importantly, this initial experiment demonstrates that MF stimulation evokes beam-like responses *in vivo*, in contrast to previous results in the isolated guinea pig cerebellum (Rokni et al., 2007;Cohen and Yarom, 1998) but in agreement with an *in vitro* autofluorescence optical imaging study (Coutinho et al., 2004).

NMDA activation of GCs evokes a beam-like response

To obtain greater target selectivity than that afforded by electrical stimulation and to confirm the initial results showing beam-like activity in response to MF-PF-PC circuit

activation, we employed a pharmacological approach to activate GCs. We microinjected NMDA (1.20 ± 0.20 nl, 500 μM) and its co-agonist, glycine (10 μM), into the cerebellar cortex bathed in a 0 Mg^{2+} Ringer's solution. NMDA receptors are expressed on GCs and account for ~30% of the excitatory response to MF input (D'Angelo et al., 1995). Conversely, adult mice do not have functioning NMDA receptors on PFs (Lonchamp et al., 2012;Piochon et al., 2007;Shin and Linden, 2005), although these receptors are expressed on PCs (Renzi et al., 2007;Piochon et al., 2007), suggesting that the NMDA will primarily activate GC dendrites and a patch of PCs and/or interneurons in the immediate vicinity of the injection. However, local activation of PCs and/or interneurons will not generate a beam-like response. NMDA/glycine microinjection evokes a beam-like activation pattern, with the largest amplitude responses evoked by injections within the GC layer between 200-350 μm below the cortical surface (Fig. 2A and C). Also, a patch-like region of activation occurs above the site of injection. The ΔF/F responses evoked by NMDA/glycine for the Beam region were 0.36 ± 0.22% at 50-150 μm, 0.75 ± 0.41% at 200-350 μm, and 0.02 ± 0.17% at 400-500 μm (Fig. 2C, n = 7 mice). The greatest magnitude response occurred when NMDA/glycine was injected at the 200-350 μm depth range and the responses were significantly different at each depth ($F_{15, 186}$ = 24.55, $P < 0.0001$ followed by *post hoc* test). The response amplitudes (ΔF/F) in the Central region were 0.61 ± 0.41% at 50-150 μm, 0.69 ± 0.50% at 200-350 μm, and 0.11 ± 0.20% at 400-500 μm. The largest amplitude responses occurred at both the 50-150 μm and 200-350 μm ranges ($F_{15, 186}$ = 32.37, $P < 0.0001$ followed by *post hoc* test). As noted**,** this is expected as the NMDA will activate neurons locally at the injection site in

both the molecular and GC layers. The lack of a response at the greatest depths below the GC layer (> 400 μm) adds further support that the responses are evoked by GC activation. The smaller response amplitude at greater depths is consistent with the mouse GC layer being ~250 μm thick beneath the ~190 μm molecular and PC layers (Oz et al., 2011;Serinagaoglu et al., 2007). At the 50-150 and 200-350 μm ranges, the responses also had the largest ML/RC ratios; 4.01 ± 2.58 and 4.60 ± 1.74, respectively ($F_{8,19} = 4.72$, P = 0.0026, followed by *post hoc* test, Fig. 2C).

To verify the responses were NMDA receptor-mediated, in three mice NMDA injections were repeated at the depth (200-350 μm) evoking a maximal response in the 0 Mg^{2+} Ringer's solution after reintroduction of 2 mM Mg^{2+} into the optical chamber bath (Fig. 2B). In the presence of Mg^{2+}, the amplitude of the ΔF/F response was significantly reduced from 0.61 ± 0.19 % to 0.16 ± 0.12 % ($t_2 = 4.50$, P = 0.045, n = 3, Fig. 2D). Similarly, the Central response was significantly reduced from 0.95 ± 0.34 % to 0.21 ± 0.08 % ($t_2 = 4.84$, P = 0.040). In the presence of 2 mM Mg^{2+}, the ML/RC ratio decreased markedly to 2.02 ± 0.89 which was significantly different from the ratio obtained by NMDA injections at 200-350 μm ($t_2 = 22.28$, P = 0.0020, Fig. 2D). Therefore, electrical stimulation of MF afferents and glutamate and NMDA microinjection in the GC layer evoke beam-like responses, implying that strong stimulation of a group of MFs or GCs activate PFs that, in turn, activate PCs.

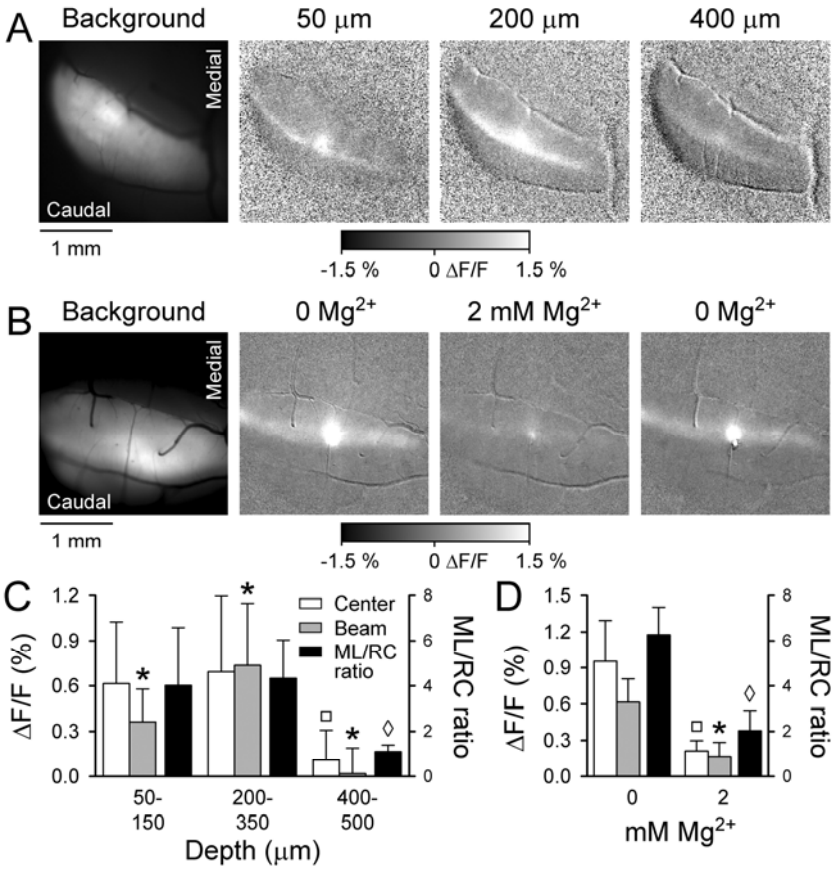

Figure 2. Granular layer stimulation by NMDA evokes beam-like response. **A**, Cerebellar activation evoked by NMDA/glycine microinjection. Left, Background fluorescence of Crus II followed by a series of grayscale images to the right showing typical Ca^{2+} responses to NMDA/glycine microinjections at 50, 200, and 400 μm below the cerebellar surface. Peak beam-like activity is evoked when NMDA/glycine is microinjected at 200–350 μm below the cortical surface, depths corresponding to the granular layer. **B**, To verify that the responses were NMDA receptor-mediated, NMDA injections were performed at a depth evoking a maximal response in the 0 mm Mg^{2+} Ringer's solution and repeated upon reintroduction of 2 mm Mg^{2+} into the optical chamber bath. **C**, Fluorescence responses (ΔF/F on left axis) are summarized for the center and beam components (Fig. 1A, ROI example) as well as the ML/RC ratios (right axis) for NMDA/glycine injection within three depth ranges below the cerebellar surface (n = 9 mice). The *, □, ◊ values are significantly different from all other values in the same group (i.e., control, beam, ML/RC). The ◊ indicates the ML/RC ratio for injection at 400–500 μm is significantly different from the ML/RC ratio for injections at either 50–150 or 200–130 μm. **D**, Summary fluorescence responses and ML/RC ratios for NMDA/glycine injections with and without Mg^{2+}. The *, □, ◊ values are significantly different from all other values in the same group (i.e., control, beam, ML/RC). The ◊ indicates the ML/RC ratio for injection at 400–500 μm is significantly different from the ML/RC ratio for injections at either 50–150 or 200–130 μm.

Peripheral stimulation evokes a beam-like response in Crus I

While the first two experiments demonstrate MF and GC stimulation result in beam-like activation *in vivo*, it can be argued neither stimulus is physiological (Bower, 2002;Bower, 2010). We estimate that the 150 μA stimulation in the WM activated axons of passage within a volume of 4×10^{-3} mm^3, a sphere with a radius of ~ 100 μm (Ranck, Jr., 1975). Based on the volume (~ 1.2 nl) of the NMDA injections and the density of GC somata (4×10^6 cells per mm^3), we estimate that at least 4000 GCs were activated (Korbo et al., 1993). It remains to be determined whether peripherally driven MF inputs produce beam-like activation patterns. In response to ipsilateral forelimb stimulation, Ca^{2+} imaging reveals beam-like responses in Crus I (Fig. 3). Although some areas of patchy activation are also evident and suggestive of localized MF input, beam-like responses extend the entire length of the exposed folium. The ML/RC ratio of the responses evoked in Crus I by forelimb stimulation was 3.48 ± 1.70, a value consistent with a beam-like pattern. The population ratio was obtained from the 19 mice in which the responses in Crus I to forepaw stimulation were determined (see Figs. 3, 4 and 5).

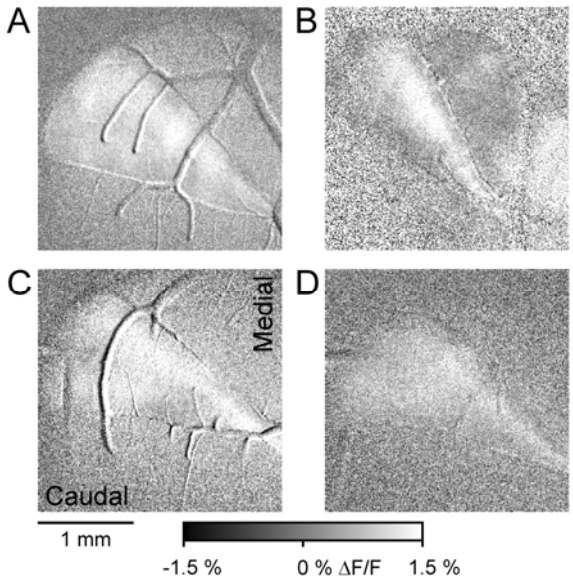

Figure 3. Ipsilateral forelimb stimulation evokes beam-like responses in Crus I. **A-D** Four examples of the beam-like Ca^{2+} responses evoked by bipolar electrical stimulation applied to the ipsilateral forepaw (10-20 V, 300 μs pulses at 100 Hz for 50-100 ms). Each example is from a different mouse. The Ca^{2+} images are shown as ΔF/F obtained by subtraction of averaged baseline images from images obtained during the stimulus (see Methods) and displayed with grayscale.

Although forelimb stimulation evokes beam-like patterns in Crus I, the contribution of PFs to the response remains unknown. This question was tested using two different approaches. First, single unit activity was recorded in the molecular layer of Crus I inside and outside of the thresholded Ca^{2+} response area as shown for an example experiment (Fig. 4A and B). For PCs recorded within the response region, simple spike activity increases significantly to the forelimb stimulation (Fig. 4C). Conversely, simple spike discharge for PCs recorded outside of the region is not modulated (Fig. 4D). In 7 mice, 108 PCs and 28 unidentified neurons were recorded. The simple spike firing of 59% (42/70) of the PCs recorded within the beam-like response region responded to the peripheral stimulus while only 3% (1/38) of the PCs

outside of the region were significantly modulated. These results are consistent with our previous studies that ~90% of the flavoprotein signal is due to post-synaptic activation (Wang et al., 2011;Wang et al., 2009;Reinert et al., 2011). The simple spike responses within the beam-like response regions had a latency of 27.7 ± 5.0 ms and duration of 16.9 ± 9.1 ms. The latencies are comparable to those reported for forelimb stimulation in the rat (Holtzman et al., 2006). Similarly, 76% (16/21) of the unidentified cells recorded within the beam-like region and 0% of the unidentified cells recorded outside of the beam region exhibited a significant change in firing.

In the second approach to testing the PF contribution to the response, discrete lesions in the molecular layer were made to assess changes in the peripheral responses medial and lateral to the lesion. Figure 5 shows the results of two experiments. Forelimb stimulation evoked beam-like Ca^{2+} responses that parallel the rostral border of Crus I (left images of Fig. 5A and B) similar to the responses evoked by PF stimulation (right images of Fig. 5A and B). The electrolytic lesions (50 μA, 1 sec, 3-5 locations) were made across the response defined by PF stimulation (green ROIs in Fig. 5C and D). Following the lesioning, PF stimulation shows that the responses proximal to the lesion were relatively intact and either blocked or greatly reduced distal to the lesion (right images in Fig. 5C and D). Importantly, the electrolytic lesions were discrete and limited to the molecular layer (Fig. 5E). The abrupt transection of the response to PF stimulation and the small lesions demonstrate that the damage to the cerebellar cortex was restricted. The extent of the lesion was further estimated in 7 experiments by directly stimulating PFs on

both the medial and lateral sides of the lesion and measuring the width of absent/decreased optical response. The average region of decreased responsiveness was 203 ± 71 μm, suggesting that beyond the transection damage is limited and consistent with the histology (Fig. 5E). Further, these results establish the PFs and cerebellar cortex are responsive and functioning on either side of the lesioned area.

Comparing the cerebellar responses to forelimb stimulation before and after lesioning shows the decrease in activation either lateral (Fig. 5C) or medial (Fig. 5D) to the lesion. The population data from 7 mice shows the amplitude of the on-beam response to forelimb stimulation (red ROIs in Fig. 5C and D) is significantly reduced to 52 ± 26% of the baseline response following the lesioning (Fig. 5F, $t_6 = 7.28$, P = 0.0003). Therefore, PFs contribute to the beam-like responses in Crus I.

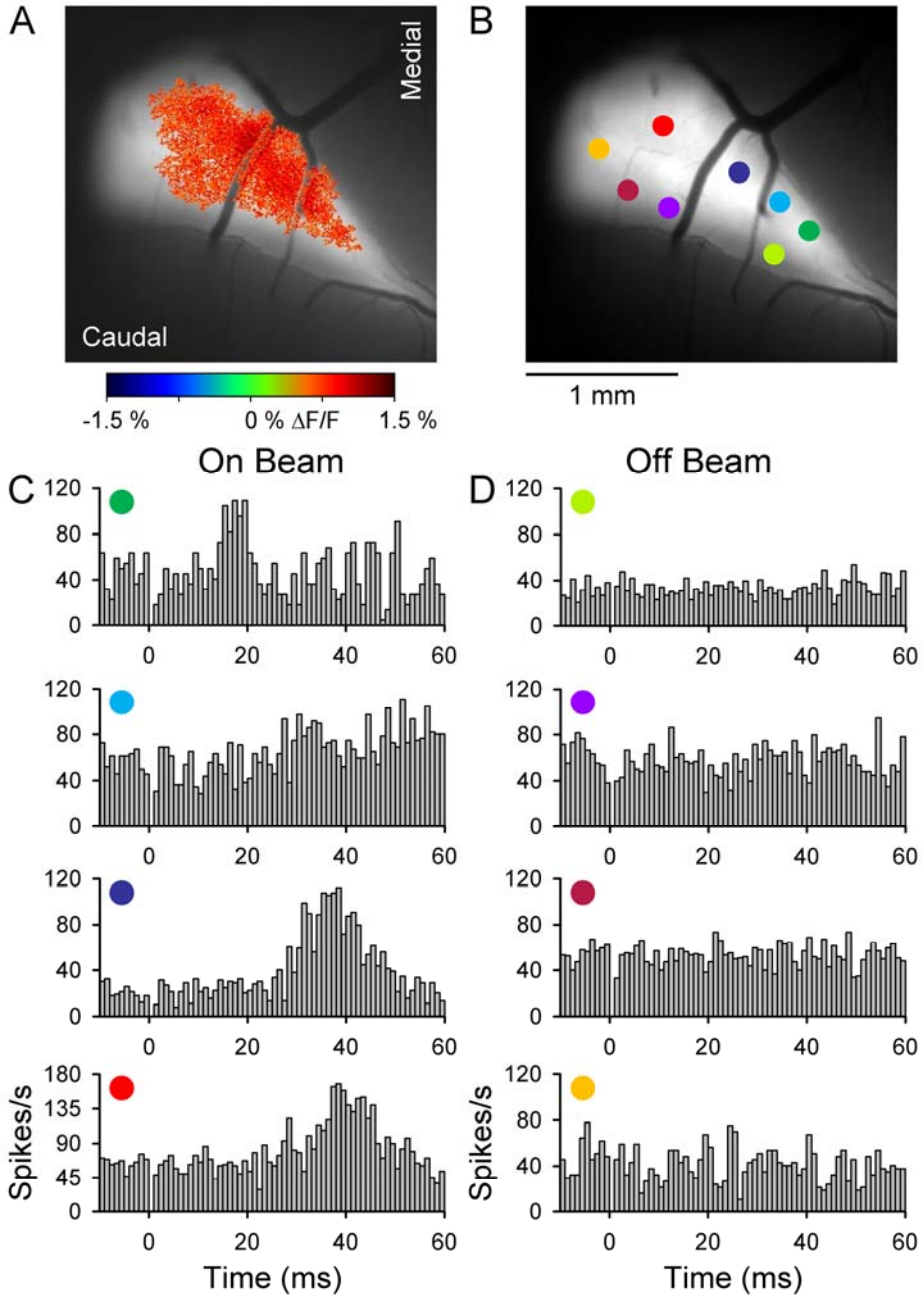

Figure 4. On and off beam PC simple spike responses in Crus I. **A** Example of the Ca^{2+} response defined by statistical thresholding (see Methods) evoked by ipsilateral forepaw stimulation overlayed on an image of the background fluorescence. **B** Recording locations for PCs recorded within (On Beam) or outside (Off Beam) of the forelimb-evoked response region in A. **C** and **D** Simple spike firing histograms corresponding to the PCs shown in B. Histograms were constructed from 100-200 trials of 300 µs, 20 v pulses. Stimulus onset at t = 0 ms and 0 ms bin is blank due to the stimulus artifact.

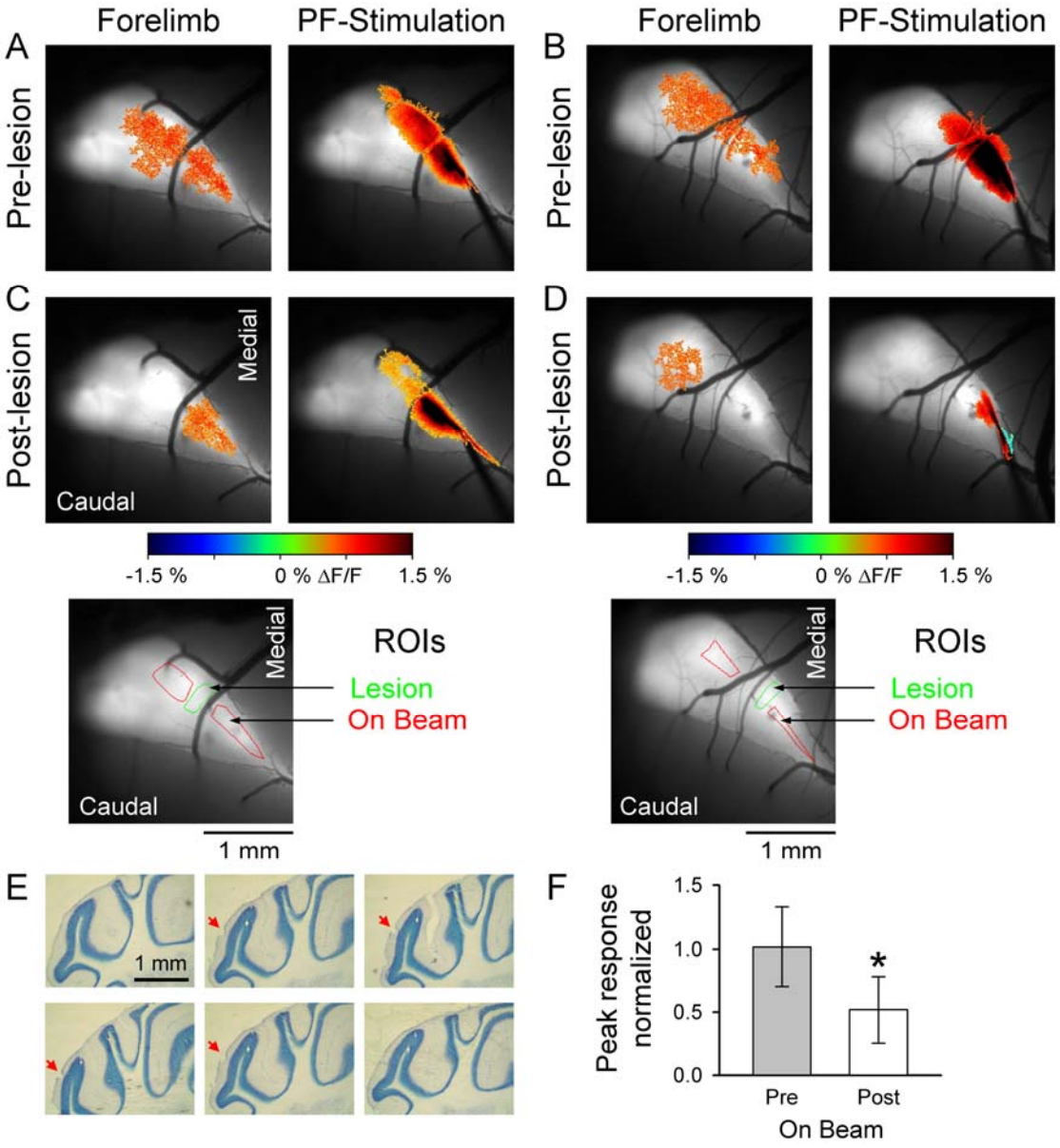

Figure 5. PFs contribute to the beam-like response in Crus I. **A** and **B** Example images from two mice showing the fluorescence responses evoked by forelimb stimulation (left) or direct PF stimulation (right). **C** and **D** After electrolytic lesioning of the molecular layer (see green ROIs in inset below), the peripherally evoked beam-like response (left) is reduced. Also, the response to direct PF stimulation is disrupted (right). Bottom images in C and D show the RO1s used to quantify the On Beam response (red) and the location of the lesion (green). **E** Consecutive 40 μm sections showing the lesion location and depth in the molecular layer (red arrow). **F** Normalized On Beam response to forelimb stimulation is significantly reduced post PF lesioning, (n = 7 mice).

Optical and single cell responses to peripheral stimulation in Crus II

Numerous studies report that peripheral inputs primarily evoke patch-like activation in the cerebellar cortex, particularly in Crus II (Santamaria et al., 2002;Bower and Woolston, 1983). These findings are in conflict with the beam-like activation found for peripheral stimulation in Crus I described above. In fact, stimulation of the ipsilateral C3 vibrissa evokes patch-like activation in Crus II as assessed by flavoprotein imaging (Gao et al., 2006). However, our initial study did not examine the responses of single cells to this peripheral input nor did it assess whether the flavoprotein imaging has the sensitivity to detect beam-like activity. Therefore, the next experiment combined monitoring the responses to vibrissal stimulation with both flavoprotein imaging and single cell recordings restricted to the molecular layer of Crus II within and outside of the response area. Both PCs and unidentified cells were recorded. As demonstrated previously (Gao et al., 2006), the flavoprotein responses to vibrissal stimulation are patch-like (Fig. 6A). Similar patch-like responses are found with Ca^{2+} imaging (see Figs 8, 9 and 10). The example data show that the PC simple spike responses are consistent with the optical responses. PCs recorded within the region of increased fluorescence (± 2 SD above background) respond with a significant increase in simple spike firing and cells recorded outside of the region do not respond (Fig. 6A and B). The correspondence between the simple spike and optical responses is also evident in the averaged simple spike responses for the 80 PCs recorded within or outside of the optical responses (Fig. 6D). Of the 33 PCs recorded within the region of increased flavoprotein fluorescence, the simple spike firing of 30 (91%) was modulated significantly by vibrissal stimulation.

Of the 47 PCs recorded outside the optical response region, the discharge of only 7 (15%) was modulated significantly. None of the PCs responded with an increase in complex spike discharge. Similar to PCs, the firing of 22 (96%) of the 23 unidentified cells located within the flavoprotein response region was significantly modulated by vibrissal stimulation. The firing of only 2 (17%) of the unidentified cells recorded outside the border was modulated. Both the simple spike response duration and response amplitude are greater for PCs recorded within versus outside of the optical response (Fig. 6C). The simple spike responses within the region of increased fluorescence have a latency of 9.8 ± 1.5 ms and duration of 10.2 ± 5.5 ms. The unidentified cells recorded within the response region exhibit a similar latency of 10.1 ± 2.5 ms and duration of 10.0 ± 5.3 ms.

We also tested whether there was a correlation between the firing rate change and the change in flavoprotein fluorescence. The correlation coefficient (ρ) between the change in firing relative to baseline and the $\Delta F/F$ at the corresponding recording location was determined for all 115 cells across 8 animals. The correlation coefficient was 0.57 and provides further evidence that the flavoprotein signal reflects the underlying neuronal activity. Therefore, vibrissal stimulation evokes MF input into Crus II in a patch-like pattern, whether assessed by single cell recordings or flavoprotein imaging, with no evidence of a beam-like response.

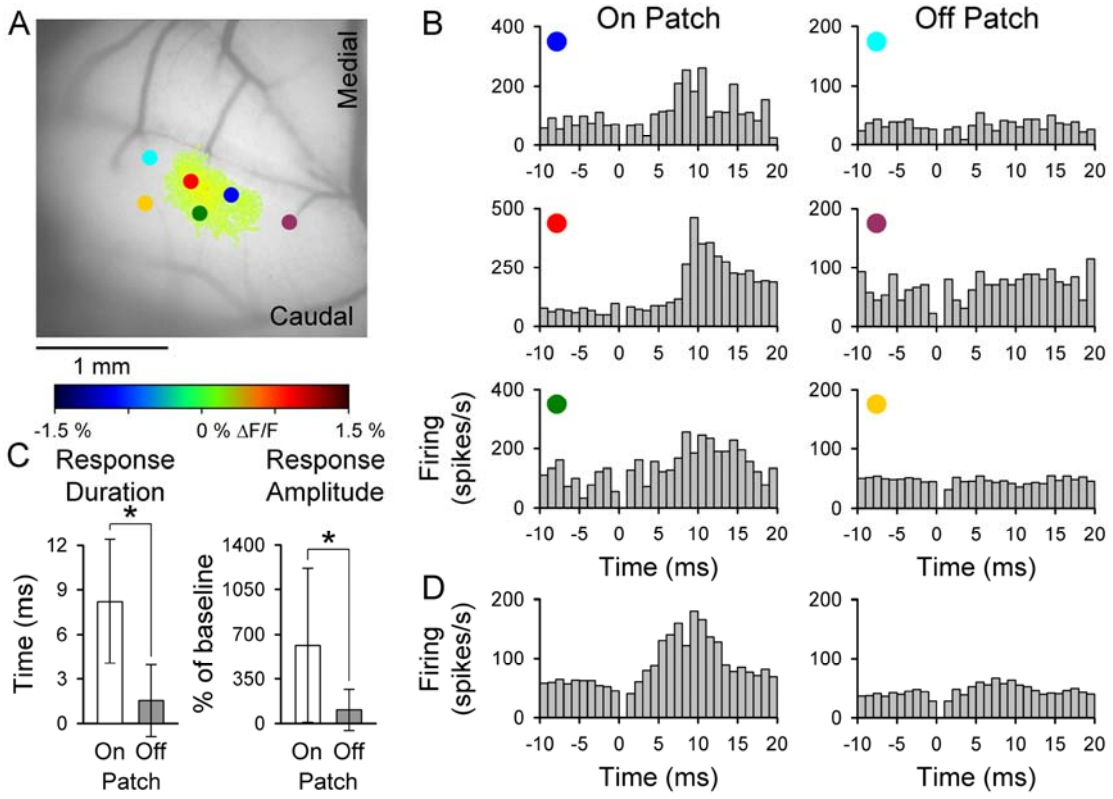

Figure 6. Spatial relation between flavoprotein and PC simple spike responses to peripheral stimulation in Crus II. **A** Ipsilateral vibrissal pad stimulation evokes patch-like increase in fluorescence that was defined by the statistical thresholding. Also shown are the recording locations (colored circles) of PCs relative to the optical response (On Patch versus Off Patch). **B** Simple spike histograms for the On Patch (left) and Off Patch (right) PCs shown in A. Each histogram was generated from 100 vibrissal stimuli. Other conventions as in Fig. 4. **C** Duration and amplitude (mean ± SD) of the significant simple spike modulation for the population of 80 PCs recorded within and outside of the response region (n = 8 animals). **D** Population histograms of simple spike firing for the 80 PCs recorded On Patch (left) and Off Patch (right) of the statistically defined optical response.

Molecular layer inhibition does not suppress the beam-like response

The next experiments addressed possible mechanisms for the beam-like responses in Crus I versus the patch-like responses in Crus II. It was hypothesized that molecular layer inhibitory interneurons control the geometry of the PCs activated by PFs and produce the patch-like responses (Bower, 2002;Santamaria et al., 2007;Santamaria et al.,

2002;Bower, 2010). Application of $GABA_A$ antagonists was reported to result in beam-like responses in PCs (Santamaria et al., 2007). We re-examined this hypothesis monitoring the flavoprotein responses in Crus II evoked by stimulation of the ipsilateral C3 vibrissa under baseline conditions and in the presence of $GABA_A$ receptor antagonists (200 μM GABAzine or 100 μM bicuculline) (Gao et al., 2006). If molecular layer inhibition underlies the patch-like geometry of cerebellar cortical activation to GC input, blocking the action of GABAergic interneurons is expected to convert the patch-like response into a more beam-like response (Santamaria et al., 2007). As shown in the example experiments, the application of $GABA_A$ receptor antagonists increases the amplitude and overall area of activation but does not result in conversion to a beam-like response (Fig. 7A). Furthermore, we measured the ML/RC ratios; if the response becomes more beam-like with blocking GABAergic transmission the ratio should increase. However, the ML/RC ratios were 1.74 ± 0.62 for the baseline, 1.87 ± 0.40 upon bicuculline application ($n = 6$ mice), and 1.89 ± 0.46 with GABAzine ($n = 3$ mice). The ratios were not significantly different for either antagonist ($P > 0.05$ for both drugs, paired Student's *t*-test, Fig. 7B). These results are in agreement with voltage-sensitive dye imaging studies *in vitro* in which blocking $GABA_A$ receptors failed to generate beam-like responses to MF stimulation (Rokni et al., 2007). Therefore, although molecular layer inhibition controls the amplitude and spatial extent of the responses (Gao et al., 2006), it does not prevent beam-like activation *in vivo*.

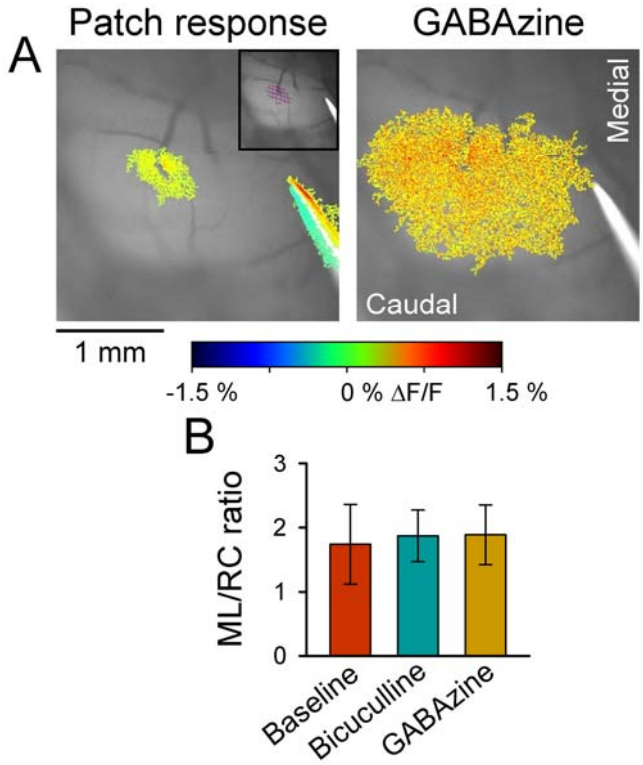

Figure 7. Blocking molecular layer inhibition does not result in beam-like responses. **A** Left image demonstrates the patch-like response in Crus II to stimulation of the ipsilateral vibrissal pad. Insert in upper right in **A** shows thresholded response region covered by grid used to measure the RC and ML extent of the response. Statistical thresholded flavoprotein response is superimposed on the background fluorescence. Right image shows application of GABAzine (SR-95531, 200 μM) increases the amplitude and area of the response but does not result in beam-like activation. Also shown in both images is the PF stimulating electrode used in all experiments to test the integrity of the cerebellar cortex. **B** Summary data of the ratio of the extent of the response in the mediolateral (ML) and rostrocaudal (RC) directions before (baseline) and after application of the $GABA_A$ antagonists, 200 μM GABAzine or 100 μM Bicuculline (n = 9 mice).

Role of excitatory amino acid transporters in the spatial pattern of the responses to peripheral input

Unresolved is why peripheral inputs evoke beam-like responses in Crus I (Figs. 3, 4 and 5) and patch-like activation in Crus II (Figs. 6 and 7). Because molecular layer inhibition does not appear to be responsible, we hypothesized that the differential

distribution of EAAT4 on PCs in Crus I and Crus II plays a role (Gincel et al., 2007). EAAT4 is the predominant glutamate transporter on PCs, is PC-specific and is expressed in parasagittal bands of zebrin-positive PCs in Crus II (Dehnes et al., 1998;Gincel et al., 2007;Nagao et al., 1997). The parasagittal distribution of EAAT4s is known to differentially modulate PC responses to both PF and climbing fiber inputs (Wadiche and Jahr, 2005;Paukert et al., 2010;Tsai et al., 2012). In contrast, EAAT4 is expressed uniformly in Crus I.

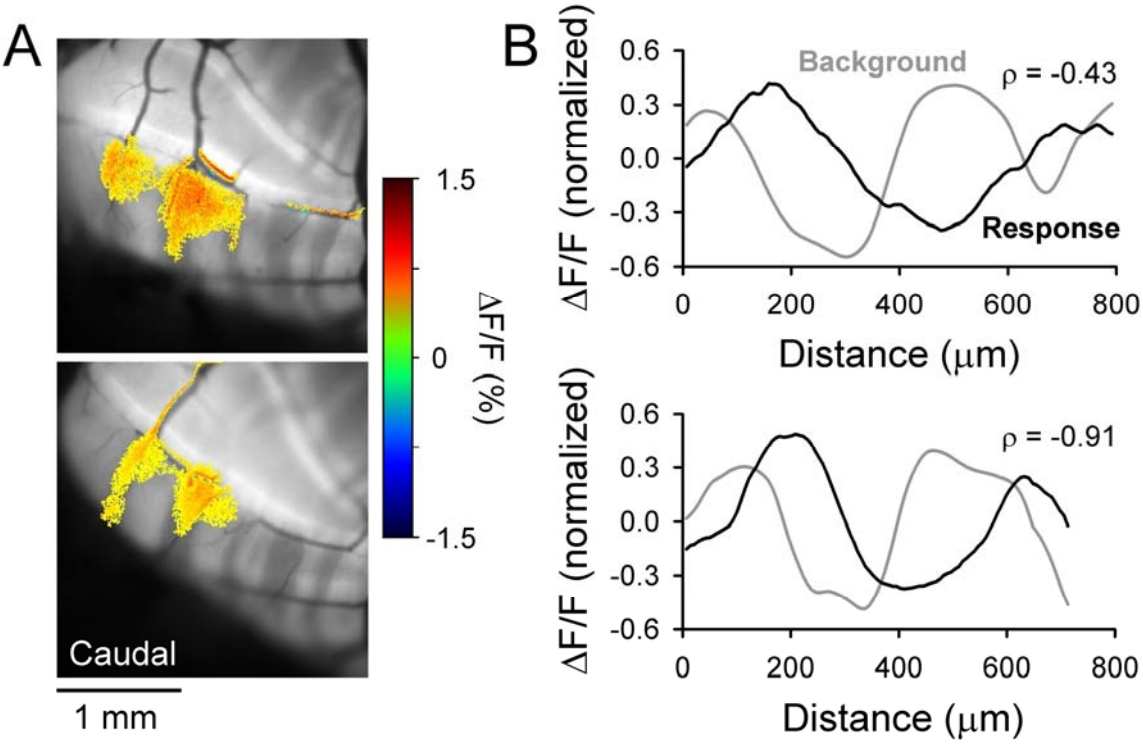

Figure 8. Spatial correspondence between $EAAT_4$ expression in PCs and the response to peripheral input in Crus II. **A** Example images of the patch-like Ca^{2+} responses in Crus II evoked by stimulation of the ipsilateral vibrissae using the $EAAT_4$ reporter mouse that expresses GFP under the control of the $EAAT_4$ promoter. The responses align with parasagittal regions expressing lower levels of the $EAAT_4$ transporter. **B** Evoked Ca^{2+} fluorescence responses (black trace) and background $EAAT_4$ fluorescence in the same folium (gray trace) corresponding to the images in **A**. Correlation coefficient (ρ) between the background fluorescence and the evoked response is shown.

To test this hypothesis, the first experiment used a reporter mouse that expresses green fluorescent protein (GFP) under the control of the EAAT4 promoter (Gincel et al., 2007). In Crus II, vibrissal stimulation evokes patch-like increases in Ca^{2+} fluorescence similar to those observed with flavoprotein imaging (compare Figs. 7 and 8). As shown for the two example experiments, the Ca^{2+} mediated responses to vibrissal stimulation are centered between the parasagittal zones with the higher expression levels of EAAT4 (Fig. 8A). Also, note the lack of a parasagittal distribution of EAAT4 in Crus I (Gincel et al., 2007). To quantify the spatial relationship between the optical responses and the distribution of EAAT4, a rectangular ROI (800 μm along the mediolateral axis of the folium and 10 μm along the rostrocaudal axis of the folium) was defined that encompassed both the responsive and non-responsive regions. The fluorescence change along the ROI was determined for both the Ca^{2+} responses and the background fluorescence of EAAT4 expression and the correlation coefficient between these two profiles was computed. The fluorescence profiles for the two example experiments show the inverse relationship between EAAT4 expression and the responses to C3 vibrissa stimulation (Fig. 8B) and the negative correlation coefficient (ρ = - 0.43 and ρ = -0.91, $P < 0.0001$). In each of the 6 mice studied, a significant inverse relationship exists between the regions responding to the peripheral stimulus and EAAT4 expression (average ρ = -0.70, range -0.43 to -0.91).

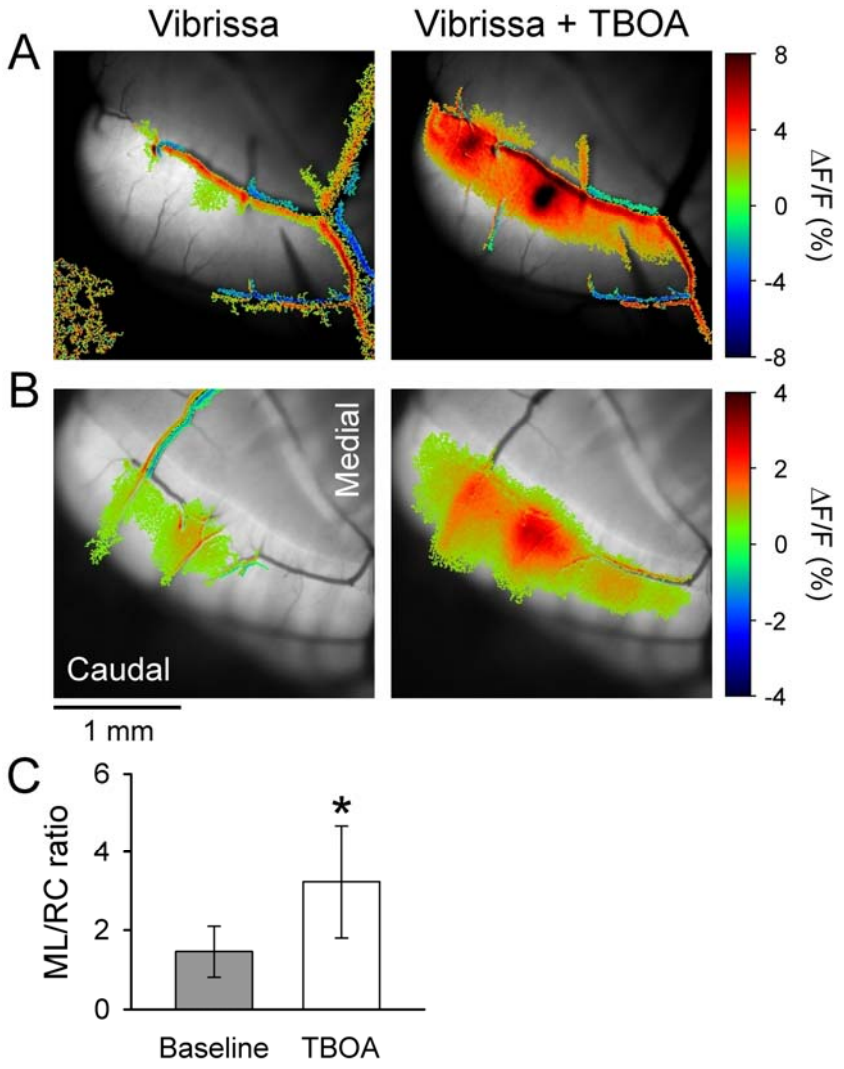

Figure 9. Blocking EAATs converts the patch-like response in Crus II to a beam-like response. **A** Statistically thresholded image of the Ca^{2+} response in Crus II to ipsilateral vibrissal stimulation (10-20 V, 300 μs pulses at 100 Hz for 50-100 ms) prior to (Vibrissa) and upon bath application of 300 μM TBOA in an FVB mouse (Vibrissa + TBOA). Also note the increased fluorescence response on or surrounding several blood vessels. This reflects the increased blood flow that accompanies activation of the cerebellar cortex (Yang et al., 1999;Mathiesen et al., 1998). Blood vessel related activation was commonly observed. **B** Same experiment as in **A** in an EAAT4 reporter mouse. **C** Ratio of ML to RC dimensions of the evoked responses in the baseline condition (white) and in the presence of TBOA (grey) based on 10 FVB and 2 EAAT4 mice.

We reasoned that if the higher level of EAAT4 in the parasagittal zones reduces the responses of PCs to MF inputs then blocking EAATs should convert the patch-like activation of Crus II into a beam-like response. Therefore, the EAAT blocker, TBOA was applied to the Ringer's solution in the optical chamber (Shimamoto et al., 1998;Dehnes et al., 1998). In both FVB (Fig. 9A) and EAAT4 reporter mice (Fig. 9B), vibrissal stimulation evokes the typical patch-like responses in Crus II. Application of TBOA increases the response amplitude and extent of the patch components, but also results in a beam-like profile. For both examples in the presence of TBOA, there are two patches of increased fluorescence embedded in a beam-like response that extends the length of the folium. The conversion to a beam-like profile was observed in all 12 mice tested (10 FVB and 2 EAAT4) and quantified using the analysis described for evaluating the effect of the GABAergic antagonists (see Fig. 7). The ML/RC ratio was 1.46 ± 0.64 for the patch-like response and increased significantly to 3.24 ± 1.44 upon application of TBOA (t_{11} = -4.73, P = 0.0006; Fig. 9C).

If the beam-like response in the presence of TBOA is driven by a general increase of excitability at the level of the granular layer, local inhibition of MF-GC synaptic transmission should affect a correspondingly local region of the beam-like response. Conversely, if the TBOA is acting at the level of the PF-PC synapse, local block of MF-GC synaptic transmission should decrease the activation along the beam-like response due to a reduction in PF activation. To test this hypothesis, the AMPA and NMDA iGluR antagonists (100 μM DNQX and 250 μM APV, 5.95 ± 2.37 nl) were injected into

the granular layer (depth of 250 μm) with the TBOA application, targeting the patch region of increased fluorescence evoked by vibrissal stimulation. Similar to Fig. 9, the two examples in Fig. 10 A and B demonstrate the conversion of the peripherally evoked patch-like response to a beam-like profile by TBOA (300 μM). With injection of the iGluR antagonists, the beam-like responses to vibrissal stimulation are reduced, both medially and laterally. For the 6 mice tested, the evoked fluorescence changes were quantified as for the WM stimulation and NMDA injection experiments (see Figs. 1 and 2). For the Beam region the average ΔF/F was 0.21 ± 0.09 % for vibrissal stimulation alone, 0.71 ± 0.31 % in the presence of TBOA and 0.45 ± 26 % for microinjection of iGluR antagonists in the presence of TBOA ($F_{17, 398} = 88.6$, $P < 0.0001$ followed by *post hoc* test). Similarly, the ΔF/F response for the Central region was 0.38 ± 0.16 % for vibrissal stimulation, 1.18 ± 0.59 % upon bath application of TBOA and 0.52 ± 0.48 % for microinjection of iGluR antagonists with TBOA ($F_{17, 398} = 190.7$, $P < 0.0001$ followed by *post hoc* test). The ML/RC ratio was 1.02 ± 0.17 for the patch-like response, increased significantly to 2.18 ± 0.63 ($t_{10} = -4.32$, $P = 0.0015$) upon application of TBOA, and decreased to 0.86 ± 0.55 ($t_{10} = 3.85$, $P = 0.0032$) with injection of the iGluR antagonists. Therefore, a focal reduction in GC activity results in decreased activation along the beam and converts a beam-like response into a patch-like response, consistent with PF mediated activation along the transverse axis of Crus II.

The ~6.0 nl injection volume of DNQX/APV is a 180 μm diameter sphere. To assess the spatial extent of the action of the injected iGluR antagonists a control

experiment was performed. Two beams were evoked by direct PF stimulation in Crus II (see example in Fig. 10D) and the iGluR antagonists were injected at a depth of ~250 μm below the cerebellar surface between the beams. We reasoned the extent to which the response to PF stimulation in the molecular layer was altered would provide an estimate of the spread of the iGluR antagonists. As shown in the example (Fig. 10D), injecting iGluR antagonists into the granular layer had no obvious effect on the response to PF stimulation demonstrating the spread into the molecular layer, and therefore, into the GC layer, is limited. The ΔF/F responses were quantified for 3 mice using the same approach as the WM stimulation experiment (see Fig. 1). The Center ROI was placed directly over the injection and the Beam ROI were measured medial and lateral to the injection site. The ΔF/F response for the Beam region was 0.96 ± 0.12 % for the baseline and 0.97 ± 0.11 % with injection of the iGluR antagonists (t_{95} = 0.82, P = 0.4149; Fig. 10E). The ΔF/F response for the Central region was 1.44 ± 0.29 % for the baseline and 1.36 ± 0.21 % with injection of the iGluR antagonists (t_{95} = 1.66, P = 0.1005; Fig. 10E). This experiment demonstrates that microinjection of iGluR antagonists into the granular layer acts to locally block the MF-GC synapse. The iGluR antagonists do not diffuse sufficiently into the molecular layer to affect PF-PC synaptic transmission. Therefore, the results obtained from the EAAT4 reporter mice and TBOA experiments strongly suggest that EAATs, including EAAT4s on PCs, are involved in modulating the spatial pattern of the response to MF inputs in the cerebellar cortex.

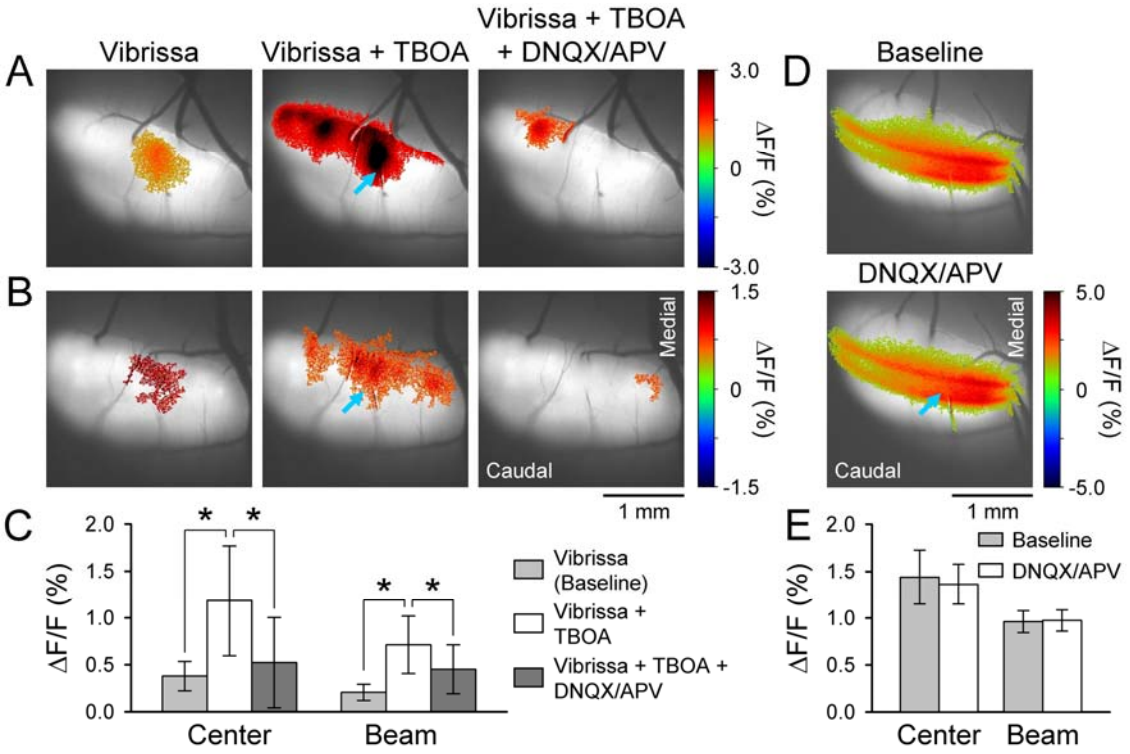

Figure 10. Microinjection of glutamate receptor antagonists into the granular layer disrupts beam-like response in Crus II. **A** and **B** Statistically thresholded images from two mice of the Ca^{2+} response evoked by ipsilateral vibrissal pad stimulation (Vibrissa), with bath application of 300 µM TBOA (Vibrissa + TBOA), and with microinjection of iGluR antagonists (100 µM DNQX and 250 µM APV, 5.95 ± 2.37 nl) into the granular layer (depth of ~250 µm). Blue arrow in the middle images points to the injection site. In both examples focal injection of iGluR antagonists into the granular layer reduces the beam-like response in the presence of TBOA. The PF stimulating electrode is evident in the experiment shown in A. Also, blood vessel related increases in fluorescence are present in both **A** and **B** (see Fig. 9). **C** Summary data (n = 6 mice) for the Center and Beam response components for the baseline with TBOA alone and TBOA with microinjection of GluR antagonists. **D** Statistically thresholded images of the Ca^{2+} response in Crus II evoked by direct PF stimulation with two electrodes before (Baseline) and after microinjection of iGluR antagonists (DNQX/APV) at a depth of 250 µm (blue arrow). **E** Summary data (n = 3 mice) for the Center and Beam responses for the Baseline and DNQX/APV injection.

Discussion

The first major finding is that MF or GC stimulation activates beam-like responses in the cerebellar cortex *in vivo*. There is also a large amplitude response directly above the site of MF or GC stimulation, consistent with the GC ascending limb axons exerting a strong influence on PCs. With electrical stimulation there remains some possibility of direct PF activation, for example, spread of current along the electrode-tissue interface. Importantly, microinjection of NMDA into the granular layer evokes a post-synaptic beam-like response. Given the lack of functioning NMDA receptors on PFs in adult mice (Shin and Linden, 2005;Qiu and Knopfel, 2007;Piochon et al., 2010), NMDA provides a highly selective method of activating GCs without activating PFs directly. PCs and cerebellar interneurons express NMDA receptors (Renzi et al., 2007;Piochon et al., 2007;Bilak et al., 1995); however, activation by focal NMDA injection would result in a patch response and not the observed beam-like activation pattern.

To our knowledge, the observation that forelimb stimulation evokes beam-like responses in Crus I is the first optical imaging evidence for the beam hypothesis. Single cell recordings confirm PC simple spike activation along the beam. Importantly, focal lesioning of PFs reduces the activation lateral and medial to the transection, strongly suggesting that PFs contribute to the transverse response. If the beam-like response was solely due to GC ascending axons, the decrease would be limited to the lesion site.

Molecular layer inhibition does not control beam-like responses

The next major finding is that molecular layer inhibition does not prevent beam-like activation of PCs (Santamaria et al., 2007;Bower, 2010). Application of $GABA_A$ antagonists does not convert patch-like responses into beam-like responses, and instead the response amplitude and extent along both the mediolateral and rostrocaudal axes increases. Conversion of the patch-like response into a beam-like response by TBOA demonstrates that optical imaging has the sensitivity to detect such changes in the activation pattern (see Figs. 9 and 10). The single cell recordings establish that the flavoprotein autofluorescence accurately represents the spatial extent of the underlying neuronal responses. Possibly the flavoprotein imaging may have failed to detect beam-like responses in PCs consisting of very brief duration excitation followed by prolonged inhibition. However, this type of response is highly unlikely given that block of $GABA_A$ receptors increases the duration of the excitation and blocks the inhibition (Bao et al., 2010;Jaeger and Bower, 1994). Therefore, present and previous results fail to support the hypothesis that molecular layer inhibition prevents beam-like responses.

Role of parasagittal zones and glutamate extracellular concentration in response pattern

The finding of patch-like responses in Crus II and beam-like responses in Crus I raises the question of the mechanism underlying the regional differences. Intriguingly, a recent study examining whisker inputs into Crus I and II observed a similar phenomenon (Bosman et al., 2010). Co-modulation in the simple spike discharge occurs in transversally located pairs of PCs in Crus I but not in Crus II. One likely explanation is

the known differences in parasagittal zonation. Crus II has zebrin-positive and -negative zones that reflect differential expression of a host of molecules on PCs (Apps and Hawkes, 2009), many of which control PC excitability and plasticity (Brasnjo and Otis, 2001;Paukert et al., 2010;Wadiche and Jahr, 2005;Wang et al., 2011;Gao et al., 2006). However, Crus I lacks this parasagittal zonation (see Figs. 8 and 9) (Sillitoe et al., 2003;Sarna et al., 2006).

One possible contributor to the patch-like responses is EAAT4. The level of EAAT4 expression on PCs is inversely correlated with glutamate concentration and extra-synaptic GluR activation (Tsai et al., 2012). As we show, the responses to peripheral input in Crus II are inversely related to EAAT4 expression. There are a number of possible explanations. However, differential release of glutamate does not appear to contribute as release is similar in regions with low and high EAAT4 levels (Tsai et al., 2012). We propose the low levels of EAAT4 play a role in generating the patch-like responses. Another possibility is that the MF projections mediating the vibrissae response preferentially terminate between zebrin II parasagittal bands and contribute to the patch-like activation. As recently reviewed (Apps and Hawkes, 2009), MFs show some but not perfect alignment with the overlying zebrin banding pattern or longitudinal zones (Ji and Hawkes, 1994;Wu et al., 1999;Voogd et al., 2003;Pijpers et al., 2006). Nor is there evidence that MF inputs selectively innervate regions of low EAAT4 expression and sparingly innervate regions of high EAAT4. For example, granular layer responses to peripheral and central inputs show activation throughout Crus I and II

(Shambes et al., 1978b;Kassel, 1980;Kassel et al., 1984). Similar maps in Crus II and lobule IX show granular layer responses to the same input that extend across overlaying zebrin positive and negative zones (Hallem et al., 1999;Chockkan and Hawkes, 1994). Therefore, it is unlikely the differential responses in relation to EAAT4 zonation are solely due to variation in the strength of the MF projections. There are other mechanisms that could contribute to patch-like versus beam-like responses, for example the recently described differential transmitter release probability at PF-PC synapses during GC high frequency bursts (van Beugen et al., 2013). Still, the present results show that PFs are activated and glutamate clearance plays an important role in whether PCs are activated in patches or beams.

The TBOA experiments support the interpretation that EAATs shape the response pattern, with foci of activation that become beam-like in the presence of TBOA (Figs. 9 and 10). What the TBOA results show is that by increasing extracellular glutamate concentration, PC excitability increases and the PF contribution becomes apparent. The change to a beam-like pattern is unlikely to reflect a generalized increase in excitability, as $GABA_A$ receptor antagonists increase excitability without producing a beam (see Fig. 7). We hypothesized that the patch-like regions are a major source of the activated PFs responsible for the beam-like response. The finding that focal injection of iGluR antagonists into the granular layer reduces the beam-like responses strongly supports this hypothesis.

Direct PF, MF or GC stimulation evokes beam-like responses in Crus II that may seem at odds with the patch-like responses to peripheral stimulation. However, parasagittal differences in EAAT4 levels do not affect electrically evoked post synaptic responses on PC spines (Tsai et al., 2012), accounting for the beam-like responses to direct electrical or NMDA stimulation. We also suggest that PF, MF or GC stimulation produces a larger and more synchronized PF input that can overcome local mechanisms controlling excitability. In contrast, peripheral stimulation produces smaller amplitude and less synchronous activation of MFs, and in turn GCs, allowing EAAT4 to have a greater role in shaping the spatial pattern of the responses. While we can only speculate on functional implications the results suggest differential requirements for processing of PF inputs, with greater responsiveness in zones expressing lower levels of EAAT4. A corollary is that the width of such processing zones is defined by EAAT4 expression levels. This is consistent with growing evidence that the parasagittal zones have differential physiological and functional properties (Apps and Hawkes, 2009). Clearly, additional studies are needed to determine if the parasagittal distribution of EAAT4 on PCs has similar effects on the response patterns in different folia.

Reconciling previous observations

The present results explain some of the reported discrepancies on the response patterns in Crus I versus II. Several studies supporting the radial hypothesis based their conclusions on patch-like PC responses to peripheral stimuli in Crus II (Santamaria et al., 2007;Bower and Woolston, 1983). There is also less evidence for PF-mediated

synchrony in Crus II than in Crus I (Wise et al., 2010;Bosman et al., 2010). Furthermore, in the cat anterior lobe, responses to various stimuli occur along several mm of a folium (Yu et al., 1985;Valle et al., 2008;Garwicz and Andersson, 1992) and these folia have narrower and more widely spaced zebrin II zones (Sillitoe et al., 2003). While we can only infer that the physiological responses in previous reports are related to EAAT4 expression levels, the evidence suggests the present findings generalize beyond Crus I and II. The results do not necessarily explain why WM stimulation in the isolated cerebellum preparation primarily evoked patch-like responses (Cohen and Yarom, 1998;Rokni et al., 2007). An anatomical comparison is not possible as these earlier studies did not report the lobules evaluated. However, differences between the previous and present studies including using an isolated preparation versus intact animal and voltage-sensitive dye versus Ca^{2+} imaging, respectively, likely explain the differences.

Summary

The present study demonstrates that, in response to peripheral inputs, PFs are activated and modulate PC activity as predicted by the beam hypothesis. However, the hypothesis also envisioned sequential activation along the PFs (Braitenberg and Atwood, 1958;Braitenberg, 1961;Braitenberg et al., 1997). Detecting sequential activity is problematic given that physiological inputs, particularly during behavior, produce complex patterns of MF inputs in space and time (Figs. 3, 8 and 9). The non-homogenous properties of the cerebellar cortex add to the complexity (Apps and Hawkes, 2009), and these factors are likely to obscure any hypothesized timing differences in PC

activity along the PFs. The present findings also demonstrate that synapses along the GC ascending limb modulate PC activity. Both the beam and patch-like elements must be integrated into our understanding of cerebellar cortical function.

CHAPTER III: *IN VIVO* OPTICAL IMAGING DEMONSTRATES ALTERED CEREBELLAR CIRCUITRY IN THE *TOTTERING* MOUSE

Introduction

One family of the Ca^{2+} channelopathies is caused by autosomal mutations of the *CACNA1A* gene that encodes the α_{1A}, pore-forming subunit of the human $Ca_v2.1$ (P/Q-type) voltage gated Ca^{2+} channel (Ophoff et al., 1996;Kramer et al., 1995). Clinical manifestations of *CACNA1A* mutations encompass a broad spectrum of symptoms subclassified into three groups: EA2, familial hemiplegic migraine type 1, or spinocerebellar ataxia type 6 (Jen et al., 2004;Jen et al., 2007;Baloh et al., 1997;Rajakulendran et al., 2010). The symptom complex and severity of disease depends on the specific mutation. EA2 is characterized by paroxysmal attacks of cerebellar dysfunction, including limb dysmetria, gait ataxia, and nystagmus that persist for hours to days. Between episodes, patients typically exhibit progressive cerebellar dysfunction, ataxia and regional cerebellar atrophy (Baloh et al., 1997;Jen et al., 2007;Denier et al., 1999). Importantly, P/Q-type Ca^{2+} channels are heavily expressed in the cerebellum, particularly in Purkinje cells (PCs) and granule cells (GCs) (Mintz et al., 1992;Fletcher et al., 1996;Westenbroek et al., 1995). Mutations in *CACNA1A* that give rise to EA2 have been shown or are predicted to cause a loss or decrease of P/Q-type Ca^{2+} channel function (Wappl et al., 2002;Spacey et al., 2004;Jen et al., 2004;Pietrobon, 2010).

The mutant *tg/tg* mouse contains a recessive missense mutation in the pore-forming region of the P/Q-type Ca^{2+} channel *Cacna1a*, orthologue of the human gene *CACNA1A* (Fletcher et al., 1996). The phenotype of the *tg/tg* mouse consists of paroxysmal dystonia, ataxia, and absence seizures. One non-episodic element of the *tg/tg* mouse phenotype is the uncoordinated, ataxic gait. Similar to EA2 patients, the *tg/tg* mouse exhibits a reduction-in-function with a 30-40% loss of P/Q-type Ca^{2+} channel current in PCs. Cerebellar histopathological findings in the *tg/tg* mouse are very limited and overt loss of PCs is only observed in animals beyond 1 year of age (Levitt, 1988;Isaacs and Abbott, 1995;Sawada et al., 2009). While frank neurodegeneration (primarily of PCs) often underlies severe ataxia in many cerebellar disorders, milder ataxia occurs in the absence of neuronal loss (for review see (Reeber et al., 2013)). In the absence of neurodegeneration, abnormalities in the cerebellar circuitry such as impaired synaptic transmission, developmental changes or altered excitability may give rise to the baseline ataxia (Ikeda et al., 2006;Matsumoto et al., 1996;Sato et al., 2009;Barnes et al., 2011;Ebner et al., 2013;Armbrust et al., 2014).

Two hypotheses have been put forward to explain the ataxia of the *tg/tg* mouse. The first attributes the ataxia to increased variability in the simple spike firing of PCs, termed "loss of the precision of pacemaking" (Walter et al., 2006;Alvina and Khodakhah, 2010b;Alvina and Khodakhah, 2010a). Similarly, loss of pacemaking is hypothesized to underlie impaired sensorimotor processing in the flocculus and the corresponding abnormal eye movements exhibited by the *tg/tg* mouse (Hoebeek et al., 2005). While it is

established *tg/tg* mouse PCs exhibit increased variability in simple spike firing, the role of the increased irregularity in the abnormal motor behavior of the *tg/tg* mouse is controversial (Glasauer et al., 2011;Stahl and Thumser, 2013;Stahl and Thumser, 2014).

Alternatively, impaired synaptic transmission in the cerebellar cortex may underlie the ataxia in the *tg/tg* mouse. P/Q-type Ca^{2+} channels play an essential role in synaptic transmitter release in the central nervous system (CNS) including in the cerebellar cortex (for review see (Ebner and Chen, 2012;Pietrobon, 2010;Catterall, 1998)). Parallel fiber (PF)-PC synaptic transmission is reduced in the *tg/tg* mouse (Chen et al., 2009;Matsushita et al., 2002). Furthermore, in *tg/tg* mice synaptic transmission is altered in the cerebral cortex (Ayata et al., 2000;Tehrani et al., 1997;Sasaki et al., 2006) and at the neuromuscular junction (Plomp et al., 2000). Therefore, decreased PC responsiveness to PF input has been hypothesized to underlie cerebellar dysfunction in the *tg/tg* mouse, and possibly in EA2 (Matsushita et al., 2002).

To gain a better understating of the mechanisms underlying the baseline ataxia exhibited by the *tg/tg* mouse, this study examines several components of the cerebellar cortical circuitry in the mutant *tg/tg* mouse *in vivo*. Using flavoprotein and Ca^{2+} optical imaging as well as single PC extracellular recordings, we demonstrate decreased function in the GC-PF-PC circuit. In contrast, the climbing fiber-PC circuit is relatively intact. Importantly, 4-aminopyridine, one of the effective pharmacological therapies in EA2, corrects the GC-PF-PC deficit. We propose that the abnormalities in the GC-PF-PC

circuit contribute significantly to the baseline ataxia in this reduction-of-function mouse model of a *CACNA1A* channelopathy.

Methods

Animal preparation

All animal experimentation was approved by and conducted in conformity with the Institutional Animal Care and Use Committee of the University of Minnesota. Male and female *tg/tg* mice on a C57BL/6 background as well as male and female C57BL/6 control mice were used for experiments in this study. Homozygous *tg/tg* mice were obtained by crossing a line of mice that have the *tg* and the semi-dominant *Os* allele, which causes oligosyndactylism; *tg/tg* homozygotes were identified at birth by the absence of oligosyndactylism. Putative *tg/tg* homozygotes were challenged with caffeine (15 mg/kg, i.p.) or psychological stress (e.g. placement in a novel cage) to verify the expression of episodic dystonia. Detailed descriptions of the preparation of animals for optical imaging have been described in previous publications (Gao et al., 2006;Reinert et al., 2004) and therefore, are described briefly. Adult mice ages 3-8 months were anesthetized by an initial intramuscular injection of 2 mg/kg acepromazine followed by an intraperitoneal injection of 2 mg/kg urethane and supplemented with 1.5 mg/kg urethane as needed. Animals were placed in a stereotaxic frame, mechanically ventilated and their body temperature feedback regulated. Depth of anesthesia was monitored via electrocardiogram and testing for responses to somatosensory stimuli. A craniotomy

exposed Crus I and II and then a watertight acrylic chamber was constructed around the exposed folia and filled with Ringer's solution gassed with 95% O_2 and 5% CO_2.

Drug administration

Glycine (L-glycine) and NMDA (N-Methyl-D-aspartic acid) were purchased from Tocris Bioscience (Bristol, UK) and were microinjected into the cerebellar cortex. 4-aminopyridine (4-AP) was also purchased form Tocris Bioscience, dissolved in Ringer's and applied to the exposed cerebellar cortex by replacing the solution in the optical chamber. Caffeine was purchased from Sigma (St. Louis, MO), dissolved in normal saline and administered intraperitoneally.

Stimulation and electrophysiological techniques

A parylene-coated tungsten microelectrode (2-5 MΩ, Fredrick Haer Co., Bowdoin, ME) was used to activate PFs in the cerebellar cortex (Cramer et al., 2013). The parameters for PF stimulation consisted of 10 pulses of 150 μA, 100 μs at 10 or 100 Hz. Peripheral responses were evoked via bipolar stimulation with two electrodes placed ~1 mm apart on either side of the ipsilateral C3 vibrissal pad 10-20 V, 300 μs pulses at 100 Hz for 100 ms (Cramer et al., 2013;Gao et al., 2006).

To activate climbing fibers (CFs), a tungsten microelectrode (see above) was stereotaxically placed in the contralateral inferior olive (Barnes et al., 2011). The principal olive was targeted to activate CFs projecting to the cerebellar hemisphere. As

the electrode was lowered, stimulation was performed at 200 μm intervals to a final location that evoked the largest responses. The stimulation protocol used 100 μA, 100 μsec pulses at 10 Hz for 1 s.

Microinjections of NMDA/glycine into the cerebellar cortex were performed by lowering a glass micropipette (1-5 MΩ) beneath the cerebellar surface and triggering single ejection pulses (75-100 kPa, 200 ms) using a pico-injection system (PLI-100; Medical Systems, Greenville, NY) (Cramer et al., 2013). The injection parameters were set to deliver as small a volume as possible over a brief duration. The volume of the injection was calculated by collecting an image of the droplet (assumed spherical) produced upon injection and measuring the diameter.

Single unit extracellular recordings of cerebellar neurons used glass-coated, platinum iridium microelectrodes (1-2 MΩ Alpha Omega, Nazareth, Israel) and conventional electrophysiological techniques (Chen et al., 2009). Recordings were restricted to the molecular layer where PCs were identified by the presence of spontaneous simple spikes and complex spikes (Gao et al., 2006;Cramer et al., 2013). All other neurons were classified as unidentified cerebellar neurons. Recordings were digitized at 32 KHz and stored online for offline analysis.

Optical imaging

The anesthetized animal in the stereotaxic frame was placed on an x-y stage mounted on a modified Nikon (Tokyo, Japan) epifluorescence microscope fitted with a 4X objective. Images of Crus I and Crus II were acquired with a Quantix cooled charge coupled device camera with 12 bit digitization (Roper Scientific, Tucson, AZ). A 100 W mercury-xenon lamp (Hamamatsu Photonics, Shizouka, Japan) with direct current (DC) controlled power supply (Opti Quip, Highland Mills, NY) was used as the light source. Images were binned 2 X 2 to yield images of 256 X 256 pixels with a resolution of ~ 10 X 10 μm per pixel.

Ca^{2+} imaging was performed by first loading the Ca^{2+} dye via a series of microinjections into the imaging field as described previously (Gao et al., 2006;Cramer et al., 2013). Images were captured using a custom Ca^{2+} filter set with excitation at 490-510 nm, a long-pass dichroic mirror of 515 nm, and emission at 520-530 nm. Flavoprotein autofluorescence imaging used a bandpass excitation filter (455 ± 35 nm), a dichroic mirror (500 nm), and a >515 nm long-pass emission filter (Gao et al., 2006;Reinert et al., 2004).

Optical imaging data analysis

A series of Ca^{2+} or flavoprotein images consisting of 40-310, 200 ms frames were acquired. Difference images were then generated by subtracting the average of nine control frames (control average) from each control and experimental frame. These

difference images were then divided by the control average, yielding images in which the intensity of each pixel reflects the ΔF/F change in fluorescence relative to the control average.

As previously published (Cramer et al., 2013) and shown in Figure 2, microinjection of NMDA/glycine results in a beam-like response and a centrally located increase in Ca^{2+} fluorescence. Quantification aimed to capture both components of the responses. Therefore, regions of interest (ROIs) were placed on the beam-like responses medial and lateral to the microinjection (Beam component). A rectangular region (area of 2500 μm^2) centered over the microinjection site (Center component) was also measured. The average ΔF/F response corresponding to peak activation (3 frames) was determined for each ROI and averaged for each series.

The dimensions of the peripherally evoked responses in Crus II were measured by first generating images of the significant evoked responses by first low-pass filtering (3 X 3) the ΔF/F image, and then determining the mean and SD of a control region. The pixels above or below this mean ± 2 SD were pseudocolored, aligned, and superimposed on an image of the folia using a custom program written in Matlab (MathWorks, Natick, MA). Based on this thresholding, the response dimensions were then measured along the rostrocaudal (RC) and the mediolateral (ML) axes of the folium to obtain the ML/RC ratio.

The response to inferior olive stimulation was measured by defining an ROI aligned over the simplex, Crus I, Crus II, and paramedian lobule. The pixel intensities within the ROI were obtained from an average of 5 difference images prior to the stimulus and 5 difference images during the peak response. The number of pixels that exhibited intensity values different from the baseline was divided by the total pixel count of the ROI to obtain the percentage of pixels that differed from the baseline during the climbing fiber response.

Electrophysiology analysis

Analysis of single unit recordings consisted of constructing peri-stimulus time histograms (1 ms bins) of spike firing 10 ms prior to stimulus onset and 40 ms post-stimulus using Spike 2 (Cambridge Electronic Design Limited, Cambridge, England). The number of trials ranged from 100-200. Cells were counted as responding to the stimulus if ≥ 3 consecutive post-stimulus bins contained firing rates greater or less than the pre-stimulus baseline mean $\pm$ 2 SDs. The latency of the response was defined as the bin with the first significant increase or decrease (onset) and the end of the response (offset) was the bin at which the firing no longer differed significantly from baseline. The duration of the response was defined as the time between onset and the offset. Response amplitude was defined as the average change in firing during the response compared to mean baseline firing. Percent change in firing from baseline was used to normalize for different firing rates among neurons.

Statistical analysis

The statistical analysis was performed using SAS (SAS Institute, Cary, NC). The ML/RC ratios of the response evoked by NMDA/Glycine microinjection were statistically evaluated using a Student's *t* test. The amplitude of the evoked fluorescence response to NMDA/Glycine, PF stimulation, and vibrissae stimulation as well as the ML/RC ratios and climbing fiber responses were evaluated using an ANOVA (within-subject design with repeated measures). For the evaluation of the 4-AP experiments, ANOVA was followed by Bonferroni *post hoc* test ($p < 0.01$). A χ^2 test was used evaluate the proportion of responsive and non-responsive PCs recorded within the patch response in WT and *tg/tg* mice. In the text and figures all values are reported as means ± SD unless otherwise noted. When describing the results of an experiment, "n" refers to the number of animals used.

Results

Reduced beam-like response evoked by direct PF stimulation

Our previous study documented spontaneous, episodic low frequency oscillations in the cerebellar cortex of the *tg/tg* mouse (Chen et al., 2009). We hypothesized that the oscillations are involved in the dramatic episodic dystonia that is one of the hallmark phenotypes of the *tg/tg* mouse. The goal of the present study was on the non-episodic, baseline ataxia observed in these mice. Therefore, the experiments were performed when these low frequency oscillations in the cerebellar cortex were not present.

Stimulation of PFs evokes a characteristic transverse beam of increased PC activity and has been extensively studied using electrophysiological and optical imaging techniques (Chen et al., 1998;Cohen and Yarom, 1999;Eccles et al., 1966a) including flavoprotein and Ca^{2+} imaging in Crus II (Reinert et al., 2004;Gao et al., 2006;Wang et al., 2011;Cramer et al., 2013). Flavoprotein imaging studies demonstrate that ~90% of the increase in flavoprotein fluorescence (the "light phase") of the evoked beam derives from the post-synaptic activation of PCs (Reinert et al., 2004;Reinert et al., 2007;Wang et al., 2011;Wang et al., 2009). Therefore, we tested PF-PC synaptic transmission by measuring the beam response evoked by PF stimulation in *tg/tg* and WT mice.

This initial experiment determined the flavoprotein response in Crus II to PF stimulation at two different stimulus frequencies, 100 and 10 Hz. The response to PF stimulation is severely diminished in the *tg/tg* mice (Fig. 1). At both 100 Hz (Fig. 1A and B) and 10 Hz (Fig. 1E and F) stimulation, the example images show that the response amplitude and mediolateral spread are diminished compared to control mice. Parallel fiber stimulation at 100 Hz evokes a 0.54 ± 0.15% change in flavoprotein fluorescence in the WT mouse (n = 8). In contrast, the same PF stimulus in *tg/tg* mice produces a 0.17 ± 0.10% fluorescence response (n = 8), a 70% reduction in the amplitude of the WT response ($F_{1,14}$ = 3854.6; $p < 0.0001$, Fig. 1C). Similarly, PF stimulation at 10 Hz evokes a 0.40 ± 0.15% fluorescence increase in WT versus a 0.12 ± 0.09% response in *tg/tg* mice and is significantly less than the WT response ($F_{1,11}$ = -2268, $p < 0.0001$, n = 8 *tg/tg*, n = 5 WT; Fig 1G).

A second measure of the response to PF stimulation is the geometry of the evoked fluorescence beam. The ML/RC ratio is calculated by measuring the extent of the ML distance of the response and dividing that quantity by the RC extent of the response. A ML/RC ratio >>1 corresponds to a response that is beam-like while ratios near 1 are more patch-like (Cramer et al., 2013). The geometry of the PF beam evoked by the PF stimulation in the *tg/tg* mouse is markedly abnormal compared to that of the WT mouse (Fig. 1A-B and E-F). At 10 Hz stimulation, the beam is truncated with a ML/RC ratio of 1.07 ± 0.41, markedly less than the WT ratio of 6.05 ± 5.67 ($F_{1,11}$ = 228.2, p < 0.0001, n = 8 *tg/tg*, n = 5 WT; Fig. 1H). The ML/RC ratio of the response evoked by 100 Hz PF stimulation in the *tg/tg* mouse is also reduced compared to WT ($F_{1,11}$ = 150.3, p < 0.0001, n = 8 *tg/tg*, n = 5 WT; Fig 1D). These observations confirm the earlier *in vitro* and *in vivo* reports of a decrease in responses to PF stimulation (Chen et al., 2009;Matsushita et al., 2002). These newer results establish that not only is the response amplitude reduced but also the medial-lateral extent to which PFs activate PCs.

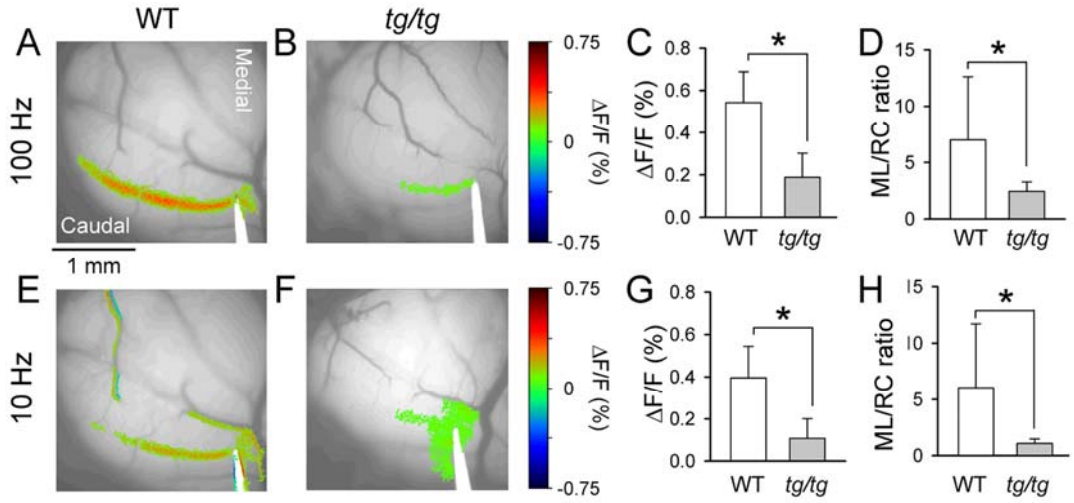

Figure 11. Beam response to direct PF stimulation is reduced in the *tg/tg* mouse. **A** and **B** Example of the flavoprotein fluorescence response evoked by direct electrical stimulation of the PFs (150 μA, 100 μs pulses at 10 or 100 Hz, 10 pulses) in the WT and *tg/tg* mouse. **C** Summary of the beam fluorescence response for the WT (white) and the *tg/tg* (gray) mouse (n = 8 WT, n = 8 *tg/tg*). **D** Summary ML/RC ratios for the beam response evoked by 100 Hz stimulation in the WT (white) and *tg/tg* (gray) mice (n = 12 WT, n = 9 *tg/tg*). **E** and **F** Examples of fluorescence responses evoked in WT and *tg/tg* mice to direct PF stimulation at 10 Hz. **G** and **H** Summaries of the fluorescence response and the ML/RC ratios evoked by 10 Hz PF stimulation for WT and *tg/tg* mice (n = 5 WT, n = 8 *tg/tg*). Note that for all figures, bars show mean ± SD and * denotes significant difference at $p<0.05$.

NMDA activation of granule cells evokes an attenuated beam-like response

To more fully evaluate the GC-PF-PC circuitry, the next experiment pharmacologically activated GCs to test PC responses to both the ascending limb and the PF component of the GC axon (Cramer et al., 2013;Sims and Hartell, 2005). As detailed previously, nano-injections of NMDA/Glycine (~ 1 nl) into the granular layer of the cerebellar cortex bathed in 0 Mg^{2+} Ringer's solution provides for selective activation of granular cells (Cramer et al., 2013). Two components of the NMDA/Glycine evoked Ca^{2+} response were measured: the central response region over the injection site, and the beam component consisting of the response medial and lateral to the central response

region (see Methods). Both the central and beam components of the response are significantly reduced in the *tg/tg* mouse as shown for example experiments (Fig. 2A and B) and the population data ($F_{3,12}$ = 201.1, p <0.0001, n = 4; Fig. 2C). Further, the ML/RC ratio of the response in the in the *tg/tg* mouse (1.45 ± 0.25) is significantly smaller than in the WT mouse (2.90 ± 1.10; t_6 = -2.54, p = 0.04, n = 4; Fig. 2D). Therefore, both the amplitude and ML/RC geometry of the NMDA/Glycine evoked beam response are significantly reduced in the *tg/tg* mouse as found for PF stimulation. These results suggest a fundamental abnormality in the GC-PF-PC circuitry in the *tg/tg* mouse.

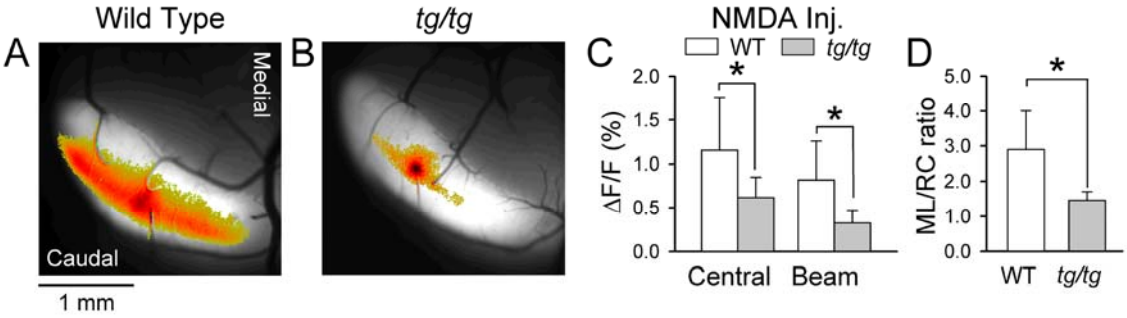

Figure 12. NMDA (NMDA/Glycine) evoked granular layer response is reduced in the *tg/tg* mouse. **A** and **B** Example of the Ca^{2+} fluorescence beam evoked by microinjection of NMDA and glycine into the granular layer of WT and *tg/tg* mice. **C** Summary of the fluorescence with NMDA (NMDA/Glycine) application for the center and beam response components in WT (white) and *tg/tg* (gray) mice (n = 4). **D** Summary ML/RC ratios for WT (gray) and *tg/tg* (white) mice (n = 4).

Peripherally evoked patch response is reduced in the tg/tg mouse cerebellar cortex

The next experiment evaluated whether the response in the cerebellar cortex to a peripheral stimulus is also reduced in the *tg/tg* mice. The response evoked by peripheral stimulation of the vibrissae is well characterized and described as a patch-like activation

of a cluster of PCs in the Crus II folium of the cerebellar cortex (Bower and Woolston, 1983;Santamaria et al., 2002;Gao et al., 2006;Cramer et al., 2013). We hypothesized that impairment of synaptic transmission in the *tg/tg* mouse would result in a reduction in the magnitude of the responses in the cerebellar cortex to peripheral stimulation. As hypothesized, both the example images (Fig. 3A and B) and population data (Fig. 3C) show the responses to C3 vibrissa stimulation are greatly attenuated in the *tg/tg* mouse compared to the WT response (0.15 ± 0.06% for the WT, n = 10 and 0.04 ± 0.05% in the *tg/tg* mouse, n = 5; $F_{1,13} = 446.7$; $p < 0.0001$).

Flavoprotein optical imaging is highly correlated with and sensitive to changes in PC simple spike firing (Cramer et al., 2013;Gao et al., 2006). To verify that the decreased responsiveness in *tg/tg* mice occurs in PCs, extracellular recordings were used to monitor changes in simple spike firing to C3 vibrissa stimulation. We recorded PCs within the optically defined patch region in WT and *tg/tg* mice. In WT mice (n = 5), 59 PCs were recorded within the patch response and of these, 44 (75%) cells exhibited an increase in simple spike firing to the vibrissa stimulus (Fig. 3D). In WT mice the peak increase in simple spike firing occurs at a latency of 9.8 ± 2.4 ms (Fig. 3G), consistent with our previous report of the simple spike latency for PCs recorced within the patch (Cramer et al., 2013). The simple spike discharge of 15 PCs (25%) was not significantly modulated by the sensory input in WT mice (Fig. 3D). In contrast, 75% (82 cells) of PCs recorded in *tg/tg* mice within the patch did not exhibit an increased simple spike discharge while 25% (28 cells) significantly increased their simple spike discharge rate.

Therefore, the percentage of modulated PCs in the patch is significantly different in the *tg/tg* mouse compared to WT ($\chi^2(1) = 35.9$, $p < 0.0001$). The overall reduction in simple spike firing to vibrissa stimulation is evidenced in the population response histograms (Fig. 3E versus F). The reduced flavoprotein fluorescence and PC responses evoked by C3 vibrissa stimulation implies that synaptic transmission is impaired at one or more sites between the periphery and the PCs in the *tg/tg* mouse. Consistent with this assertion, the 25 PCs with significant simple spike responses to C3 stimulation exhibit an increased response latency of 11.8 ± 3.5 ms compared to the 9.8 ± 2.4 ms latency of WT PCs ($F_{1,9} = 8.95$, $p = 0.004$; Fig. 3G). Furthermore, the response duration is reduced ($F_{1,9} = 36.75$, $p < 0.0001$; Fig. 3H) as well as the amplitude of the evoked change in PC simple spike firing ($F_{1,9} = 7.59$, $p = 0.008$, n = 6 for *tg/tg*, n = 5 for WT; Fig. 3I) in the *tg/tg* mouse compared to WT.

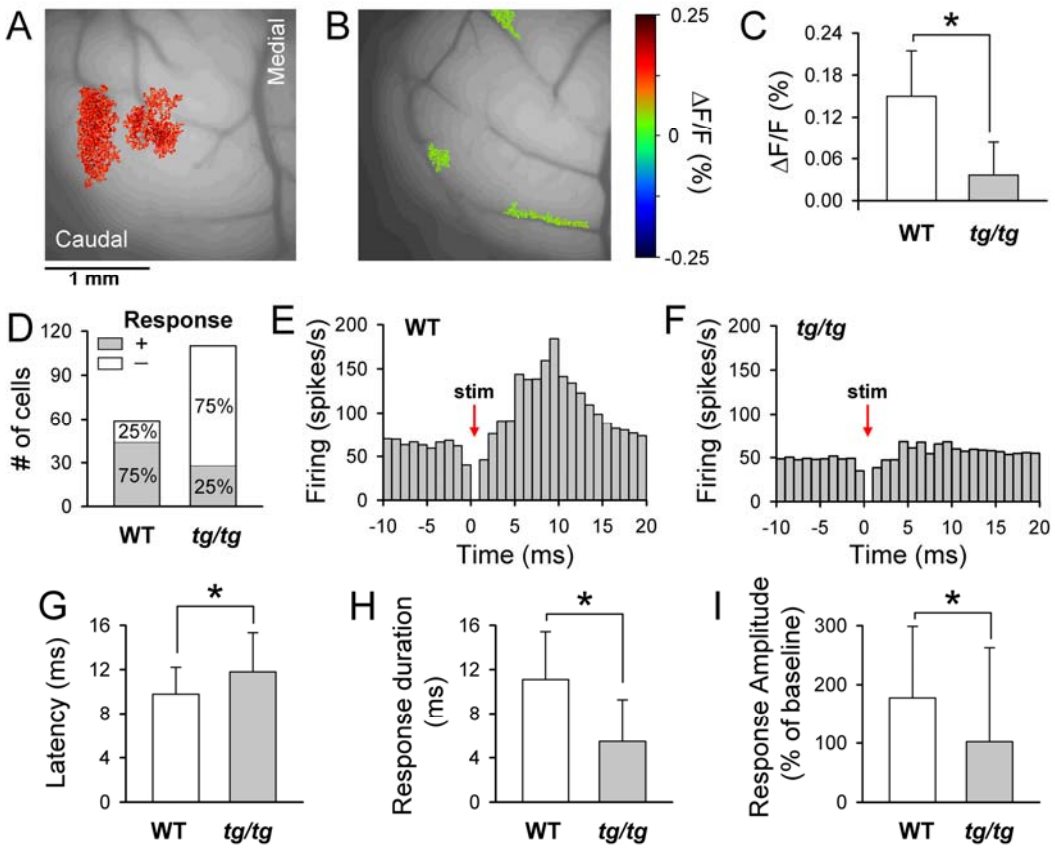

Figure 13. Patch response evoked by peripheral sensory input is reduced in the *tg/tg* mouse cerebellar cortex. **A** Example of the flavoprotein response defined by statistical thresholding evoked by ipsilateral vibrissal pad stimulation in the WT mouse versus the response **B** observed in the *tg/tg* mouse. **C** Summary of patch fluorescence response (ΔF/F %) for the WT (blue) and the *tg/tg* (orange) mouse. Responses are shown as mean ± S.D. (n = 5 WT, n = 10 *tg/tg*). **D** Number of PCs recorded within the patch region that exhibited a significant increase in simple spikes (gray) in response to peripheral stimulation and the number of PCs that did not exhibit a response (white) in WT and *tg/tg* mice. A total of 59 PCs were recorded from 5 WT mice and a total of 110 PCs were recorded in 6 *tg/tg* mice. **E** and **F** PC response duration and firing for the WT and *tg/tg* PCs that exhibited a significant increase in firing to the vibrissa stimulus (+) as well as the aggregate response of all PCs (all) recorded within the patch response region. **G** Summary response latency for the peak response in all PCs the significantly increased simple spike firing in WT (white) and *tg/tg* (gray) mice. **H** and **I** Summary histograms of all of the PCs recorded in WT (**H**) and *tg/tg* (**I**) mice.

Effects of 4-aminopyridine (4-AP) on responses to PF stimulation

A critical finding in support of the hypothesis that irregularity in the simple spike firing plays a causal role in the ataxia of the *tg/tg* mouse is that the 4-AP normalizes the PC discharge (Walter et al., 2006;Alvina and Khodakhah, 2010b). However, 4-AP has multiple actions that alter neuronal excitability including increasing synaptic transmissions (Smith et al., 2000;Molgo et al., 1980;Lundh, 1978), including at the PF-PC synapse (Walter et al., 2006). These multiple actions open the possibility that the 4-AP may also act by rescuing the deficit in PF-PC synaptic transmission. We tested this possibility by applying 4-AP in relation to PF stimulation at 5, 10, and 250 μM concentrations.

Application of 4-AP to the chamber Ringer's produces a marked improvement in both the amplitude and mediolateral extent of the response to PF stimulation at both 10 and 100 Hz (Fig. 4A and B). The amplitude of the response to PF stimulation is increased at both the 10 Hz stimulus frequency ($F_{3,16}$ = 1867.1, p <0.0001, n = 4) and 100 Hz ($F_{3,16}$ = 1616.1, p < 0.0001, n = 4, Fig. 4C). Particularly impressive is the improvement in the ML/RC ratio in which 4-AP results in a beam-like response in the *tg/tg* mouse at both the 10 Hz ($F_{3,17}$ = 100.25, p < 0.0001, n = 9) and 100 Hz ($F_{3,17}$ = 20.17, p < 0.0001, n = 9, Fig. 4D) stimulus frequencies. The increases in the amplitude of the response and ML/RC ratio by 4-AP are almost to WT levels. Further, the 4-AP changes in the response amplitude occur at concentrations as low as 5 μM. Therefore, the

improvement in the ataxia by 4-AP in *tg/tg* mice may be due to restoration PF-PC synaptic transmission (Alvina and Khodakhah, 2010b).

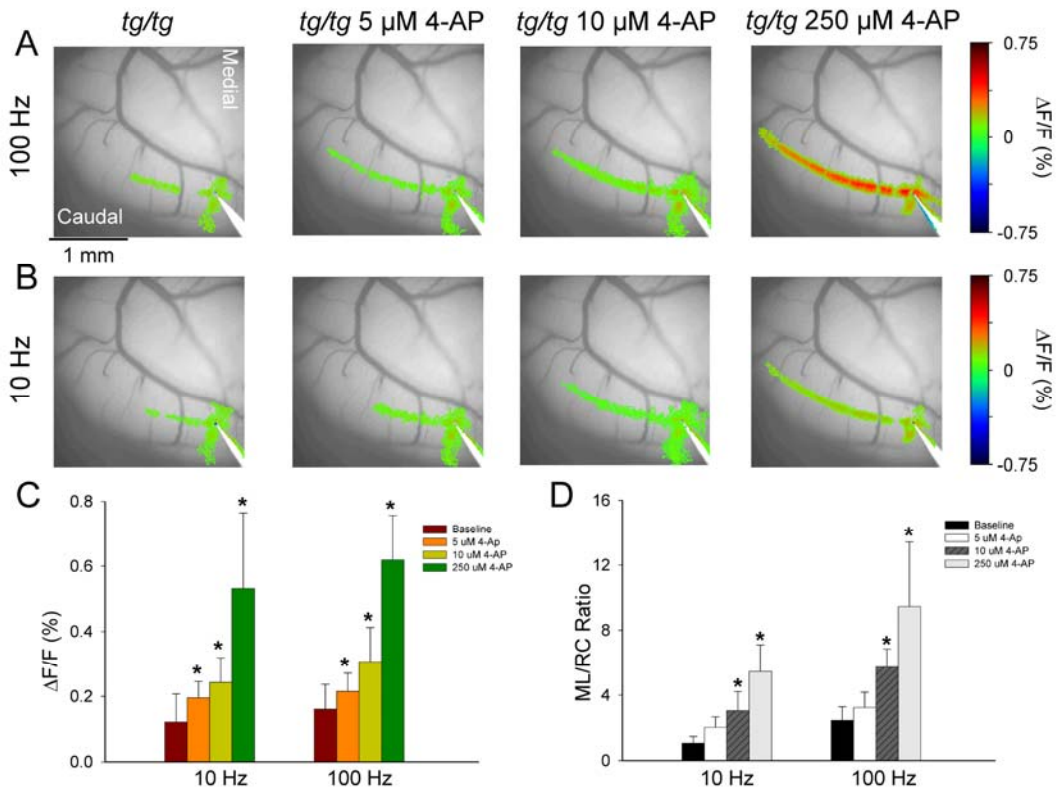

Figure 14. 4-AP rescues the beam response to PF stimulation in the *tg/tg* mouse. **A** and **B** Example flavoprotein fluorescence beam evoked by direct PF stimulation at 100 Hz (**A**) and 10 Hz (**B**) followed by bath application of 5, 10, or 250 µM 4-AP in *tg/tg* mice. **C** and **D** Population summaries of the fluorescence response (**C**) and the ML/RC ratios (**D**) of the beam response in the *tg/tg* mouse (n = 4).

Climbing fiber response is unaltered in the tg/tg mouse cerebellar cortex

Abnormal CF input to PCs is associated with motor impairments including ataxia (Barnes et al., 2011;Chen et al., 2010;Horn et al., 2013). Therefore we examined the responses evoked by electrical stimulation of the contralateral inferior olivary nucleus in the *tg/tg* mouse. The evoked response consisted of parasagittal bands of increased fluorescence in both *tg/tg* and WT mice as shown in the example images (Fig. 5A and B) and consistent with previous optical imaging studies (Barnes et al., 2011;Gao et al., 2003;Rokni et al., 2007). The response to CF stimulation is similar between WT and *tg/tg* mice ($F_{1,10}$ = 3.77, p = 0.055, n = 6; Fig. 5C) consistent with a previous study (Matsushita et al., 2002).

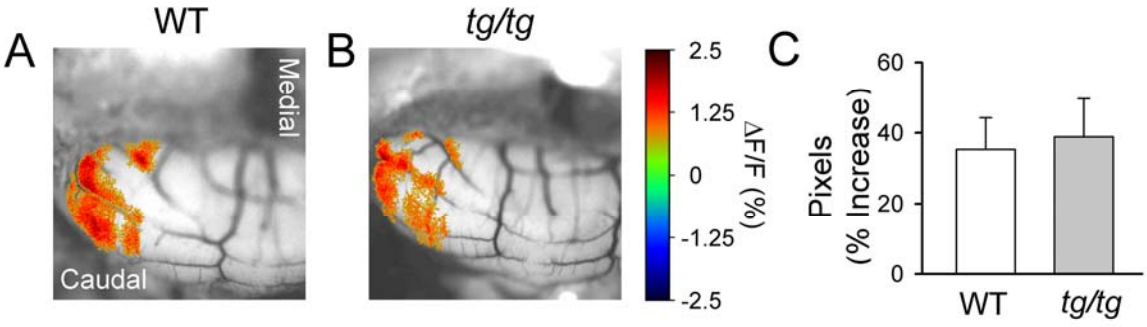

Figure 15. Climbing fiber response is intact in the cerebellar cortex of the *tg/tg* mouse. **A** Example of the flavoprotein response evoked by electrical stimulation (100 μA, 100 μsec pulses at 10 Hz for 1 s) of the contralateral inferior olivary nucleus in the and **B** the *tg/tg* mouse. **C** Summary of the climbing fiber response shown as % change in pixel intensity between baseline and stimulus application in WT and *tg/tg* mice (n = 6).

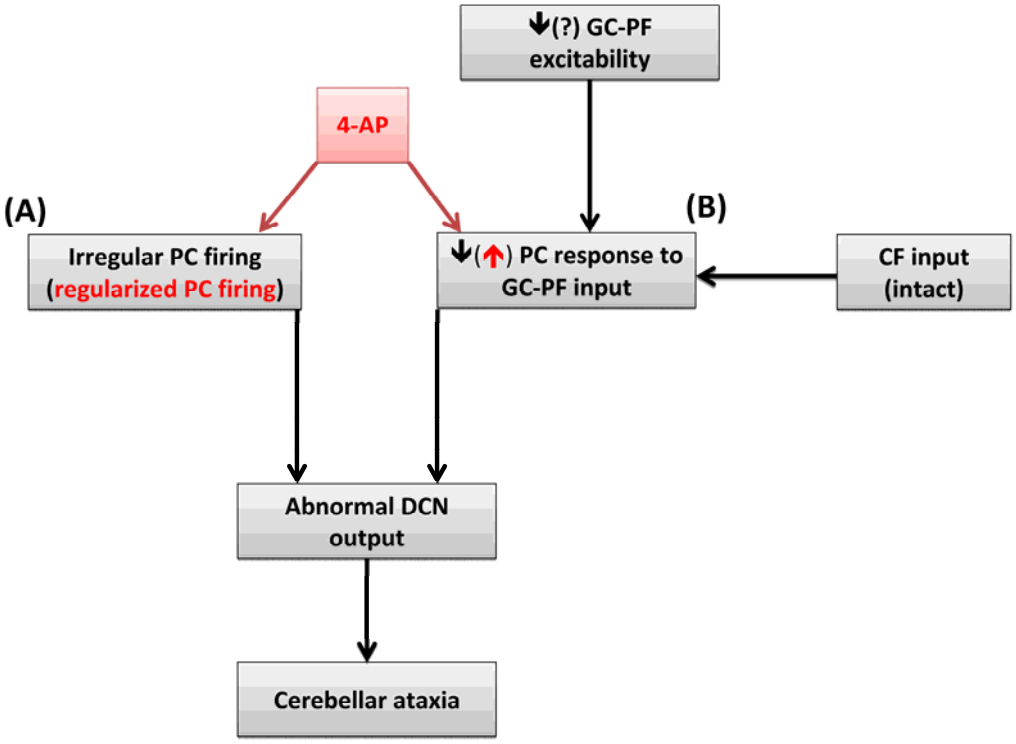

Figure 16. Two mechanisms of cerebellar dysfunction in P/Q channelopathies. **A** proposes that irregular PC firing results in cerebellar dysfunction while **B** proposes that reduced PC responses produces cerebellar dysfunction and ataxia (note that the hypotheses are not mutually exclusive).

Discussion

The major finding in this study is the reduced responses in the cerebellar cortex to inputs mediated by the GC-PF circuitry in the *tg/tg* mouse as assessed by *in vivo* optical imaging and single unit electrophysiology. The responses to electrical stimulation of PFs or pharmacological activation of GCs are reduced. Not only is there a reduction in the amplitude but also in the beam-like geometry of the responses, demonstrating that the GC-PF-PC circuit is highly abnormal in the *tg/tg* mice. Further, the response to whisker stimulation is reduced as demonstrated by both decreased flavoprotein activation and

modulation of simple spike firing. Previous *in vitro* investigations of PC response to PF inputs in the *tg/tg* mouse have been conflicting, with one reporting intact synaptic transmission (Zhou et al., 2003) and another reporting impaired transmission (Matsushita et al., 2002). An *in vivo* examination of the evoked PF response in the *tg/tg* mouse cerebellum reported a reduced response (Chen et al., 2009). The present results provide substantial evidence using multiple approaches that PF-PC synaptic transmission is reduced in the *tg/tg* mouse. Given the fundamental role this circuit is hypothesized to play in the cerebellar cortical function (Braitenberg, 1961;Thach et al., 1992;Ito, 2002;Marr, 1969;Hansel et al., 2001;Albus, 1971), and that GCs provide up to 200,000 inputs to a PC, we hypothesize that the reduced fidelity of GC-PF-PC synaptic transmission contributes to the baseline ataxic phenotype of the *tg/tg* mouse.

Presynaptic or postsynaptic contributions to the reduced PC responses in the tg/tg mouse

The reduced PC response to PF stimulation or GC activation, both the amplitude and mediolateral extent, shows that the excitability of either the PFs or PCs is impaired in the *tg/tg* mouse. Considering the large contribution of P/Q-type Ca^{2+} current in PF synaptic transmission (Mintz et al., 1995), a deficit in PF glutamate release might be expected in the *tg/tg* mouse. However, paired-pulse facilitation, a measure of presynaptic release, does not differ in *tg/tg* and WT mice (Matsushita et al., 2002;Zhou et al., 2003). In the *tg/tg* mouse, the loss of pre-synaptic P/Q-type Ca^{2+} channel function is

compensated for by other voltage-gated Ca^{2+} channels at numerous central synapses and neuromuscular junctions (Plomp et al., 2000), including on PFs and CFs (Matsushita et al., 2002). Based on these previous findings, the impaired response may be primarily due to postsynaptic dysfunction.

If as argued above, glutamate release from PFs is not the main mechanism for the decreased responsiveness, there are several other possibilities. First, PF or GC excitability could be reduced. To our knowledge, neither possibility has been investigated. P/Q-type Ca^{2+} receptors are found throughout cerebellar GCs and are particularly enriched at PF presynaptic varicosities (Kulik et al., 2004). Second, AMPA receptors on PCs could be reduced. In another *CACNA1A* mutant, the *rocker* mouse that exhibits reduced PF-PC transmission in the absence of impaired paired-pulse facilitation, it was found that AMPA receptors on PCs are diminished (Kodama et al., 2006). Again, in the *tg/tg* mouse, whether AMPA receptors on PCs are reduced or have decreased responsiveness has not been studied to our knowledge.

The third possibility is a reduction in PC excitability due to reduced P/Q-type Ca^{2+} currents. This mechanism is highly likely given that P/Q-type Ca^{2+} channels account for 70-80% of voltage-gated P/Q-type Ca^{2+} currents on WT PCs (Mintz et al., 1992;Llinas et al., 1992). Also, compensatory enhancement of L-type Ca^{2+} channel expression occurs in *tg/tg* PCs (Campbell and Hess, 1999). Diminished and/or changes in the voltage-gated Ca^{2+} channels on PCs in *tg/tg* mice could affect the integration of PF

inputs. Alterations in PC dendritic morphology have been described in the *tg/tg* mouse, including ectopic dendritic spines and altered dendritic geometry (Rhyu et al., 1999), which could decrease somatic responses by altering current spread down the dendritic processes (Roth and Hausser, 2001;Vetter et al., 2001). This would not only be in the amplitude of the responses but also spatial information processing. Therefore, reduced P/Q-type Ca^{2+} currents in PCs could explain the reduced mediolateral extent of PF-mediated activation and reduced responses to peripheral inputs.

Impaired synaptic transmission and ataxia

Both the gait ataxia and eye movement abnormalities exhibited by the *tg/tg* mouse have been attributed to increased variability in the simple spike firing of PCs (Walter et al., 2006;Alvina and Khodakhah, 2010b;Alvina and Khodakhah, 2010a;Hoebeek et al., 2005). While the irregularity of PC simple spike firing is established in the *tg/tg* mouse, a causal role between the irregular firing and the abnormal motor behavior is not uniformly accepted (Glasauer et al., 2011;Stahl and Thumser, 2013;Stahl and Thumser, 2014). For example, the therapeutic efficacy of 4-AP in improving eye movement impairments in the *tg/tg* mouse failed to demonstrate benefit (Stahl and Thumser, 2013). Regularization of *tg/tg* mouse PC firing *in vitro* with the voltage-gated K^+-channel blocker, 4-AP, provides critical evidence for the hypothesis that normalization of simple spike discharge accounts for the motor impairment observed with 4-AP administration *in vivo* (Alvina and Khodakhah, 2010b). However, 4-AP has multiple actions that alter neuronal excitability including increasing synaptic transmission (Smith et al.,

2000;Molgo et al., 1980;Lundh, 1978). In WT mice, low concentrations of 4-AP increase PF-PC synaptic transmission, but not the responses to white matter stimulation. In this study, 4-AP rescues both the decreased responses and mediolateral activation to PF stimulation found in the *tg/tg* mouse. Therefore, the therapeutic action of 4-AP is likely to involve improving the response of PCs to PF inputs. While these observations do not rule out the contribution of the regularization of simple spike firing, clearly other mechanisms are important (see Fig. 16).

Alternatively, impaired GC-PF-PC circuitry in the *tg/tg* mouse may contribute to the ataxia (Matsushita et al., 2002;Pietrobon, 2010). An important role for impaired synaptic transmission in this circuit is further supported by a recent study showing granule cell-specific deletion of the P/Q-type Ca^{2+} channels recapitulates the three phenotypic elements of the *tg/tg* mouse, including ataxia (Maejima et al., 2013). Therefore, deficient synaptic transmission at the PF-PC synapse, independent of PC dysfunction, can produce an ataxic phenotype. Reduced synaptic transmission at PF-PC synapses has been described in a number of diseases associated with impaired motor coordination and cerebellar ataxia independent of P/Q-type Ca^{2+} channel alterations, including spinocerebellar ataxia types 5 (Ikeda et al., 2006;Armbrust et al., 2014) and 15 (Matsumoto et al., 1996) as well as dentatorubral-pallidoluysian atrophy (Sato et al., 2009).

The findings of reduced flavoprotein responses and a decrease in the number of modulated PCs to sensory input further supports that synaptic transmission is impaired in the *tg/tg* mouse cerebellar cortex and possibly at synapses outside of the cerebellum. Reduced cerebellar cortical activation to sensory input also demonstrates that a fundamental impairment of information processing occurs in the cerebellum of the *tg/tg* mouse. As discussed above, loss of information processing in the cerebellar cortex can produce abnormal motor control and ataxia. However, if the decrease in cerebellar responsiveness to sensory input is exacerbated by loss of fidelity in synaptic transmission at synapse(s) prior to entering the cerebellar cortex, information would be degraded to an even greater extent than if limited to the cerebellum. Disrupted proprioceptive sensory integration outside of the cerebellum can produce non-cerebellar ataxia (Sghirlanzoni et al., 2005;Spinazzi et al., 2010). Therefore, the ataxia in the *tg/tg* mouse may reflect the accumulation of subtle impairments in synaptic transmission to the cerebellum in addition to poor integration of these inputs in the cerebellar cortex resulting in deficits in motor control.

In conclusion, this first detailed *in vivo* assessment of the cerebellar cortical circuitry in the *tg/tg* mouse demonstrates impaired GC-PF-PC synaptic transmission and reduced cerebellar responses evoked by sensory input. Therefore, the ataxia of the *tg/tg* mouse is likely to involve pathological changes beyond irregular simple spike firing.

CHAPTER IV: ABNORMAL EXCITABILITY AND EPISODIC LOW FREQUENCY OSCILLATIONS IN THE CEREBRAL CORTEX OF THE *TOTTERING* MOUSE

Introduction

The hallmark of episodic channelopathies is that neural circuits transiently enter an abnormal excitability state resulting in paroxysmal neurological dysfunction (for reviews see (Ryan and Ptacek, 2010;Kullmann, 2010)). One family of Ca^{2+} channelopathies is caused by mutations of the *CACNA1A* gene that encodes the α_{1A}, pore-forming subunit of the $Ca_v2.1$ (P/Q-type) voltage gated Ca^{2+} channel (Ophoff et al., 1996;Kramer et al., 1995). Non-CAG expansion mutations of the *CACNA1A* gene include EA2 and familial hemiplegic migraine type 1 (FMH1) (Jen et al., 2004;Jen et al., 2007;Baloh et al., 1997;Rajakulendran et al., 2010). Typically, EA2 involves a decrease and FMH1 an increase of $Ca_v2.1$ function (Wappl et al., 2002;Spacey et al., 2004;Jen et al., 2004;Tottene et al., 2002).

Motor dysfunction is a prominent feature of EA2 with episodes of cerebellar dysfunction that include limb and gait ataxia and oscillopsia (Rajakulendran et al., 2012). Interictally patients may exhibit nystagmus and progressive cerebellar dysfunction linked to cerebellar atrophy (Baloh et al., 1997;Jen et al., 2007;Denier et al., 1999). The most widely studied model of EA2 is the *tg/tg* mouse that has a recessive mutation in the pore-forming region of the P/Q-type Ca^{2+} channel gene, *Cacna1a*, ortholog of the human

CACNA1A gene (Fletcher et al., 1996). Similarly, the *tg/tg* motoric phenotype includes mild ataxia and a dramatic paroxysmal dystonia that are linked to cerebellar dysfunction (Campbell et al., 1999;Neychev et al., 2008;Raike et al., 2013;Walter et al., 2006;Chen et al., 2009;Hoebeek et al., 2005).

However, P/Q-type Ca^{2+} channels are distributed widely throughout the CNS, with high expression levels in the cerebral cortex and hippocampus as well as the cerebellum (Mintz et al., 1992;Fletcher et al., 1996;Westenbroek et al., 1995). Further, P/Q-type Ca^{2+} channels are central to neurotransmitter release (Pietrobon, 2010;Catterall, 1998). Therefore, it is not unexpected that EA2 patients and *tg/tg* mice have non-cerebellar dysfunction. Patients have a high incidence of migraine headaches and the associated transient aura of visual, motor, and somatosensory disturbances (Jen et al., 2004). Other non-cerebellar findings in EA2 include epilepsy, cognitive impairment, abnormal EEG, and elevated cortical excitability (Jen et al., 2001;Jouvenceau et al., 2001;Van and Szliwowski, 1996;Rajakulendran et al., 2012;Baloh, 2012;Helmich et al., 2010). As for the ataxia, many of these clinical features are episodic. The *tg/tg* mouse has absence seizures with rhythmic polyspike EEG bursts (Noebels and Sidman, 1979;Kostopoulos et al., 1987). Cerebral cortical abnormalities in *tg/tg* mice include decreased glutamatergic and GABAergic signaling (Ayata et al., 2000;Tehrani et al., 1997), decreased muscarinic acetylcholine receptor density (Liles et al., 1986) and increased norepinephrine innervation (Levitt and Noebels, 1981).

Previously, we described episodic, LFOs in the cerebellar cortex of *tg/tg* mice that are coupled to the dystonic attacks (Chen et al., 2009). Therefore, we hypothesized that similar oscillations may occur in the cerebral cortex. This study demonstrates episodic LFOs of very high power throughout the cerebral cortex of anesthetized *tg/tg* mice. Representing a highly abnormal excitability state, the LFOs may contribute to non-cerebellar dysfunction in P/Q-type Ca^{2+} channelopathies.

Methods

Animal preparation

All of the animal studies were approved by and conducted in conformity with the Institutional Animal Care and Use Committee of the University of Minnesota. Male and female *tg/tg* mice on a C57BL/6 background as well as male and female C57BL/6 control mice (WT) were used in this study. Homozygous *tg/tg* mice were obtained by crossing a mouse line containing the *tg* allele and the semi-dominant allele *Os,* which causes oligosyndactalism. The first step in identifying *tg/tg* homozygotes was by the absence of oligosyndactalism at birth. Putative *tg/tg* homozygotes were then challenged with caffeine (15 mg/kg, i.p.) or psychological stress (i.e., placement in a novel environment) to verify the expression of episodic dystonia prior to experimentation (Fureman and Hess, 2005).

Detailed descriptions of the anesthetized mouse preparation for optical imaging of the cerebellar cortex have been described in previous publications (Gao et al.,

2006;Reinert et al., 2004). The approach used here is similar except for the exposure and imaging of the cerebral cortex instead of the cerebellar cortex. Therefore, the preparation is only described briefly. Adult mice ages 3-8 months were anesthetized by an initial intramuscular injection of 2.0 mg/kg acepromazine followed by an intraperitoneal injection of 2.0 mg/kg urethane and supplemented with 1.5 mg/kg urethane as needed. Animals were placed in a stereotaxic frame, mechanically ventilated and their body temperature feedback regulated. Depth of anesthesia was monitored via electrocardiogram and testing for responses to somatosensory stimuli. A craniotomy (~7.00 mm x 6.75 mm) was performed to expose the cerebral cortex and the dura removed. A watertight acrylic chamber was constructed around the exposed cortex and filled with Ringer's solution gassed with 95% O_2 and 5% CO_2.

Drug administration

Caffeine and acetazolamide (5-acetamido-1,3,4-thiadiazole-2-sulfonamide) were purchased from Sigma-Aldrich (St. Louis, MO). DNQX (6,7-dinitroquinoxaline-2,3-dione), APV (D-(-)-2-amino-5-phosphonopentanoic acid), L-NAME (NG-nitro-L-arginine methyl ester hydrochloride), indomethacin (1-(4-chlorobenzoyl)-5-methoxy-2-methyl-1*H*-indole), tetrodotoxin (octahydro-12-(hydroxymethyl)-2-imino-5,9:7,10a-dimethano-10a*H*-[1,3]dioxocino[6,5-*d*]pyrimidine-4,7,10,11,12-pentol), GABAzine (6-imino-3-(4-methoxyphenyl)-1(6*H*)-pyridazinebutanoic acid hydrobromide), MPEP (2-methyl-6-(phenylethynyl)pyridine hydrochloride), LY 367385 ((*S*)-(+)-α-amino-4-carboxy-2-methylbenzeneacetic acid), ω-Agatoxin (ω-Agatoxin TK), and 4-AP (4-

aminopyridine) were purchased from Tocris Bioscience (Bristol, UK). All drugs, except caffeine, were dissolved in normal Ringer's solution and applied to the surface of the exposed cerebral cortex by replacing the solution in the optical chamber. Caffeine was dissolved in normal saline and administered intraperitoneally.

Optical imaging and neural activity acquisition and analysis

The anesthetized animal in the stereotaxic frame was placed on an x-y stage mounted under a high-speed, cooled CCD macroscope (Nikon AZ-100) with a 1X (Fig. 10) or 2X (all other figures) objective with a 512 X 512 CCD chip at 16 bit digitization. Binning on the CCD chip was done to achieve a pixel resolution of ~35 X 35 μm (1X) or ~28 X 28 μm (2X).

A series of flavoprotein images (i.e., an imaging period) consisting of 625 frames (200 ms) each were acquired for all experiments except for those shown in Figure 10 which consisted of a series of 1500 ms frames. Difference images were then generated by subtracting the average of nine control frames (control average) from each control and experimental frame. These difference images were then divided by the control average, yielding images in which the intensity of each pixel reflects the change in fluorescence ($\Delta F/F$) relative to the control period (Reinert et al., 2004;Gao et al., 2006). Images of the $\Delta F/F$ were used to illustrate the spontaneous oscillations in the *tg/tg* versus WT mice (see Fig. 1). Time points in the image series were selected and at each time point 10 frames (5 frames before and 5 frames after the time point) were averaged. Resultant images were

scaled to ± 5 % ΔF/F for pseudocolor display using Metamorph (Molecular Devices, Sunnyvale, CA).

The spectral content of the optical data was obtained as described previously (Chen et al., 2009) and therefore, is described only briefly. Images were low-pass filtered using a 13 X 13-pixel mean filter, then the optical signal for each pixel linearly detrended, and transformed into the frequency domain using a 2,048-point fast Fourier transform (FFT) algorithm. The power spectrum was computed using a 50% Hanning window with 25% overlap. The spectral content and power were analyzed in visually defined regions of interest (ROIs) over the left and right cerebral hemispheres. The ROIs were chosen to exclude non-cortical structures within the imaged field (i.e., the superior sagittal sinus, cranium, and acrylic chamber). This procedure was applied to each image acquisition period. As described in the Results, the average power spectrum from WT and *tg/tg* mice differed markedly between 0.035-0.11 Hz (see Fig. 2A) which was defined as the frequency band of interest. Subsequent analyses of the optical signals focused on this frequency band. Also as described in the Results, *tg/tg* mice exhibited very high power at these LFOs and values greater than 3 standard deviations above the mean WT power were defined as a high power state. In the population summaries of experimental conditions and genotype, the power within the ROIs with the frequency band of interest were averaged across multiple imaging periods.

Based on the spectral analysis, maps of the frequency, power, and phase shifts were generated for the ROIs as described previously (Chen et al., 2009). Within the frequency band of interest and for pixels with power above the high power state threshold, frequency maps represent the dominant frequencies at each pixel and the power maps illustrate the power of the oscillations at the dominant frequencies. The phase shift map indicates the degree to which oscillations are in or out of phase across the exposed cortex.

In some experiments flavoprotein optical imaging was acquired simultaneously with extracellular single-unit neural activity. Single-unit extracellular recordings of cerebral cortical neurons used glass-coated, platinum iridium microelectrodes (1–2 MΩ; Alpha Omega, Nazareth, Israel) and conventional electrophysiological techniques (Chen et al., 2009;Cramer et al., 2013;Haider et al., 2006). Recordings were conducted throughout the extent of the cerebral cortical layers. The single cell recordings were digitized at 32 kHz and stored online. Spikes were sorted offline using Spike2 (Cambridge Electronic Design, Cambridge, UK) and periods of spontaneous activity corresponding to temporal windows of image acquisition were exported for analysis in Matlab (The MathWorks, Natick, MA). The spike trains were converted into instantaneous firing rate with 200 ms binning using fractional intervals, a method used to determine the instantaneous firing rate in equal bins based on the inverse of the interspike intervals (Popa et al., 2012;Chen et al., 2009). The mean firing rate for each spike train period was subtracted from the instantaneous firing rate. The spectral content was

obtained using a 2,048-point FFT algorithm (Chen et al., 2009). The spectral content of the spontaneous flavoprotein response was determined within a 540 X 540 μm ROI visually aligned over the location of the single-unit recording (see examples in Fig. 5). The spectral content of the simultaneously acquired optical and single-unit activity between 0.035-0.11 Hz was then detrended and the correlation coefficient (r) between these power spectra computed using Matlab. For the examples comparing the power between single-unit firing and the optical activity, the power was normalized due to the widely different nature of the two signals.

Optical imaging of responses to direct cortical and whisker stimulation

In experiments examining cerebral cortical responses, direct cortical stimulation was delivered via a paralyene-coated tungsten microelectrode (2-5 MΩ, Frederick Haer, Bowdoin, ME) positioned ~ 1 mm lateral and ~1 mm rostral to bregma and lowered to a depth of ~265 μm below the cortical surface. Stimulation parameters consisted of 5 pulses of 200 μA, 100 μs at 5 Hz. Peripheral whisker stimulation was applied using a pico-injection system (PLI-100; Medical Systems) to deliver a series of air-puffs to the left C2 whisker. The whiskers on the left whisker pad were trimmed short except for whisker C2. The air-puff stimulus consisted of 5 pulses of 9 PSI, 120 ms at 5 Hz applied to the C2 whisker, 1 cm from its base (Devonshire et al., 2010). For both the intracortical and whisker stimulation, the experimental design was to avoid the LFO frequencies. After a 100 s baseline period of images were acquired, direct cortical or air-puff stimulation was delivered continuously, at random intervals between 6-8 s in duration.

The stimulus program was written in Spike2. During the 200 s imaging interval following the baseline period, 25-33 stimuli were delivered. The average (mean ± SD) number of stimuli applied per imaging period was 29 ± 1 for *tg/tg* mice and 28 ± 1 for WT. This inter-stimulus-interval corresponds to a frequency of 0.125-0.167 Hz, outside of the frequency band of the LFOs.

Analysis of the flavoprotein response to direct cortical or whisker stimulation consisted of determining the spectral content within a 700 μm X 700 μm ROI visually aligned over the cortical response region. For the response evoked by air-puff whisker stimulation, a single ROI was defined over the contralateral somatosensory cortex. For direct cortical stimulation, ROIs were defined over both the ipsilateral and contralateral response regions. The average power between 0.125-0.167 Hz (the range of the stimulus frequencies) was then computed for the ROI(s) per image acquisition period, similar to a previous report (Llano et al., 2009).

Western blotting

WT and *tg/tg* cerebral cortices were dissected and then homogenized in brain extraction buffer: 0.25 M Tris-HCl pH 7.5 with protease inhibitors (1183617001, Roche, Basal Switzerland). Protein concentration was determined with the Bradford method (Bradford regent and technique, Sigma-Aldrich) and 30 μg neuronal nitric oxide synthase (nNOS) or 60 μg endothelial nitric oxide synthase (eNOS) of total protein were denatured and run on a 4-15% gradient gel (BioRad, Hercules, CA) and blotted on mid-sized

nitrocellulose membrane. Membranes were blocked for ~ 1 hour with 5% blocking buffer (5% w/v milk in 1X PBS) with 0.1% v/v Tween-20. Membranes were incubated with nNOS (ab1376, AbCam Inc., Cambridge, UK) or eNOS (NBP1-19824, Novus Biologicals, Littleton, CO) antibody overnight at 4° C, washed three times with 1X PBS with 0.1% Tween-20 and incubated with anti-goat (nNOS) or anti-rabbit (eNOS) horse radish peroxidase secondary antibody for 2 hours. Samples were also probed with mouse anti-α-tubulin (T5168, Sigma-Aldrich) as loading control. Images of the membranes were acquired with ImageQuant (General Electric, Fairfield, CT) and protein levels quantified using ImageQuant densitometric analysis software.

Statistical analysis

The statistical analysis was performed using SAS (SAS Institute, Cary, NC). The effects of various drugs and evoked cortical responses were statistically evaluated with ANOVA (within-subject design with repeated measures). Statistical evaluation of protein expression levels between WT and *tg/tg* mice was performed using a Student's *t* test. In the text and figures all values are reported as mean ± SD. When describing the results of an experiment, "n" refers to the number of animals used.

Results

Transient, low frequency oscillations in the cerebral cortex of tg/tg mice

In the initial experiments autofluorescence optical imaging was used to examine the spontaneous activity in the cerebral cortex of the anesthetized *tg/tg* mouse *in vivo*.

During the course of these experiments, oscillations in the flavoprotein fluorescence developed spontaneously throughout the exposed cerebral cortex. As shown for an example experiment, the oscillations in the *tg/tg* mouse consist of large amplitude fluorescence changes (ΔF/F) across most of the cerebral cortex (Fig. 1A and B). The time courses of the ΔF/F (Fig. 1B) based on four ROIs in the frontal and parietal cortices bilaterally (colored circles in Fig. 1A) reveal a periodicity of ~16 s frequency (~ 0.0625 Hz), similar to the LFOs observed in the cerebellar cortex of the *tg/tg* mouse (Chen et al., 2009). The large amplitude of the changes in flavoprotein fluorescence (± 5 ΔF/F) are consistent with extensive shifts in cortical neuronal activity (Reinert et al., 2004;Reinert et al., 2011;Cramer et al., 2013). In contrast, WT mice do not exhibit the large amplitude LFOs observed in *tg/tg* mice. As shown for a control animal (Fig. 1C and D), the spontaneous activity across the cerebral cortex consists of much smaller amplitude fluctuations (± 0.7 % ΔF/F) at higher frequencies (~0.2-0.4 Hz).

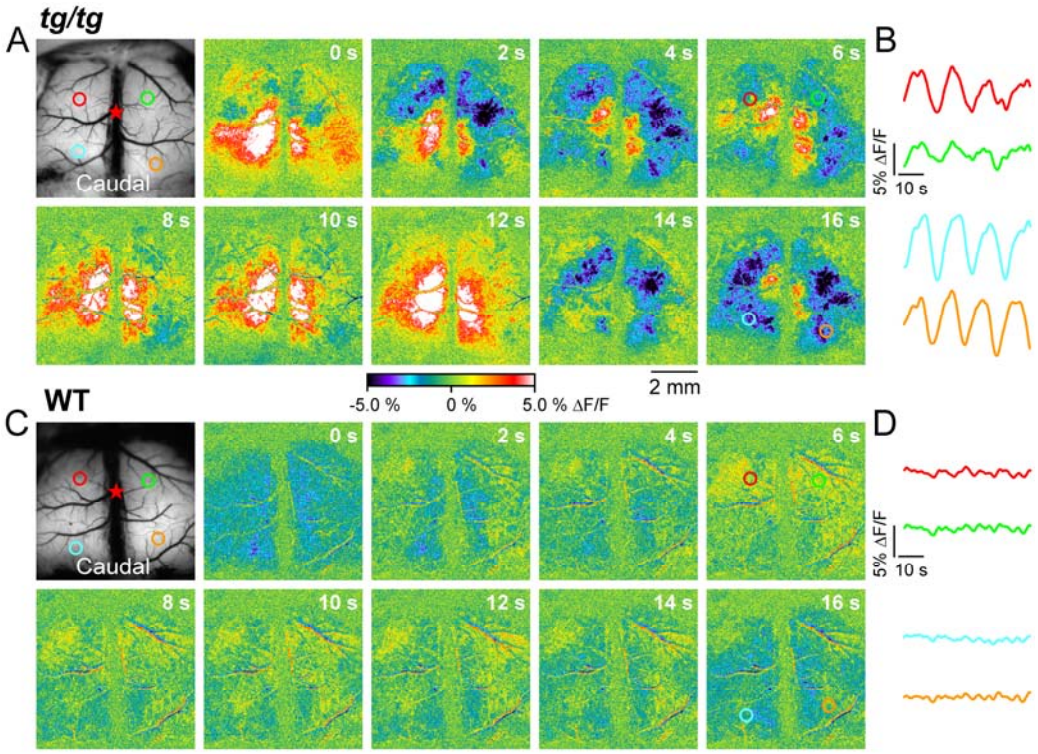

Figure 17. Spontaneous low frequency oscillations (LFOs) in the cerebral cortex of the *tg/tg* mouse. **A** Background fluorescence image of the cerebral cortex with color coded ROIs used to quantify the fluorescence change over time. The red star indicates the location of bregma in this and all subsequent figures. The pseudocolored images show the spontaneous change in flavoprotein fluorescence (ΔF/F) in the cerebral cortex of a *tg/tg* mouse at 2 s intervals over a 16 s period. Note the large cyclical fluctuations at this periodicity throughout the exposed cortex. **B** Traces of the ΔF/F over time for the ROIs depicted in the background image in **A** demonstrate large amplitude, LFOs in both hemispheres. **C** Background image followed by pseudocolored images of the spontaneous change in flavoprotein activity in a WT mouse. **D** Traces of the ΔF/F over time for the ROIs depicted in the background image in **C** show only small amplitude fluctuations at higher frequencies.

Because the LFOs in the *tg/tg* mouse are spontaneous and transient, the first step was to quantitatively define this abnormal state based on the frequencies and magnitude of the oscillations. A two step spectral analysis of the autofluorescence signal was performed, similar to the approach used to quantify LFOs in the cerebellar cortex (Chen

et al., 2009). In the first step, power as a function of frequency was determined for 947 imaging periods (each imaging period consisted of 125 s of consecutive images) of spontaneous activity in 34 *tg/tg* mice and in 308 sessions in 20 WT animals. Because the goal was to statistically define the occurrence of the episodic, large amplitude LFOs observed in *tg/tg* mice (Fig. 1A and B), the analysis is based on the activity in both hemispheres. Comparison of the average power versus frequency plots across all periods and animals establishes that strong oscillations occur in a frequency band between 0.035-0.11 Hz in the *tg/tg* mouse but not in the WT mouse (Fig. 2A). Therefore, we selected this range as the frequency band of interest.

In the second step, the occurrence rate of power in this frequency band was determined across all imaging periods. The power levels in *tg/tg* mice span three orders of magnitude, with a long tail extending into very high power levels (Fig. 2B, white bars). Therefore, we used a $\log_{10}$ scale for the x-axis (Fig. 2B). Imaging periods with these higher power values correspond to the LFOs shown for the example *tg/tg* mouse in Fig. 1A and B in which the average power between 0.035-0.11 Hz was 541 ± 754. In contrast, the power distribution in WT animals is confined to much lower values (Fig. 2B, gray bars) as shown for the example WT mouse in Fig. 2C and D in which the average LFO power was 24 ± 17. Therefore, the distributions show the existence of two states, low and high power. We defined the high power state as when the average power between 0.035-0.11 Hz exceeded the average power in the WT animal (16.3 ± 17.8) by three standard deviations (> 69.7). This threshold corresponds to a p-value < 0.003. The

high power state occurred spontaneously in 21 of 34 *tg/tg* mice and in 311 of 947 (32.8%) imaging periods. Conversely, using this threshold, there was only a single instance of a high power state in 1 of 20 WT animals out of 308 (0.003%) imaging periods. Based on this analysis, the power versus frequency plots show the marked differences in power between the high and low power state in *tg/tg* mice as well as between the high power state in *tg/tg* mice versus average power in WT mice (Fig. 2C).

Using the low frequency band of interest and the definition of a high power state, spectral analysis was used to generate maps of the frequency, power and phase superimposed onto a background image of the cerebral cortex. In these maps only pixels with power values greater than the threshold for a high power state are shown. For a *tg/tg* mouse in the high power state, maps of the spontaneous LFOs in the cerebral cortex (Fig. 3, top) show that the oscillation frequencies can be markedly uniform across the cortex; however, power typically varies greatly in different regions (see also Figs. 4, 9 and 11). For the *tg/tg* mouse in Fig. 3, a region of very high power is centered in the right hemisphere, ~1mm caudal to bregma and ~1mm lateral to the midline. The phase map shows regions with LFOs in phase both within and between the hemispheres. The phase map also illustrates the complex temporal relationships in the oscillations over the cerebral cortex. Conversely, in the example WT mouse (Fig. 3, bottom), there are only small regions within the occipital cortex that exceed threshold for the high power state. Note that because our definition of high power state is based on the average power across the cerebral cortex, it does not imply that individual pixels or regions do not exceed the

threshold in WT animals. The spectral maps illustrate the spatial extent and dynamic nature of the LFOs in the *tg/tg* mouse during the high power state.

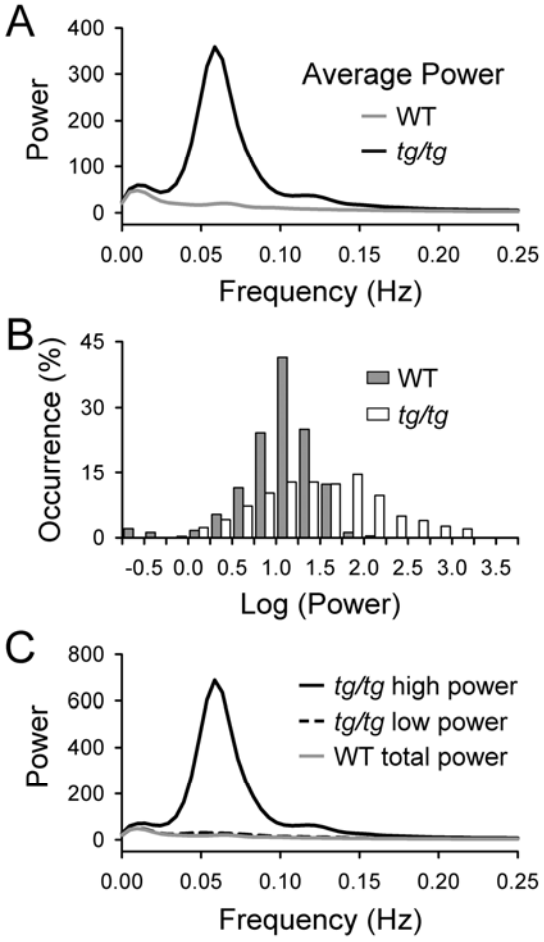

Figure 18. Transient, high power LFOs in the *tg/tg* mouse cerebral cortex. **A** Power versus frequency plot demonstrates the average power in the cerebral cortex of *tg/tg* (black) and WT mice (gray) obtained from 947 imaging periods in *tg/tg* mice (n = 34) and 308 imaging periods in WT mice (n = 20). Spectral analysis demonstrates that the greatest power in the *tg/tg* mouse cerebral cortex is within a frequency band of 0.035-0.11 Hz. Therefore, we focused on this frequency range for the remaining analysis. **B** Occurrence rate (as a percentage of total number of imaging periods) is plotted versus the $\log_{10}$ of the average power histogram of 947 imaging periods in the *tg/tg* mouse (white bars) and 308 imaging periods in the WT mouse (gray bars). An imaging period was defined as high power if the average power was > 69.7, a level corresponding to the mean power exhibited by WT mice (gray trace, 16.3 ± 17.8) plus three standard deviations. **C** Power versus frequency plots of the high power state (black trace) and low power state (black dashes) averaged across all imaging periods from *tg/tg* mice. Average power versus frequency pots across all imaging periods from WT mice (gray trace).

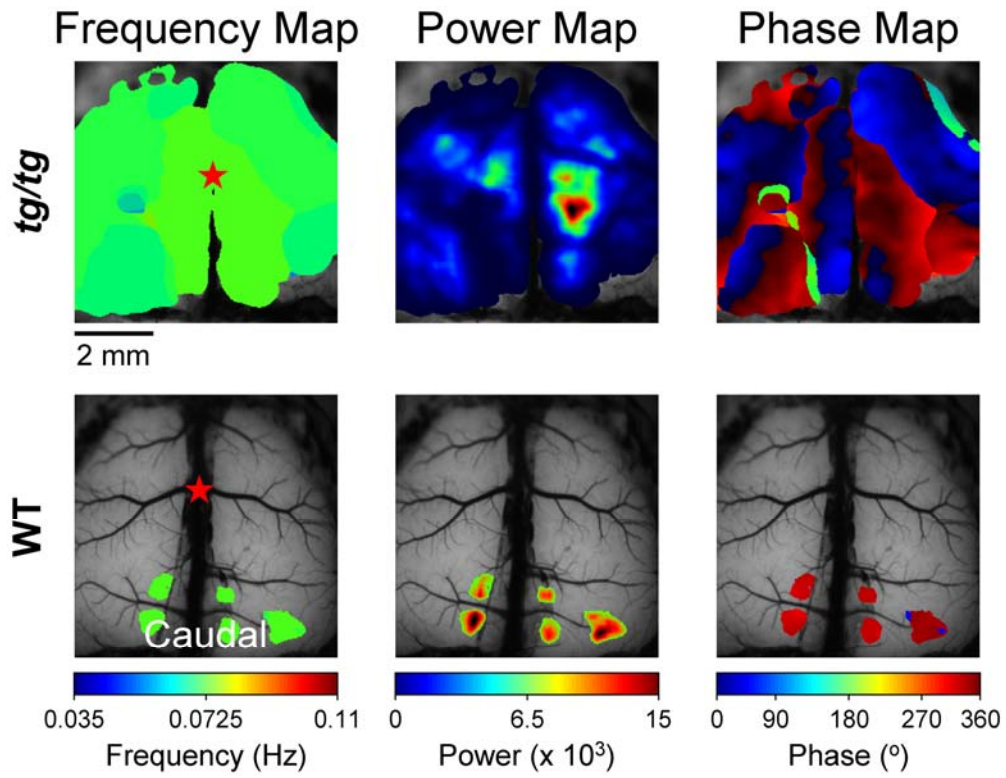

Figure 19. Frequency, power and phase maps of the spontaneous activity in the cerebral cortex of *tg/tg* and WT mice. Spectral analysis demonstrates the frequency (left), power (middle) and phase (right) maps for an example *tg/tg* mouse (top) and the WT mouse (bottom) superimposed on background fluorescence images of the cerebral cortex.

Neural contribution to low frequency oscillations in the cerebral cortex

The spontaneous occurrence of the high power LFOs suggests the cerebral cortical network is not stable in the *tg/tg* mouse and can enter an abnormal excitability state. A primary question is the neuronal contribution to this oscillatory activity. To evaluate the role of neuronal activity in the LFOs, 10 μM of tetrodotoxin (TTX) was bath applied to block voltage gated Na^+ channels and suppress action potentials (Kao, 1966). In the *tg/tg* mice, the TTX was applied only after a minimum of 6 contiguous imaging periods confirmed the presence of the high power state in the cerebral cortex because we were specifically interested in the neural contribution to the high power LFOs. As shown

in the example experiment (Fig. 4), TTX suppresses the high power LFOs throughout much of the *tg/tg* cerebral cortex with only discrete, smaller regions still exhibiting high power oscillations. For the population, TTX significantly decreases the power in the LFOs by 40% ($F_{1,8} = 58.8$, $p < 0.0001$; n = 5, Fig. 6E). This finding confirms a large neural contribution to the LFOs. The application of TTX in WT mice reduces the power ~75% ($F_{1,6} = 174.9$; $p < 0.0001$, n = 4; Fig. 4D) and demonstrates, as expected, that TTX greatly reduces excitability. However, TTX did not completely block the high power state in *tg/tg* mice. This observation suggests that once established, the high power LFOs are not solely dependent on action potential generation or intracortical connections.

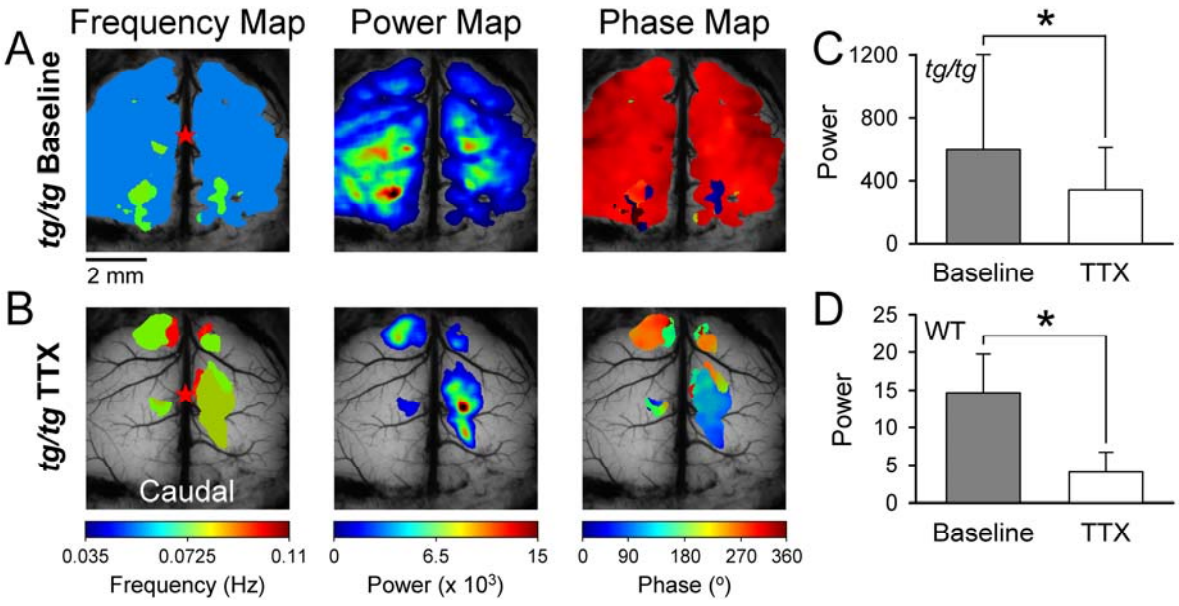

Figure 20. TTX suppresses but does not block high power LFOs in the *tg/tg* mouse. **A** Example frequency, power, and phase maps of spontaneous, high power cerebral cortical activity in the *tg/tg* mouse. **B** Frequency, power, and phase maps of the same mouse after bath application of 10 μM TTX. **C** Summary of the average baseline power in *tg/tg* mice (gray; for all figures, bars show mean ± SD and * denotes significant difference at $p<0.05$) and the resulting power in the presence of TTX (white, n = 5). **D** Summary of the average baseline power (gray) in WT mice and upon TTX application (white, n = 4).

In the next experiment we characterized the relationship between the LFOs and cerebral cortical neural activity in the *tg/tg* mouse. Extracellular single-unit recordings of the spontaneous discharge of neurons in the cerebral cortex were obtained simultaneously with flavoprotein imaging. For the single-unit data, we recorded all neurons encountered on tracts beginning at the cortical surface to 860 μm, a depth corresponding to cortical layer VI in the mouse (DeFelipe et al., 2002). In 5 *tg/tg* mice, 278 imaging periods (125 s duration) were acquired with recordings of 131 cerebral cortical neurons. A spectral analysis was performed on the simultaneously obtained optical and neuronal firing data for each imaging period. The analysis was restricted to a ~290 μm^2 ROI aligned over the recording electrode (see example ROIs in Fig. 5). As shown for several example cell recordings, the neuronal firing contains frequencies within the 0.035-0.11 Hz band of interest and the normalized power spectrum closely mirrors the spectral content in the flavoprotein signal in the same region (Fig. 5C and D). The firing of other cortical neurons had less power at these low frequencies or did not match the power in the optical signal (Fig. 5B and E). To quantify the neural-optical relationship, the correlation was computed between the power spectrum of the optical and neural data within the 0.035-0.11 Hz band of interest. The correlation coefficients (r-values) range from -0.82-0.99. However, for the vast majority of neurons the r-values are positive. Of the 278 recording periods, 148 (53%) exhibited $r > 0.7$ and the overall mean r-value was 0.54 ± 0.47 (critical value for significance ($p \leq 0.05$) is $r_{15} \geq \pm 0.48$). Therefore, the firing of the majority of cortical neurons in *tg/tg* mice oscillate at the same low frequencies observed

in the optical recordings. The results from application of TTX and the single-unit recordings show neuronal activity contributes to the LFOs.

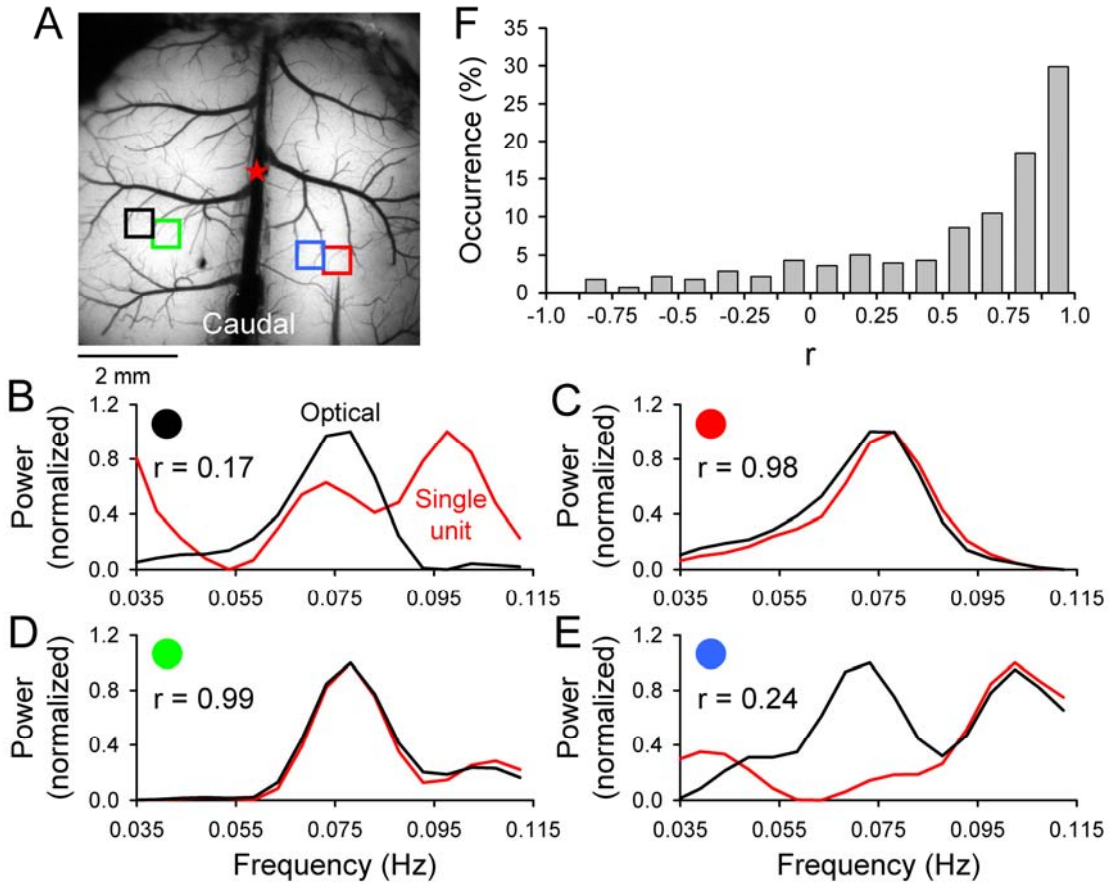

Figure 21. Power comparison between simultaneously acquired flavoprotein fluorescence and single-unit extracellular recordings in the *tg/tg* mouse. **A** Background image of the cerebral cortex with colored ROIs used to compute the power in the optical signal (see Methods) shown in the example traces in **B-E**. **B-E** Four examples of the normalized power for the optical (black) and the single-unit firing (red) and the computed r-value. **F** Histogram of occurrence rate versus r-values for the comparison of the optical and single-unit power for each of the 278 imaging periods (125 s duration) acquired with single-unit recordings of 131 cerebral cortical neurons in 5 *tg/tg* mice.

Contribution of P/Q-type Ca^{2+} channels and synaptic transmission to the LFOs

The next question addressed whether a decrease in P/Q-type Ca^{2+} channel function underlies the high power LFOs observed in the *tg/tg* mouse. Therefore, we tested whether acute reduction in P/Q-type Ca^{2+} current in the WT mouse with 1.5 μM of the specific P/Q-type Ca^{2+} channel blocker, ω-Agatoxin (Teramoto et al., 1993), would recapitulate the LFOs observed in the *tg/tg* mouse. Based on previous reports of the *in vivo* efficacy of 100 nM ω-Agatoxin (Hoebeek et al., 2005), 1.5 μM likely blocks the majority of cortical P/Q channels. In WT animals, ω-Agatoxin produced a significant increase in the power of LFOs from 17.2 ± 13.3 to 33.1 ± 32.3 ($F_{1,6}$ = 18.4, p < 0.0001, n = 4, Fig. 6C). As shown in example spectral maps (Fig. 6A), there are regions within the cerebral cortex with increased power in the frequency band of interest. However, the power levels did not enter the high power state and remained well within the power levels observed in WT mice. A complimentary question is whether a further reduction in P/Q-type Ca^{2+} channel function in the *tg/tg* mouse results in the transition to a high power state. Because we were specifically interested in the transition from low to a high power state in this experiment, the ω-Agatoxin was applied only after a minimum of 6 contiguous imaging periods confirmed the presence of a low power state. Both the example experiment (Fig. 6B) and the population results (Fig. 6D) show that ω-Agatoxin does not result in high power LFOs in the *tg/tg* mouse. The power of the LFOs (60.7 ± 49.6) in the presence of ω-Agatoxin was not significantly different ($F_{1,6}$ = 0.01, p = 0.92, n = 4; Fig. 6D) and nearly identical to baseline power (60.2 ± 46.1). Taken together, these two experiments suggest that a reduction in the P/Q-type Ca^{2+} current favors the

development of network instabilities in the cerebral cortex as evidenced by the spontaneous high power state in the *tg/tg* mouse and by the increased LFO power in WT mice in the presence of ω-Agatoxin. However, as ω-Agatoxin did not produce a high power state in WT or *tg/tg* mice, the mechanisms underlying LFOs must involve changes in the cerebral cortical circuitry beyond an acute reduction in P/Q-type Ca^{2+} channel function.

The next series of experiments assessed if the instability in the *tg/tg* cerebral cortex is unmasked by altering the balance of excitation or inhibition. As noted in the Introduction, abnormalities in both glutamate and GABA neurotransmission are present in the *tg/tg* mouse cerebral cortex (Ayata et al., 2000;Tehrani and Barnes, Jr., 1995;Tehrani et al., 1997). Given that the majority of fast excitatory inputs, either *via* thalamocortical or corticocortical projections, are mediated by post-synaptic ionotropic glutamate receptors (AMPA and NMDA) (Sherman and Guillery, 2011), we bath applied 100 μM DNQX and 200 μM APV to block fast glutamatergic neurotransmission. As for the experiments blocking P/Q-type Ca^{2+} channels, we applied the antagonists in the low power state. In WT mice, DNQX and APV result in a significant reduction in the low frequency power (example maps, Fig. 7B), decreasing baseline power from 22.0 ± 23.0 to 13.0 ± 20.3 ($F_{1,6}$ = 10.2, p = 0.0023, n = 4; Fig. 8A). As expected, in the WT cerebral cortex, blocking ionotropic glutamate receptors decreases spontaneous cortical activity.

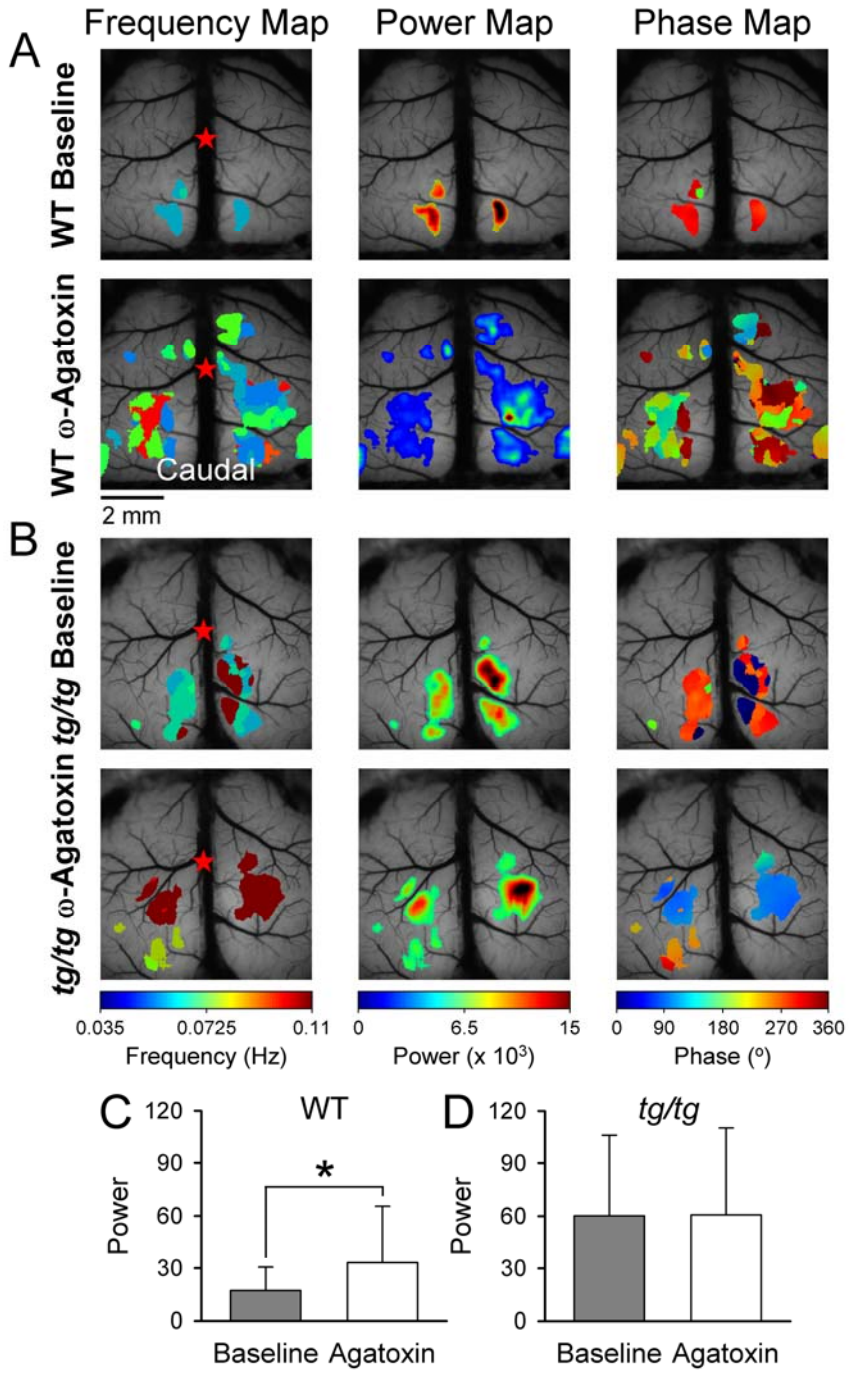

Figure 22. ω-Agatoxin blockade of P/Q-type Ca^{2+} channels increases LFO power in WT but not in *tg/tg* mice. **A** Example maps from a baseline imaging period (top row) in a WT mouse show small regions of high power that expand upon application of 1.5 µM ω-Agatoxin. **B** Example maps for the same experiment in a *tg/tg* mouse. ω-Agatoxin application does not alter the power of the spontaneous activity in the *tg/tg* mouse cerebral cortex. **C** and **D** summarize the average power in the baseline period (gray) and upon application of ω-Agatoxin (white) in the WT (**C**, n = 4) and *tg/tg* mouse (**D**, n = 4).

In contrast and unexpectedly, DNQX/APV in the *tg/tg* mouse produces a significant increase in power from 11.2 ± 13.8 to 61.2 ± 117.0 ($F_{1,18}$ = 177.4, p < 0.0001, n = 10; Fig. 7A and 8B) and resulted in a high power state in 3 of 10 *tg/tg* mice. However, on average, blocking ionotropic glutamate receptors does not produce the high power state observed spontaneously in *tg/tg* mice and nor did DNQX/APV application result in the extremely high power values observed spontaneously in *tg/tg* mice (Fig. 2). These findings suggest that reduced post-synaptic, ionotropic glutamatergic activation contributes to the LFOs and increases the likelihood of a high power state.

In the cerebral cortex, excitatory glutamatergic synaptic transmission also involves metabotropic receptors, mainly type 1 and 5 (Ferraguti and Shigemoto, 2006;Alexander and Godwin, 2006). Furthermore, given the slower time of action of these receptors on post-synaptic neurons, one could hypothesize a role in the LFOs. Therefore, we also tested the effect of blocking metabotropic glutamate receptors by applying MPEP (30 μM), a metabotropic glutamate receptor type 5 antagonist, and LY36738 (50 μM), a metabotropic glutamate receptor type 1 antagonist into the optical chamber. This cocktail of MPEP and LY367385 reliably blocks metabotropic glutamate receptor activity in the cerebral cortex of mice (De and Sherman, 2012). The application of MPEP and LY367385 significantly increases power in the LFOs in *tg/tg* mice (39.4 ± 22.6 to 115.2 ± 98.7, $F_{1,6}$ = 52.5, p < 0.0001, n = 4; Fig. 8D), therefore, on average reaching a high power state. Furthermore, MPEP and LY367385 resulted in the high power state in 3 of 4 *tg/tg* mice. In contrast, inhibition of metabotropic glutamate

receptors in WT mice significantly reduces the power of spontaneous cerebral cortical activity from 21.0 ± 13.5 to 15.3 ± 8.5 ($F_{1,6}$ = 12.7, p = 0.0008, n = 4; Fig. 8C). Similar to blocking ionotropic glutamate receptors, though more effective, reducing metabotropic receptor activation increases the likelihood of entering a high power state.

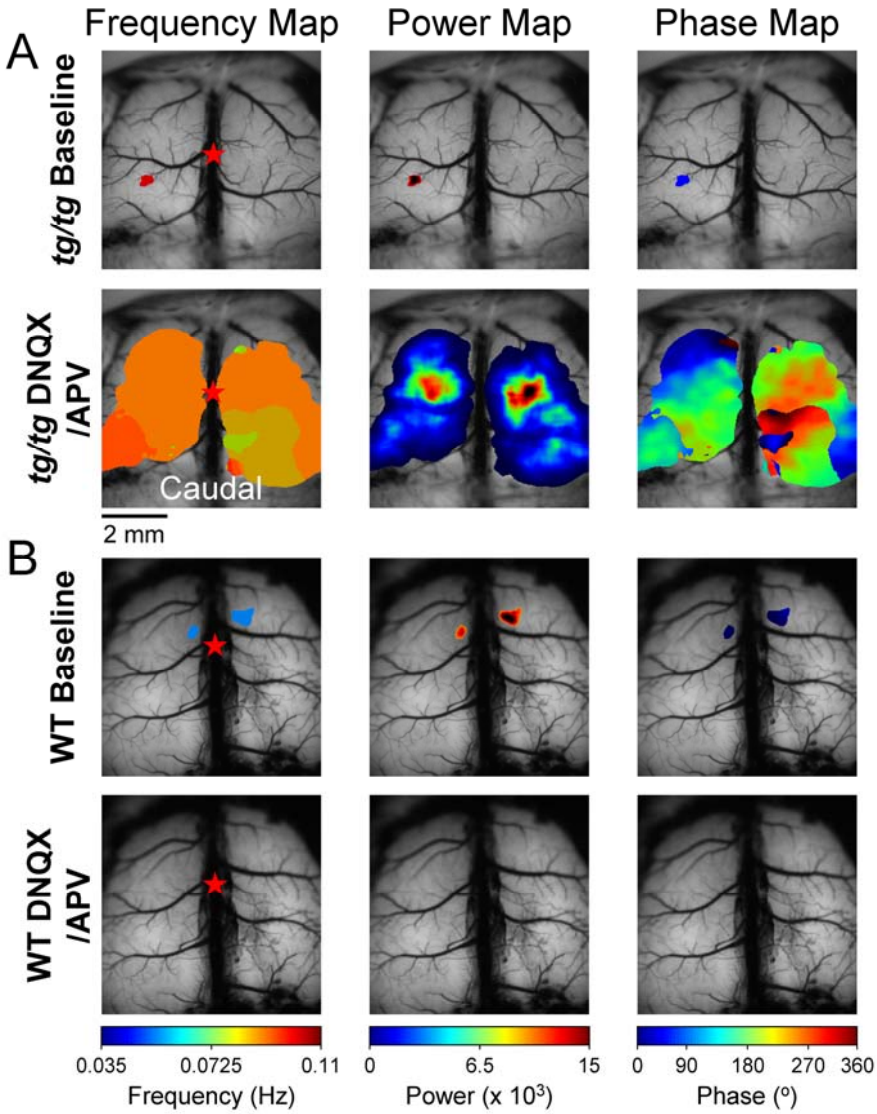

Figure 23. DNQX/APV application increases the high power domains in the cortex of *tg/tg* mice but not WT mice. **A** Spectral analysis demonstrates a large increase in high power domains upon application of DNQX and APV (100 and 200 µM, respectively) compared to baseline activity (top row) in the *tg/tg* mouse. **B** Baseline power (top row) is suppressed by DNQX/APV application (bottom row) in the WT mouse.

In the cerebral cortex of the *tg/tg* mouse, there is a decrease in the efficacy of fast GABAergic inhibition (Tehrani and Barnes, Jr., 1995;Tehrani et al., 1997). Therefore, one possibility is that the increase in LFOs is due to a reduction in cortical inhibition. We tested whether suppression of $GABA_A$ergic transmission in the *tg/tg* cortex facilitates a transition to the high power state. Application of 1 μM of the $GABA_A$ receptor antagonist GABAzine does not change the baseline LFO power (9.6 ± 7.3 to 7.2 ± 5.4, $F_{1,8} = 5.57$; p = 0.0211; n = 5, data not shown). The results based on blocking glutamatergic and GABAergic receptors show that high power LFOs are not due to an increase in excitability. Instead, the LFOs are facilitated by a reduction in excitatory synaptic transmission.

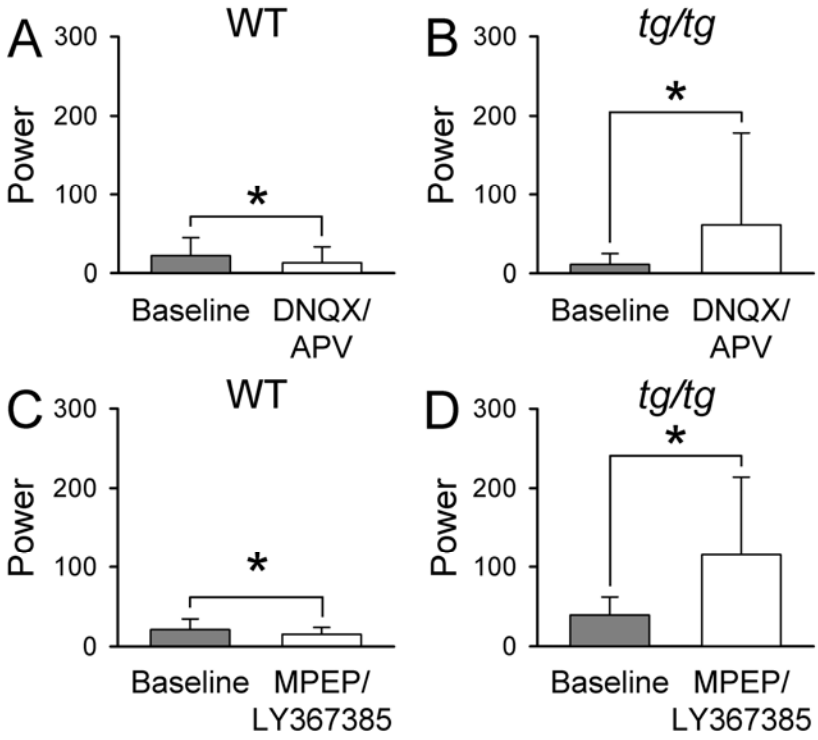

Figure 24. Blocking ionotropic and metabotropic glutamate receptors facilitates high power LFOs in the *tg/tg* mouse. **A** Bath application of DNQX/APV (white) to the cerebral cortex causes a significant decrease in the power compared to the baseline (gray) state in WT mice (n = 4). **B** Power is significantly increased from baseline (gray) in the presence of DNQX/APV (white) in the *tg/tg* mouse (n = 10). **C** Bath application of the metabotropic glutamate receptor type 5 antagonist MPEP (30 μM) and the metabotropic glutamate receptor type 1 antagonist LY367385 (50 μM) results in a significant decrease in power (white) compared to baseline (gray) in WT mice (n = 4). **D** In contrast, blockade of metabotropic glutamate receptors in *tg/tg* mice results in a significant elevation of the power (white) compared to baseline (gray, n = 4).

Contribution of NO signaling to cerebral cortical LFO activity

The suppressive effects produced by TTX, the firing discharge of cerebral cortical neurons, and the facilitatory actions of blocking ionotropic and metabotropic glutamate receptors imply a major neural contribution to the LFOs observed in the *tg/tg* mouse cerebral cortex. However, we also tested blood flow contributions to LFOs, particularly given the high incidence of migraine in patients with *CACNA1A* mutations (Jen et al.,

2004) and reports of altered nitric oxide signaling in the cerebellum of the *tg/tg* mouse (Frank-Cannon et al., 2007;Rhyu et al., 2003). Two prominent pathways exist in the cerebral cortex to regulate neurovascular coupling: the neuronal nitric oxide synthase (nNOS) pathway that produces nitric oxide (NO) in response to neural activation and the cyclooxygenase (COX) pathway that produces multiple signaling molecules including prostaglandins in response to astrocyte activation (Attwell et al., 2010).

In order to parse their relative contributions to the LFOs, we separately blocked the NOS and prostaglandin pathways, applying the blockers in the low power state. L-NAME (1 mM) was applied to inhibit NOS mediated production of NO (Moore and Handy, 1997). Unexpectedly, blocking NOS results in a dramatic increase in the LFOs in the *tg/tg* mouse (Fig. 9A). The spectral maps from an example experiment show that across most of the cerebral cortex the LFOs exceed the high power threshold and there are large regions of very high power (Fig. 9A) similar to that observed spontaneously (Fig. 1). On average, L-NAME increases power 10 fold in the cerebral cortex of the *tg/tg* mouse ($F_{1,10} = 41.1$, $p < 0.0001$; n = 6, Fig. 9C). Application of L-NAME produced a high power state in 6 of 6 *tg/tg* mice. In contrast, L-NAME in WT mice resulted in only a modest increase in baseline power ($F_{1,6} = 4.15$, $p = 0.0465$; n = 4, Fig. 9C) and never resulted in a high power state.

The observation that L-NAME evokes LFOs in the cerebral cortex of the *tg/tg* mouse coupled with the demonstration that nNOS expression is elevated in the

cerebellum of the *tg/tg* mouse (Frank-Cannon et al., 2007;Rhyu et al., 2003) led us to examine the protein expression levels of nNOS and eNOS in the cerebral cortices of *tg/tg* and WT mice. Densitometric analysis of nNOS protein levels normalized to the α-Tubulin control shows that protein expression is unchanged in the cerebral cortex of the *tg/tg* mouse versus WT mice (t_6 = -1.85, p = 0.11, n = 4 each of WT and *tg/tg*; Fig. 9E). Similar to the nNOS result, Western blot analysis of eNOS levels in the cerebral cortex shows no difference between *tg/tg* and WT mice (t_6 = -1.35, p = 0.23, n = 4 each of WT and *tg/tg*; Fig. 9F). We did not examine cerebral cortical expression of inducible nitric oxide synthase because previous studies have demonstrated very low expression levels in the absence of acute pathological insult (Calabrese et al., 2007).

Bath application of indomethacin (100 μM) to inhibit COX mediated production of prostaglandins (Vane, 1971;Faraci, 1992) does not result in the transition from the low to the high power state in the *tg/tg* cerebral cortex. In fact, the baseline power did not change significantly ($F_{1,6}$ = 4.4, p = 0.0403; n = 4, Fig. 9D). Similarly, indomethacin in WT mice did not result in a high power state, producing a very modest increase in LFO power from 8.9 ± 12.2 to 15.0 ± 11.9 ($F_{1,6}$ = 7.3, p = 0.0091; n = 4, Fig. 9D).

Together these results suggest that the NO signaling plays a major role in the transition from low to high power state in the *tg/tg* mouse. In contrast, the prostaglandin pathway controlling cerebral blood flow does not. As both nNOS and eNOS expression is similar between the *tg/tg* and WT mice, the effect of L-NAME in the *tg/tg* mouse in

generating abnormal LFOs is not due to the disruption of a high basal level of NO production.

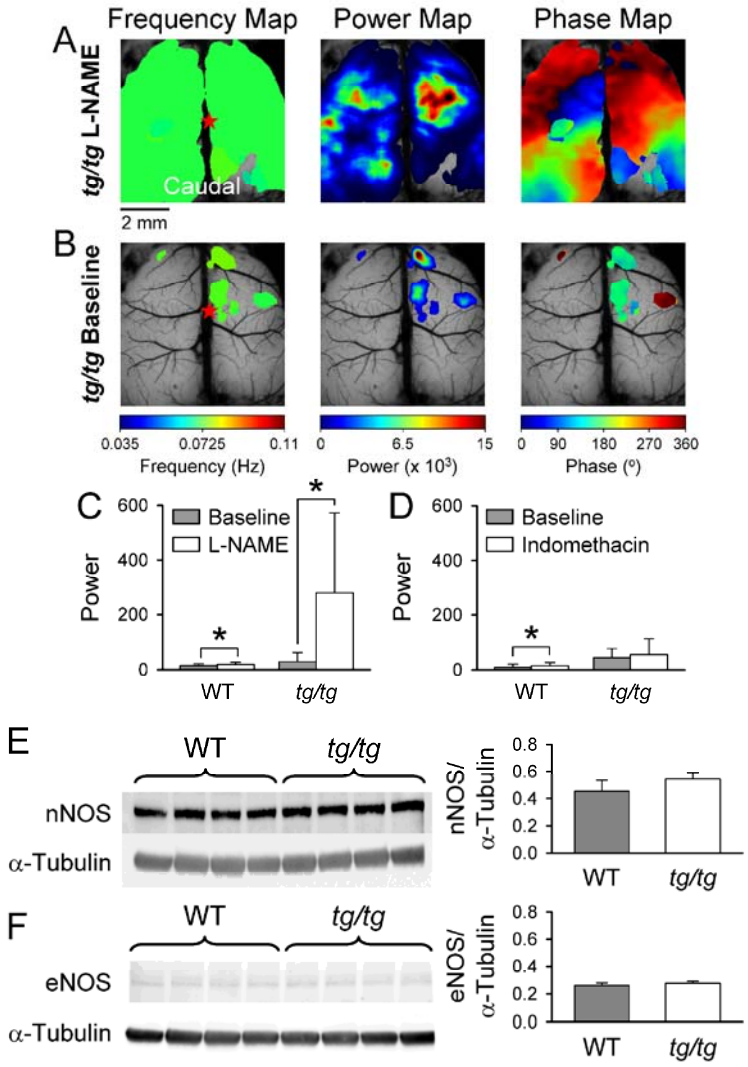

Figure 25. Blocking NO-synthase facilitates LFOs in the cerebral cortex. **A** Frequency, power, and phase maps showing large regions of high power in a *tg/tg* mouse cerebral cortex upon bath application of 1 mM L-NAME, a non-specific nitric oxide (NO) synthase antagonist. **B** Example maps of the spontaneous activity in the same *tg/tg* mouse prior to NO synthase blockade. **C** and **D** Summaries of the average power during the baseline period (gray) in WT and *tg/tg* mice in the presence (white) of either L-NAME or the cyclooxygenase inhibitor, indomethacin (WT, n = 4 for both drug treatments; *tg/tg*, indomethacin n = 4, L-NAME n = 6). **E** Western blot (left) of total cerebral cortical protein probed for neuronal NO-synthase and α-Tubulin loading control in WT (n = 4) and *tg/tg* (n = 4) mice. Summary (right) of densitometric analysis of neuronal NO-synthase protein expression normalized to α-Tubulin in WT (gray) and *tg/tg* (white) mice. **F** Similar to E, Western blot (left) of endothelial NO-synthase protein expression in WT (n = 4) and *tg/tg* (n = 4) mice with α-Tubulin control. Densitometric analysis (right) of endothelial NO-synthase expression in WT (gray) and *tg/tg* (white).

Abnormal cerebral cortical responses to sensory input and direct cortical stimulation in tg/tg mice

Given the highly abnormal activity in the cerebral cortex of the *tg/tg* mouse, the next question was if the *tg/tg* mouse cerebral cortex differs from WT mice in sensory evoked cortical activation or the response to direct cortical stimulation. Stimulation of the C2 whisker used a 5 Hz train at random intervals between 6-8 s. The stimulus application strategy was designed to avoid the frequency band of the LFOs. The response amplitude was defined as the power evoked in the stimulus frequency range (0.125-0.167 Hz) (Llano et al., 2009). In both WT and *tg/tg* mice air-puff delivered to C2 evokes a patch of activity in the contralateral barrel cortex (Fig. 10A). The response in *tg/tg* mice is reduced relative to WT ($F_{1,6} = 7.0$, $p = 0.0089$, n = 4 each for WT and *tg/tg*; Fig. 10B) and demonstrates a deficit in the processing of sensory inputs into the somatosensory cortex.

The reduction in the response to C2 whisker puff could occur outside of the cerebral cortex. Therefore, we also investigated direct intracortical stimulation in the motor cortex using a brief 5 Hz train at random intervals between 6-8 s. Direct cortical stimulation evokes a response ipsilateral to the stimulating electrode and a transcallosal, contralateral response (Fig. 10C). As for whisker puff, the ispilateral and contralateral responses are lower in the *tg/tg* compared to the WT mice as shown in the example power maps. The population data confirms the response to direct cortical stimulation in the *tg/tg* mouse is significantly reduced both ipsilaterally ($F_{1,6} = 24.0$, $p < 0.0001$, n = 4) and

contralaterally ($F_{1,6}$ = 8.7, p = 0.0037, n = 4) compared to WT mice (Fig. 10D). Therefore, the responses to both sensory input and direct cortical simulation is reduced in the *tg/tg* mouse cerebral cortex and the later result demonstrates a deficit in information processing that is intrinsic to the cerebral cortex.

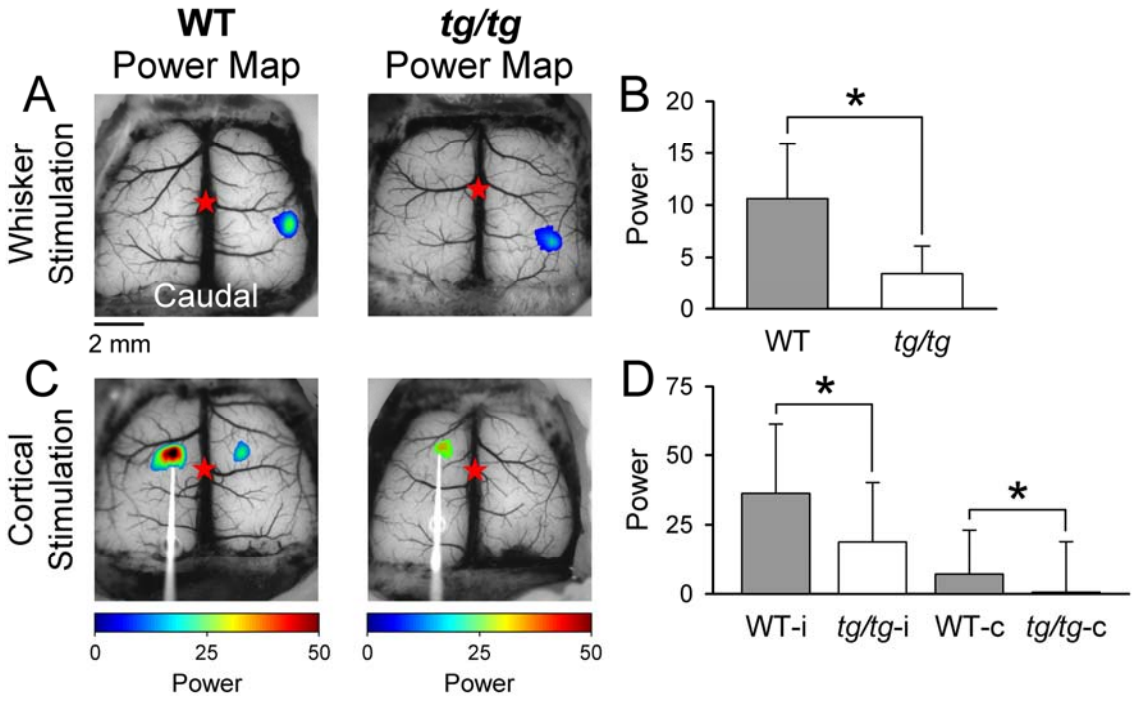

Figure 26. Cortical responses to direct electrical stimulation and sensory input are reduced in the *tg/tg* mouse. **A** Example power maps of evoked response to air-puff stimulation of the left, C2 whisker in WT (left) and *tg/tg* (right) mice. The air-puff stimulus consisted of train of 5 pulses of 9 PSI, 120 ms at 5 Hz delivered at random intervals of 6-8 s. These maps were generated at the frequencies of the stimulation (0.125-0.167 Hz) and not at the LFO frequency. Note a 1X objective was used, resulting in a larger imaged area compared to other figures. **B** Population summary of the power of the cortical response evoked by whisker stimulation in the WT and *tg/tg* mouse (n = 4 each). **C** Similar power maps of the response to direct cortical stimulation of the motor cortex using trains of 5 pulses of 200 µA, 100 µs at 5 Hz in the WT mouse (left) and the *tg/tg* mouse (right). Stimulation electrode is evident on left. **D** Summary of the power evoked by cortical stimulation in the ipsilateral (-i) cortex (i.e., the side with the stimulating electrode) and the contralateral (-c) response in WT and *tg/tg* mice (n = 4 each).

LFOs are decreased by therapeutic agents used to treat EA2, acetazolamide and 4-aminopyridine.

We reasoned that if the LFOs in the cerebral cortex are important in the neurological abnormalities in patients with *CACNA1A* mutations, the agents used to treat EA2, acetazolamide (ACTZ) and 4-aminopyridine (4-AP), should reduce the LFO activity in *tg/tg* mice. As shown in the example experiment, bath application of the carbonic anhydrase inhibitor ACTZ (4 mM) nearly eliminates the LFO activity in a high power state to within the baseline range (Fig. 11A and C). On average, the power of the LFOs is reduced significantly by ACTZ from 218.7 ± 82.0 to 44.0 ± 51.9 ($F_{1,6}$ = 173.9, p < 0.0001, n = 4; Fig. 11C) and converted from the high power state to a low power state in all of the *tg/tg* mice tested. Similarly, as shown in an example experiment (Fig. 10B) and the average data, bath application of 500 μM 4-AP, a K^+ channel antagonist, during the high power state also greatly reduces the power of the LFOs from 377.2 ± 273.0 to 173.7 ± 208.6 ($F_{1,10}$ = 57.0, p < 0.0001, n = 6; Fig. 11D), though not quite as effectively as ACTZ. Therefore, the high power LFOs that characterize the *tg/tg* mice are markedly decreased by the two common EA2 therapies.

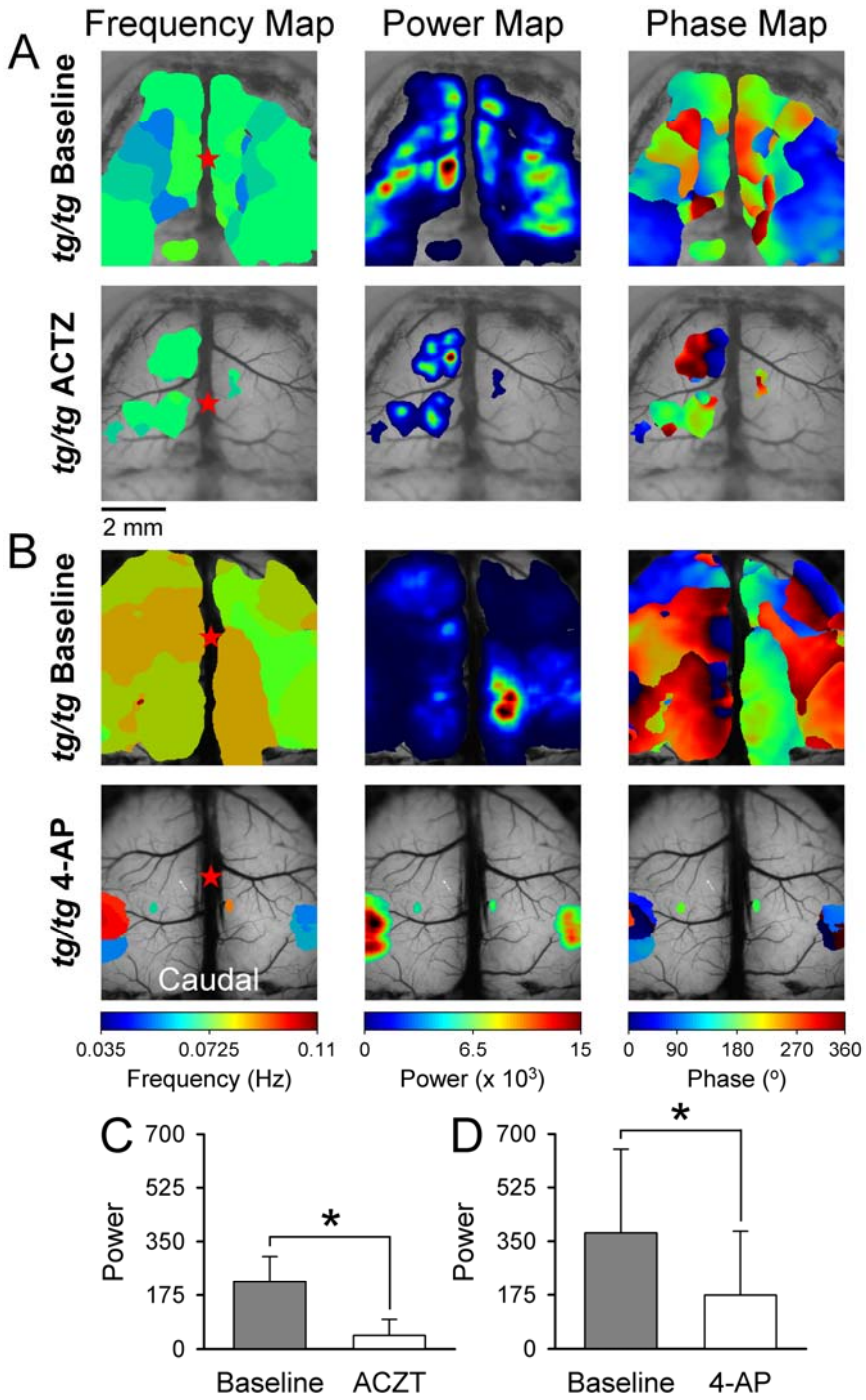

Figure 27. High power LFOs are reduced by therapeutic agents used to treat EA2. **A** and **B** Examples of the frequency, power, and phase maps demonstrate the high power LFOs in the *tg/tg* mouse cerebral cortex in the baseline period (top row) and following (bottom row) application of either ACZT or 4-AP. **C** and **D** Summaries of average baseline (gray bars) power and the average power upon drug application (white bars), either ACZT (n = 4) **C** or **D** 4-AP (n = 6).

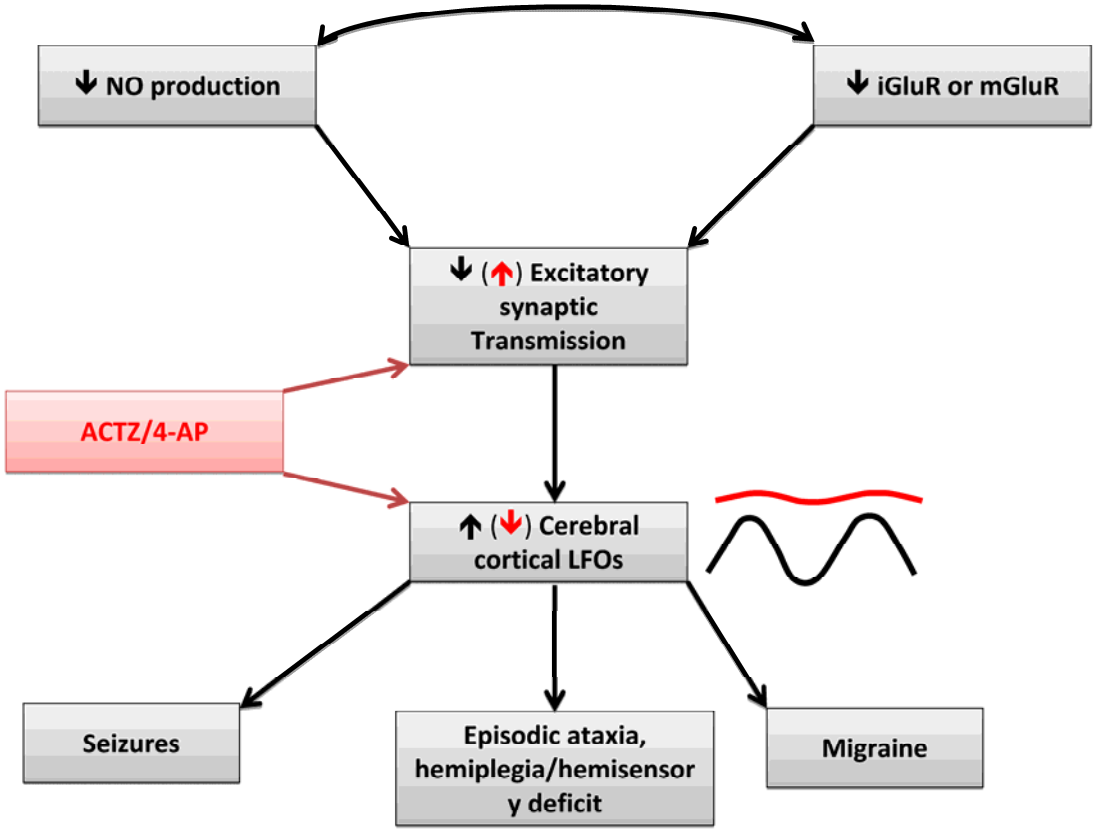

Figure 28. Mechanism of cerebral cortical dysfunction in P/Q channelopathies. The abnormal LFO activity is facilitated by a reduction in excitatory synaptic transmission in the cerebral cortex. The therapeutic agents (ACZT and 4-AP) reduce the LFOs by facilitating excitatory synaptic transmission. The LFOs represent the fundamental instability in the cerebral circuitry that produces episodic symptoms.

Discussion

The major finding in this study is the presence of episodic and highly abnormal LFOs in the cerebral cortex of the *tg/tg* mouse. The oscillations are at the same frequencies observed in the cerebellar cortex, highlighting that the *tg/tg* mutation results in similar instabilities in widely different circuits within the CNS (Chen et al., 2009). The transient nature of the LFOs in the *tg/tg* mouse cerebellar and cerebral cortices

emphasizes the multi-faceted, episodic dysfunction characteristic of many channelopathies. Episodic abnormalities are particularly marked in the P/Q-type Ca^{2+} channelopathies (Rajakulendran et al., 2012).

Cerebral cortical oscillations represent an abnormal excitability state

Several observations demonstrate that the LFOs represent pathological CNS activity. The high power state is almost never observed in WT mice. In contrast, the power levels in the 0.035-0.11 Hz frequency band in *tg/tg* mice are over two orders of magnitude greater than the average power in WT mice (Fig. 2B and C). The responses to several pharmacological agents are strikingly aberrant in *tg/tg* mice. For example, blocking ionotropic or metabotropic glutamate receptors, as expected, reduces LFO power in WT but increases LFO power in *tg/tg* mice. Inhibition of NOS results in high power LFOs in the *tg/tg* cerebral cortex but not in WT mice. In WT controls, TTX virtually eliminates LFO power as blocking action potentials greatly suppresses neuronal activity in normal animals, including sensory input (Sachidhanandam et al., 2013) and cortico-cortical connections (Chen et al., 2013;Khalilov et al., 2003). Although TTX greatly reduces the LFOs in *tg/tg* mice, the high power state was not eliminated suggesting that local cellular, action potential independent mechanisms can support the oscillations. Similarly, local mechanisms appear capable of generating the LFOs in the cerebellar cortex (Chen et al., 2009). In agreement with previous *in vitro* demonstrations of abnormalities in the somatosensory thalamus and cortex (Sasaki et al., 2006;Ayata et al., 2000), the cortical responses to both somatosensory inputs and to intracortical

stimulation are reduced, suggesting that normal information processing is disrupted. Decreased post-synaptic response to parallel fiber stimulation also occurs in the cerebellar cortex of the *tg/tg* mouse (Chen et al., 2009;Matsushita et al., 2002). Overall, cerebral cortical excitability and synaptic transmission is abnormal in *tg/tg* mice.

Role of synaptic transmission in the low frequency oscillations

The high power LFOs in the *tg/tg* mouse are not solely due to an acute decrease in P/Q-type Ca^{2+} channel function. In WT mice, acutely blocking P/Q-type Ca^{2+} channels with ω-Agatoxin increases the power of the spontaneous cortical activity within the 0.035-0.11 Hz frequency band; however, the power remains well below the high power threshold. Furthermore, ω-Agatoxin does not induce high power LFOs in the *tg/tg* mice. The latter finding may reflect that changes in the makeup of voltage-gated Ca^{2+} channels at axon terminals compensate for the loss of P/Q-type Ca^{2+} channels (Zhou et al., 2003;Qian and Noebels, 2000;Pardo et al., 2006;Kaja et al., 2007b;Campbell and Hess, 1999). At some central and peripheral synapses the compensation is nearly complete (Qian and Noebels, 2000;Pardo et al., 2006;Kaja et al., 2007b) and additional antagonism of P/Q-type Ca^{2+} channels may not increase the baseline deficit. The lack of high power LFOs in the presence of ω-Agatoxin in WT animals argues that other developmental/compensatory mechanisms are operative in the *tg/tg* mouse and these changes bias the cerebral cortex to generate high power LFOs. In support of the concept that developmental/compensatory changes are important in the pathological CNS activity, the episodic dystonia does not appear before ~21 days of age in the *tg/tg* mouse (Green

and Sidman, 1962;Meier and MacPike, 1971;Seyfried and Glaser, 1985). A recent study of an EA2 allelic disorder, spinocerebellar ataxia type 6, demonstrated that the *CACNA1A* gene encodes a transcription factor crucial for normal neuronal development in addition to its role encoding the P/Q-type Ca^{2+} channel (DU et al., 2013). Therefore, a constellation of developmental and compensatory alterations in the *tg/tg* mouse contribute to the instabilities in the cerebral cortex that lead to the high power LFOs.

Although there is compensation for the reduction in P/Q-type Ca^{2+} channel function in *tg/tg* mouse, synaptic transmission is abnormal. In *tg/tg* mice, reductions in glutamatergic synaptic transmission occurs in the cerebellum (Matsushita et al., 2002;Chen et al., 2009), thalamus (Caddick et al., 1999) and cerebral cortex (Sasaki et al., 2006;Ayata et al., 2000). In support of reduced synaptic transmission in the cerebral cortex, the present results show decreased ipsilateral and contralateral responses to direct cortical stimulation. We reasoned that a reduction in glutamatergic synaptic transmission in *tg/tg* mice produces instability in the cerebral cortical circuitry and that further compromise of glutamatergic synaptic transmission may increase the instability. In agreement, LFO power and the probability of entering the high power state increases with blocking ionotropic or metabotropic glutamate receptors. Given the importance of inhibitory interneurons in generating cerebral cortical oscillations (Buzsaki and Wang, 2012;Wang, 2010) and as GABAergic transmission is impaired in *tg/tg* mice (Sasaki et al., 2006;Tehrani and Barnes, Jr., 1995), one could hypothesize that inhibitory networks play a role in the LFOs. Although it is well documented that blocking $GABA_A$ receptors

increases cerebral cortical excitability and produces seizures (Chagnac-Amitai and Connors, 1989;Dichter and Ayala, 1987), blocking $GABA_A$ receptors did not have a significant effect on the LFOs. These observations suggest normal excitatory synaptic transmission constrains the cerebral cortical network from entering the high power state in *tg/tg* mice.

Role of nitric oxide signaling in the low frequency oscillations

NO is an additional factor involved in the cerebral cortical LFOs as L-NAME mediated inhibition of NOS reliably produces the high power state in the *tg/tg* mouse. The contribution of NO signaling likely goes beyond modulation of cerebral blood flow, as blocking COX mediated cerebral blood flow regulation does not produce high power LFOs. NO signaling influences multiple pathways resulting in many downstream effects including modulating neurotransmission, transcription, and vascular tone (Calabrese et al., 2007). Despite similar levels of nNOS and eNOS expression in the *tg/tg* and WT mice, there is a fundamental difference in the cerebral cortical response to NOS blockade between the WT and *tg/tg* mice. Because a reduction in basal NO production reliably increases LFO activity in *tg/tg* mice, downstream signaling must serve to dampen the aberrant cerebral cortical activity that occurs during the high power state. Although there is not a consensus among reports, it is notable that NO modulates the activity of voltage-gated Ca^{2+} channels, including facilitating channel activity (Ohkuma et al., 1998;Chen et al., 2002;Jian et al., 2007;Chen and Schofield, 1995;Hirooka et al., 2000) (see however (Carabelli et al., 2002;D'Ascenzo et al., 2002;Schuchmann et al., 2002;Yoshimura et al.,

2001)). In the *tg/tg* mouse, NO may facilitate voltage-gated Ca^{2+} channel conductance and help compensate for the reduced activity of the mutant P/Q-type Ca^{2+} channels and impaired synaptic transmission.

Role for low frequency oscillations in episodic cortical dysfunction

Many studies in the *tg/tg* mouse have focused on the motor phenotypes, mild ataxia and episodic dystonia, that have been attributed to cerebellar dysfunction (Walter et al., 2006;Raike et al., 2013;Neychev et al., 2008;Campbell et al., 1999). In the human *CACNA1A* diseases, cerebral cortical symptoms are common including migraine and epilepsy as well as sensory motor and cognitive impairments (Jen et al., 2001;Jouvenceau et al., 2001;Van and Szliwowski, 1996;Baloh et al., 1997;Rajakulendran et al., 2012;Nachbauer et al., 2014). These diverse findings are thought to reflect abnormalities in either neurovascular coupling (migraine) or abnormal synaptic transmission (epilepsy). The LFOs in *tg/tg* mice provide a possible mechanism for transient cerebral cortical dysfunction in EA2. Therefore, the reduction of LFOs by ACZT and 4-AP argue for a connection between the oscillations in *tg/tg* mice and the human P/Q-type Ca^{2+} channelopathies. In EA2 patients, ACTZ reduces the frequency and severity of ataxic bouts (Griggs et al., 1978) and ameliorates non-cerebellar features including migraine attacks and abnormal EEG activity (Neufeld et al., 1996;Zasorin et al., 1983). Similar to ACTZ, 4-AP effectively decreases attack frequency and severity, interictal ataxia, and migraine occurrence in EA2 patients (Lohle et al., 2008;Strupp et al., 2004;Jung et al., 2010).

In conclusion, abnormal synaptic transmission is central to the episodic LFOs in the cerebral cortex of the *tg/tg* mouse. This conclusion is based on the observations that decreased glutamatergic synaptic transmission and NO synthesis facilitates high power LFOs. The conclusion is reinforced by the corollary findings that LFOs are reduced by 4-AP, an agent that enhances intracellular Ca^{2+} influx and neurotransmitter release (Smith et al., 2000), as well as by ACTZ a drug with multiple effects including the enhancement of NO production (Aamand et al., 2009). In addition to glutamatergic synaptic transmission, the role of NO signaling in the LFOs suggests a deficit in neurovascular coupling. The highly abnormal excitability state represented by the cerebral cortical LFOs is a novel finding and offers a potential mechanism for the non-cerebellar dysfunction in P/Q-type Ca^{2+} channelopathies (Fig. 28).

The findings also raise numerous questions about the LFOs including how they are triggered, propagated within the cerebral cortex and the functions disrupted.

CHAPTER V: FINAL DISCUSSION AND FUTURE EXPERIMENTS

Functional implications of regional differences in PF mediated PC activation

As outlined in the Introduction, the role of PFs in the computations performed by the cerebellar cortex is controversial. Chapter 2 demonstrates that previous apparently contradictory results on whether PFs activate patches or beams of PCs may be due to regional differences in PC phenotype. Therefore, the transfer of information between the mossy fiber-GC inputs to PCs is not uniform. The new findings in Chapter 2 provide evidence of a more complex role for PFs in cerebellar computations and function. An important question arises from these findings: what role do regional differences in the pattern of PF mediated PC activation play in the cerebellar control of movement?

Based on the findings in Chapter 2 and other recent work (Ebner et al., 2012;Apps and Hawkes, 2009), the regional differences in the pattern of GC-PF-PC activation could act to coordinate the movements of different body parts across parasagittal zones of PCs. This view would be an update of an established hypothesis that representations of the body are separately encoded in each of the DCN and that the DCN operate as parallel loops, each controlling different aspects of movement (Thach et al., 1992). The PFs serve to link PCs and synchronize the actions of different body regions encoded within DCN producing coordinated movement. The hypothesis predicts that the spatial pattern of co-activated PCs would depend on the number of joints and/or synergistic muscle

groups co-activated to perform a particular movement. Tasks necessitating coordination across multiple body regions (e.g., multi-joint movements) and, therefore, coordination across the cerebellar nuclei would require the beam-like activation of PCs.

Alterations in PF-mediated PC activation disrupt normal motor control

Mutant mice provide evidence for the fundamental importance of differences in parasagittal zones to the computations performed by the cerebellum and subsequent motor output. Departures from the normal parasagittal organization of the cerebellar circuitry exhibit impaired motor control. Examples of this are the mutant *tg/tg* mouse and a mouse model of the human disorder spinocerebellar ataxia type 5 (SCA5). Both mice exhibit abnormalities in the cerebellar circuitry resulting in altered patterns of PC activation (Armbrust et al., 2014). Both mouse lines also exhibit little evidence of neurodegenerative PC loss until an advanced age, therefore, reducing a major cofound to understanding how abnormalities in the cerebellar circuitry produce impaired motor control (Levitt, 1988;Isaacs and Abbott, 1995;Sawada et al., 2009;Armbrust et al., 2014).

As described in Chapter 3, the circuitry of the *tg/tg* mouse exhibits fundamental departures from the cerebellar circuitry of WT mice. The responses to PF and GC stimulation are impaired. Specifically, both the amplitude and the mediolateral extent of PC activation evoked by either direct electrical stimulation of PFs or the pharmacological activation of GCs are attenuated compared to WT mice. Similarly, the sensory evoked

PC patch response is nearly absent in the *tg/tg* mouse. The altered responsiveness of PCs to GC and PF input likely contributes to the ataxia exhibited by the *tg/tg* mouse and supports the hypothesis that PFs are integral to normal cerebellar motor control.

Similar to the *tg/tg* mouse, a recently described mouse model of the human disorder SCA5 also exhibits altered PF to PC excitability (Armbrust et al., 2014). SCA5 is a neurodegenerative disease characterized by limb and gait ataxia (Ranum et al., 1994;Burk et al., 2004) and is caused by mutations in *SPTBN2* (Ikeda et al., 2006) the gene encoding the β-III spectrin protein. β-III spectrin is highly expressed in PCs and plays a role in anchoring and restricting the movement of EAAT4 and mGluR1α in the PC plasma membrane. The anchoring function is disrupted in known mutant forms of β-III spectrin (Jackson et al., 2001;Ikeda et al., 2006;Armbrust et al., 2014). As described above, both EAAT4 and mGluR1α are non-uniformly expressed at higher levels in parasagittal zones of zebrin II+ PCs.

As in the human disorder, the SCA5 mice exhibit progressive cerebellar degeneration and impaired motor coordination. Flavoprotein autofluorescence and Ca^{2+} optical imaging in SCA5 mice demonstrated multiple abnormalities in the cerebellar circuitry. The mGluR1 component of the postsynaptic PC response is impaired. Similarly, mGluR1 mediated postsynaptic long-term potentiation to PF input is reduced in SCA5 mice. In addition, the mGluR1-dependent long-latency patch response to high frequency PF stimulation is

reduced in SCA5 mice and the long-latency patches do not exhibit long-term potentiation.

The altered sub-cellular localization of mGluR1 was found to underlie several of the cerebellar circuit abnormalities in the SCA5 mouse. Similarly, the sub-cellular mislocalization of EAAT4 may also contribute to cerebellar dysfunction. Though not investigated, one could hypothesize that the abnormal localization of mGluR1 and EAAT4 extends to the parasagittal expression of these proteins, further contributing to impaired motor coordination in the SCA5 mouse. The hypothesis would be consistent with the finding that intrathecal infusion of an antisense oligonucleotide to EAAT4 (but not the glial glutamate transporters EAAT1, EAAT2, or EAAT3) is sufficient to produce cerebellar ataxia (Maragakis et al., 1997;Raiteri et al., 2002).

In conclusion, the *tg/tg* and SCA5 mouse are two examples of how alterations in the spatial pattern and strength of PF mediated PC activation cerebellar cortex in the absence of significant PC loss may disrupt normal cerebellar function.

Future experiments to determine the mechanism of reduced PF mediated PC response in the tg/tg mouse cerebellar cortex

The findings in Chapter 3 demonstrate that the response to PF or GC stimulation is reduced, both the amplitude and mediolateral extent. The implication is that the excitability of GCs, PFs and/or PCs is impaired in the *tg/tg* mouse. However, paired-pulse facilitation, a measure of presynaptic release, does not differ between *tg/tg* and WT mice (Matsushita et al., 2002;Zhou et al., 2003) suggesting the impaired response is not due to altered synaptic release. If glutamate release from PFs is not responsible for the decreased responsiveness, there are several other mechanisms that could account for this phenomenon.

First, PF and/or GC excitability could be reduced. To test GC and PF excitability, *in vivo* two-photon Ca^{2+} imaging could be utilized. The strategy is to use an adeno-associated viral vector to sparsely express a Ca^{2+} indicator, GCaMP, in the cerebellar GCs of *tg/tg* and WT mice (Jackman et al., 2014;Akerboom et al., 2012;Tian et al., 2012). Restricting the Ca^{2+} indicator to a sparse population of granule cells affords the ability to specifically identify granule cells based on their distinctive morphology and avoid contamination of the Ca^{2+} signals from other cell types (e.g., PCs) that may also be transduced by the virus. Two photon imaging is critical to achieve single cell resolution, allowing the identification of PF axons and GC somata *in vivo*. The remaining approach is similar to that outlined in Chapter 3. An electrical stimulus is applied to the ipsilateral C3 vibrissae and the responses of the PFs and GC somata compared between WT and *tg/tg* mice. This

approach tests if there is a decrease in the excitability of the GCs and/or the PFs in the *tg/tg* mouse. If a deficit is found, 4-AP application is tested to determine if the reduced GC response in the *tg/tg* is rescued. It would also be interesting to test if the other major therapy in EA2, ACTZ rescues the reduced responsiveness (Griggs et al., 1978). Another possible mechanism for the attenuated PF-PC response in the *tg/tg* mouse is that AMPA receptors on PCs could be reduced. In another *Cacna1a* mutant, the *rocker* mouse that similarly exhibits reduced PF-PC transmission in the absence of impaired paired-pulse facilitation, AMPA receptors on PCs are diminished (Kodama et al., 2006). In the *tg/tg* mouse, whether AMPA receptors on PCs are reduced or have decreased responsiveness has not been examined, to our knowledge. Therefore, an important next step would be to measure the AMPA receptor number and density on PCs in the *tg/tg* mouse. One approach would be to employ a similar freeze-fracture technique as was used to examine the *rocker* mouse PCs (Kodama et al., 2006;Tanaka et al., 2005).

The third possible mechanism is a reduction in PC excitability due to reduced P/Q-type Ca^{2+} currents. This mechanism is highly likely given that P/Q-type Ca^{2+} channels account for 70-80% of voltage-gated P/Q-type Ca^{2+} currents on WT PCs (Mintz et al., 1992;Llinas et al., 1992). Also, compensatory enhancement of L-type Ca^{2+} channel expression occurs in *tg/tg* PCs (Campbell and Hess, 1999). Diminished and/or changes in the voltage-gated Ca^{2+} channels on PCs in *tg/tg* mice could affect the integration of PF inputs. Furthermore, alterations in PC dendritic morphology have been described in the *tg/tg* mouse, including ectopic dendritic spines and altered dendritic geometry (Rhyu et

al., 1999), which could decrease somatic responses by altering current spread down the dendritic processes (Roth and Hausser, 2001;Vetter et al., 2001).

To test if *tg/tg* mouse PCs exhibit abnormal excitability, whole cell voltage and current clamp recordings of PCs in cerebellar slices could be performed (Ovsepian and Friel, 2008). The whole cell recording configuration allows the comparison of depolarization induced PC responses between *tg/tg* and WT mice. Measures of PC electroresponsiveness such as action potential threshold as well as depolarizing current evoked initial firing rate and train duration could be obtained. Furthermore, alterations of any of the measures of PC electroresponsiveness could be further investigated to determine the specific channels that contribute to any PC abnormalities in the *tg/tg* mouse.

Future experiments to test functional consequences of parasagittal differences in cerebellar excitability

The observation that a beam of PCs is evoked in Crus I while patches are evoked in Crus II to sensory stimuli prompts the question: what is the functional role of parasagittal differences in the pattern of PC activity evoked by mossy fiber-GC input? To answer this important question, the patterns of PC responses to peripheral sensory input throughout the cerebellum should be investigated. Based on the finding that expression levels of EAAT4 influence the spatial extent of PC activation to GC-PF input, the known expression profile of EAAT4 provides a basis for predicting the responses in different

folia. For example, similar to Crus I other folia including lobules VIb, VII, IX, and X as well as the flocculonodular lobule uniformly (or nearly uniformly) express EAAT4 (Gincel et al., 2007;Apps and Hawkes, 2009;Hawkes and Herrup, 1995). The remaining folia exhibit parasagittal bands of high and low EAAT4 expression similar to Crus II. While extrapolation of the response patterns found in Crus I and Crus II to folia with similar EAAT4 expression profiles is tempting, it is possible that factors in addition to EAAT4 influence the geometry of the PC response to mossy fiber-GC-PF input. Furthermore, the other factors may be non-uniformly distributed in the cerebellar cortex in a pattern that is out of register with EAAT4 expression.

The systematic mapping of peripherally evoked PC responses in as many folia as possible would provide further validation of the findings in Chapter 2. Additionally, the mapping results would demonstrate whether the differential contribution of PFs to the responses in Crus I and Crus II is generalizable to the cerebellar cortex or if further regional variations exist. The experimental approach would be a modified version of the Ca^{2+} imaging utilized in Chapter 2 as it affords the spatial and temporal sensitivity to define the response patterns evoked by peripheral input to the cerebellar cortex (Cramer et al., 2013;Gao et al., 2006). Because the strategy is to examine as much of the cerebellar cortex as possible, bulk loading of Ca^{2+} indicator is impractical. A mouse line expressing a genetically encoded calcium indicator, such as GCaMP, specifically in PCs is needed to visualize superficial folia across the cerebellar cortex (Zariwala et al., 2012). Ca^{2+} optical imaging *in vivo* is used to monitor the response in the cerebellar cortex to stimuli applied

to various peripheral locations. The pattern of the evoked PC responses could then be used to construct a response map of the cerebellar cortex to sensory inputs. While sensory mapping of the cerebellar cortex has been performed previously in rodents (Shambes et al., 1978b;Shambes et al., 1978a;Bosman et al., 2010;Bower and Kassel, 1990), these studies examined a limited number of folia and the electrophysiological techniques used are not optimal for large scale spatial mapping.

A multi-folia map of peripherally evoked PC activation patterns could serve as a guide for investigating the series of questions. First, are different patterns of PC activation (i.e., beams and patches) produced in the cerebellar cortex of awake mice during motor behavior? Similar to previous awake imaging studies (Najafi et al., 2014;Chen et al., 2009), the mouse line expressing GCaMP in PCs would undergo a survival surgery to secure a head-post to the cranium and prepare the bone for transcranial optical imaging of the cerebellar cortex. The animal with its head fixed is secured over a running wheel (Najafi et al., 2014) and the motor behavior monitored. This configuration allows the synchronized monitoring of the limbs, trunk, and tail kinematics simultaneous with the optical imaging to determine if patches and/or beams of PC activation occur during locomotion.

An association between movements and patterns of PC activation (i.e., beams and patches) would provide the framework to address the next question: what role does the pattern of PC activity play in motor control? An optogenetic approach is well suited to

testing this question as it affords the spatiotemporal control as well as the cell type specificity necessary to target a subpopulation of PCs (Witter et al., 2013;Fenno et al., 2011;Chaumont et al., 2013;Nguyen-Vu et al., 2013). The experimental design is similar to the awake mapping investigation described above, though the animals in this experiment express both the light gated, third generation inhibitory chloride pump halorhodopsin (eNpHR3.0) and GCaMP in PCs. The dual PC specific expression of eNpHR3.0 and GCaMP3 allows the simultaneous monitoring and manipulation of PC activity.

The strategy is to use the Ca^{2+} optical imaging to define regions of the cerebellar cortex that exhibit locomotion (or another motor behavior) evoked PC beams and regions that exhibit PC patches. After a baseline period, photostimulation is delivered to inhibit a subpopulation of PCs within the patch or beam. The hypothesis predicts that partial disruption of the synchronous activation of PCs will impair the coordination of the corresponding movement. The changes observed would provide insight into the distinct roles of beam versus patch activation. For example, does inhibition of patch regions effect more distinct aspects of locomotion (i.e., single joints) and does inhibition of beams more global aspects (i.e., multi-joint coordination)?

The next experiment would address the corollary question of the effects of activating a patch or beam of PCs on motor control? Instead of inhibiting a subpopulation of PCs, this experiment excites PCs activated during normal motor control using the excitatory,

light-gated cation channel, channelrhodopsin-2 (ChR2) in PCs. Using the same behavioral evaluation proposed for optogenetic inhibition of PCs, this experiment will asses how beam versus patch activation of PCs effects locomotion. These experiments are crucial to determine the functional role of different patterns of PC activation in motor behavior and, therefore the role PFs serve in the cerebellar cortex.

In conclusion, expanded mapping of the patterns of PC activation in response to sensory inputs followed by the mapping of patterns of PC activation in awake mice is an important extension of the initial findings discussed in Chapter 2. Furthermore, the manipulation of patterns of synchronous PC activity in awake mice would provide insight into the functional role of PC beams and patches and, therefore the role of PFs in motor control.

Cerebral cortical LFOs and phenotypic abnormalities in the *tg/tg* mouse

The results of Chapter 4 raise an important question: what are the functional consequences of the high power, cerebral cortical LFOs in the *tg/tg* mouse? The complex phenotype of the *tg/tg* mouse consisting of distinct episodic abnormalities, paroxysmal dystonia and absence seizures, requires additional experiments to link the cerebral LFOs to a phenotypic trait. However, two pieces of evidence suggest that the cerebral LFOs contribute to attacks of episodic dystonia. First, the attacks evolve in a highly reproducible and stereotypical progression reminiscent of a "Jacksonian march" (Jackson,

1870;Charcot J.M. and Pitres A., 1877), implying the systematic spread of abnormal neural activity across a region of the brain with a highly organized somatotopy, such as the motor cortex. The cerebellum is not known to contain a similar somatotopic organization (Shambes et al., 1978b;Shambes et al., 1978a;Kassel et al., 1984;Bower and Woolston, 1983;Rowland and Jaeger, 2005;Allen et al., 1977;Allen et al., 1978). Second, a *Cacna1a* mouse line that expresses one mutant P/Q-type Ca^{2+} channel *tg* allele and one null allele throughout the CNS (Tottering^{haplo} mice) exhibits heightened sensitivity to attack triggers compared to the Tottering$^{PC\text{-}haplo}$ mouse that expresses one *tg* allele and one null allele in PCs but is otherwise heterozygous at the P/Q-type Ca^{2+} channel gene locus (Raike et al., 2013). The difference in trigger sensitivity between these two mouse lines suggests that structures outside the cerebellum contribute to the motor attack.

Alternatively, if the cerebral cortical LFOs do not contribute to the episodic dystonia, the LFOs could relate to other episodic abnormalities known to occur in P/Q-type Ca^{2+} channelopathies. In the human *CACNA1A* diseases, cerebral cortical symptoms such as migraine and epilepsy as well as sensory motor and cognitive impairments are common (Jen et al., 2001;Jouvenceau et al., 2001;Van and Szliwowski, 1996;Baloh et al., 1997;Rajakulendran et al., 2012;Nachbauer et al., 2014). These diverse findings are thought to reflect abnormalities in either neurovascular coupling (migraine) or abnormal synaptic transmission (epilepsy). The LFOs in *tg/tg* mice provide a possible mechanism for transient cerebral cortical dysfunction in EA2. Therefore, the reduction of LFOs by ACZT and 4-AP argue for a connection between the oscillations in *tg/tg* mice and the

human P/Q-type Ca^{2+} channelopathies. In EA2 patients, ACTZ reduces the frequency and severity of ataxic bouts (Griggs et al., 1978) and ameliorates non-cerebellar features including migraine attacks and abnormal EEG activity (Neufeld et al., 1996;Zasorin et al., 1983). Similar to ACTZ, 4-AP effectively decreases attack frequency and severity, interictal ataxia, and migraine occurrence in EA2 patients (Lohle et al., 2008;Strupp et al., 2004;Jung et al., 2010). The efficacy in reducing cerebral LFOs by the agents commonly used to treat EA2 suggests that the LFOs represent a mechanism that contributes to EA2 pathogenesis.

Cerebellar and cerebral LFOs in the tg/tg mouse

As discussed, some features of the episodic dystonia exhibited by the *tg/tg* mouse are inconsistent with abnormal motor activity deriving solely from the cerebellum. Despite this, there is substantial evidence supporting the necessary contribution of the cerebellum to episodes of dystonia (Campbell et al., 1999;Neychev et al., 2008;Raike et al., 2013;Walter et al., 2006;Chen et al., 2009). A new model is required that incorporates the roles of both the cerebellum and the cerebral cortex in the episodic dystonia.

The cerebellar output *via* the projections of DCN neurons influences the activity of many central motor areas. For example, many cerebral cortical areas receive cerebellar input *via* thalamic nuclei including primary motor cortex, premotor cortex, prefrontal cortex, and posterior parietal areas (Allen and Tsukahara, 1974;Evarts and Thach, 1969;Bostan

et al., 2013). Cerebral cortical areas receiving of cerebellar output also project back to the same region in the cerebellum, forming recurrent loops (Strick et al., 2009). The DCN also projects to sensorimotor areas of the basal ganglia (Bostan and Strick, 2010;Bostan et al., 2010;Hoshi et al., 2005) which in turn form looped projections with many cerebral cortical areas (Alexander et al., 1986). Therefore, the recurrent interconnections of the cerebellum-thalamus-basal ganglia-cerebral cortical systems may serve as a conduit by which abnormal cerebellar activity in the *tg/tg* mouse drives pathological activity in other central motor structures and leads to the rhythmic muscle contractions characteristic of episodes of dystonia (Chen et al., 2009;Campbell and Hess, 1999;Scholle et al., 2010;Raike et al., 2013;Fan et al., 2012).

Support for this hypothesis is provided by a recent investigation of the abnormal circuitry underlying the development of Rapid-Onset Dystonia-Parkinsonism (RDP) (Calderon et al., 2011;Fremont and Khodakhah, 2012). The study illustrates how the synergistic interactions of pathological activity in different CNS structures produce motor impairment. The motor phenotype of the pharmacological RDP mouse model exhibits both parkinsonian symptoms attributed to basal ganglia dysfunction and a generalized dystonia attributed to cerebello-basal ganglia dysfunction. The authors tested the motor cortical contribution to the hypothesized cerebello-basal ganglia derived dystonia and found that bilateral TTX application to the motor cortex reduced the frequency and severity of dystonia. Furthermore, the dystonia exhibited by the RDP mouse is ameliorated by eliminating cerebellar output or disrupting cerebellar projections to the

basal ganglia by lesioning the centrolateral nucleus of the thalamus (Calderon et al., 2011). The phenotype of the RDP mouse exhibits some similarities to the *tg/tg* mouse. Therefore, it is plausible that the cerebello-thalamo-basal ganglo-cerebral cortical circuitry contributes to the propagation of the abnormal LFOs from the cerebellar to cerebral cortex of the *tg/tg* mouse to produce the episodic attacks of dystonia.

Future experiments to investigate functional consequences of cerebral cortical LFOs and cerebellar-cerebral cortical interaction in episodic dystonia

A primary question raised by Chapter 4 is if the LFOs in the cerebral cortex of the *tg/tg* mouse are involved in the episodic dystonia. To address this question, the experimental design consists of transcranial flavoprotein and two-photon Ca^{2+} imaging in the awake *tg/tg* mouse cerebral cortex in conjunction with simultaneous electromyographic and video behavioral recordings to monitor the dystonic attacks. Both imaging methodologies are needed as flavoprotein allows monitoring the LFOs throughout large regions of the cerebral cortex and the two-photon imaging allows monitoring individual neurons and glia during the attacks.

A head restraint devices is surgically implanted in *tg/tg* mice (Chen et al., 2009) and the cerebral cortex prepared for transcranial imaging (Hishida et al., 2011;Yang et al., 2010;Drew et al., 2011;Drew et al., 2010). A small burr hole is placed in the cranium to allow microinjection of drugs and Ca^{2+} indicator for those animals undergoing two-

photon imaging (Lee et al., 2006;Houweling and Brecht, 2008). In the restrained animals baseline activity is monitored followed by a challenge with caffeine, a reliable attack trigger. The ensuing attack is monitored and the analyses focused on the spectral content of the flavoprotein fluorescence as well as the glial and neuronal Ca^{2+} response during the baseline, the dystonic attacks and the post attack period in relation to the behavior. In conjunction with serum fluorescence labeling, two-photon measurements of cerebral blood flow dynamics are also acquired and evaluated for the baseline, attack, and post attack periods to determine if alterations in neurovascular coupling occur during attacks (Drew et al., 2010;Drew et al., 2011).

Using the spectral analysis developed in Chapter 4, the first goal is to determine if upon attack initiation the cerebral cortex exhibits LFOs as observed in anesthetized *tg/tg* mice. The hypothesis predicts that the LFOs will be highly coupled with the episodic dystonia. In particular, the analyses focus on whether the LFOs occur in the motor areas of the cerebral cortex. The two-photon Ca^{2+} imaging data is similarly analyzed to determine if the neurons or glia exhibit LFO activity. If both cell types exhibit oscillations, additional analyses are performed to determine which cell type develops oscillations first relative to attack onset, and ultimately whether both cell types are necessary for the episodic dystonia.

The frequency band and the power of the LFOs may deviate from the anesthetized mouse as was observed in a similar previous comparison of the cerebellar LFOs between the

anesthetized and awake state (Chen et al., 2009). The exact timing between the LFOs and the motor attacks will be evaluated. A correlation between the onset of LFOs and dystonia would support the hypothesized link between the abnormal cerebral cortical activity and the dystonic phenotype of the *tg/tg* mouse. Furthermore, the two-photon data would provide insight into possible cellular mechanisms of both the LFOs and the attacks.

If a relationship is found between the cerebral cortical LFOs and the attacks, the next experiments test if the oscillations are necessary for episodes of dystonia. In the first experiment, the agents (4-AP and ACTZ) shown to suppress the cerebral cortical LFOs in the anesthetized mouse and used to treat the human P/Q-type Ca^{2+} channelopathies are infused into the cerebral cortex of the *tg/tg* mice prior to exposing the mice to an attack trigger to determine if suppression of the LFOs and the dystonia occurs concurrently. A reduction in the attack frequency, severity and/or duration with 4-AP or ACTZ in conjunction with the absence of LFOs would demonstrate that the cerebral cortex contributes to the attacks. If the attacks are blocked this would suggest the LFOs are integral to the episodic dystonia. In contrast, if the therapeutic agents suppress the cerebral cortical LFOs without affecting the attacks, it would imply that the cerebral LFOs are not necessary for the dystonic episodes.

The final experiments test how the LFOs in the cerebellar cortex relate to the LFO activity in the cerebral cortex. To test this question, simultaneous optical imaging of the

cerebral cortex and multi-unit extracellular recordings of cerebellar PCs. In this way, the temporal relationship of the onset of LFOs may be compared between these two structures, and the initiating structure identified. Based on previous studies demonstrating that the cerebellum is necessary for episodic attacks (Campbell et al., 1999;Neychev et al., 2008;Raike et al., 2013;Walter et al., 2006;Chen et al., 2009), the hypothesis predicts that the cerebellar cortex initiates the abnormal LFOs in the *tg/tg* mouse CNS. Also, the effect of manipulating the LFOs in the cerebellar cortex has on the cerebral cortex or vice-versa would be studied. For example, how does reducing ACZT or 4-AP applied to the cerebral cortex alter the LFOs in the cerebellum? Conversely, how does blocking LFOs in the cerebellar cortex with L-type Ca^{2+} channel blockers (Chen et al., 2009) effect the LFOs in the cerebral cortex? This set of experiments would be highly informative on how the cerebral cortex and cerebellar cortex interact to generate the LFOs and episodic dystonia.

Literature Cited

Aamand R, Dalsgaard T, Jensen FB, Simonsen U, Roepstorff A, Fago A (2009) Generation of nitric oxide from nitrite by carbonic anhydrase: a possible link between metabolic activity and vasodilation. Am J Physiol Heart Circ Physiol 297:H2068-H2074.

Abbott LC, Isaacs KR, Heckroth JA (1996) Co-localization of tyrosine hydroxylase and zebrin II immunoreactivities in Purkinje cells of the mutant mice, tottering and tottering/leaner. Neuroscience 71:461-475.

Abercrombie ED, Jacobs BL (1987) Single-unit response of noradrenergic neurons in the locus coeruleus of freely moving cats. I. Acutely presented stressful and nonstressful stimuli. J Neurosci 7:2837-2843.

Ahn AH, Dziennis S, Hawkes R, Herrup K (1994) The cloning of zebrin II reveals its identity with aldolase C. Development 120:2081-2090.

Akerboom J, et al. (2012) Optimization of a GCaMP calcium indicator for neural activity imaging. J Neurosci 32:13819-13840.

Albus JS (1971) A theory of cerebellar function. Math Biosci 10:25-61.

Alexander GE, DeLong MR, Strick PL (1986) Parallel organization of functionally segregated circuits linking basal ganglia and cortex. Annu Rev Neurosci 9:357-381.

Alexander GM, Godwin DW (2006) Metabotropic glutamate receptors as a strategic target for the treatment of epilepsy. Epilepsy Res 71:1-22.

Allen GI, Gilbert PF, Marini R, Schultz W, Yin TC (1977) Integration of cerebral and peripheral inputs by interpositus neurons in monkey. Exp Brain Res 27:81-99.

Allen GI, Gilbert PF, Yin TC (1978) Convergence of cerebral inputs onto dentate neurons in monkey. Exp Brain Res 32:151-170.

Allen GI, Tsukahara N (1974) Cerebro-cerebellar communication systems. Physiol Rev 54:957-1006.

Alvina K, Khodakhah K (2010a) KCa channels as therapeutic targets in episodic ataxia type-2. J Neurosci 30:7249-7257.

Alvina K, Khodakhah K (2010b) The therapeutic mode of action of 4-aminopyridine in cerebellar ataxia. J Neurosci 30:7258-7268.

Angner RT, Kelly RM, Wiley RG, Walsh TJ, Reuhl KR (2000) Preferential destruction of cerebellar Purkinje cells by OX7-saporin. Neurotoxicology 21:395-403.

Apps R, Garwicz M (2000) Precise matching of olivo-cortical divergence and cortico-nuclear convergence between somatotopically corresponding areas in the medial C1 and medial C3 zones of the paravermal cerebellum. Eur J Neurosci 12:205-214.

Apps R, Hawkes R (2009) Cerebellar cortical organization: a one-map hypothesis. Nat Rev Neurosci 10:670-681.

Armbrust KR, Wang X, Hathorn TJ, Cramer SW, Chen G, Zu T, Kangas T, Zink AN, Oz G, Ebner TJ, Ranum LP (2014) Mutant beta-III Spectrin Causes mGluR1alpha Mislocalization and Functional Deficits in a Mouse Model of Spinocerebellar Ataxia Type 5. J Neurosci 34:9891-9904.

Armstrong DM, Rawson JA (1979) Activity patterns of cerebellar cortical neurones and climbing fibre afferents in the awake cat. J Physiol 289:425-448.

Asanuma C, Thach WR, Jones EG (1983a) Anatomical evidence for segregated focal groupings of efferent cells and their terminal ramifications in the cerebellothalamic pathway of the monkey. Brain Res 286:267-297.

Asanuma C, Thach WT, Jones EG (1983b) Brainstem and spinal projections of the deep cerebellar nuclei in the monkey, with observations on the brainstem projections of the dorsal column nuclei. Brain Res 286:299-322.

Asanuma C, Thach WT, Jones EG (1983c) Cytoarchitectonic delineation of the ventral lateral thalamic region in the monkey. Brain Res 286:219-235.

Asanuma C, Thach WT, Jones EG (1983d) Distribution of cerebellar terminations and their relation to other afferent terminations in the ventral lateral thalamic region of the monkey. Brain Res 286:237-265.

Attwell D, Buchan AM, Charpak S, Lauritzen M, MacVicar BA, Newman EA (2010) Glial and neuronal control of brain blood flow. Nature 468:232-243.

Austin MC, Schultzberg M, Abbott LC, Montpied P, Evers JR, Paul SM, Crawley JN (1992) Expression of tyrosine hydroxylase in cerebellar Purkinje neurons of the mutant tottering and leaner mouse. Brain Res Mol Brain Res 15:227-240.

Ayata C, Shimizu-Sasamata M, Lo EH, Noebels JL, Moskowitz MA (2000) Impaired neurotransmitter release and elevated threshold for cortical spreading depression in mice with mutations in the alpha1A subunit of P/Q type calcium channels. Neuroscience 95:639-645.

Balaban CD, Fredericks DA, Wurpel JN, Severs WB (1988) Motor disturbances and neurotoxicity induced by centrally administered somatostatin and vasopressin in conscious rats: interactive effects of two neuropeptides. Brain Res 445:117-129.

Balaban CD, Severs WB (1991) Toxic effects of somatostatin in the cerebellum and vestibular nuclei: multiple sites of action. Neurosci Res 12:140-150.

Baloh RW (2012) Episodic ataxias 1 and 2. Handb Clin Neurol 103:595-602.

Baloh RW, Yue Q, Furman JM, Nelson SF (1997) Familial episodic ataxia: clinical heterogeneity in four families linked to chromosome 19p. Ann Neurol 41:8-16.

Bao J, Reim K, Sakaba T (2010) Target-dependent feedforward inhibition mediated by short-term synaptic plasticity in the cerebellum. J Neurosci 30:8171-8179.

Barbour B, Keller BU, Llano I, Marty A (1994) Prolonged presence of glutamate during excitatory synaptic transmission to cerebellar Purkinje cells. Neuron 12:1331-1343.

Barmack NH, Qian Z, Yoshimura J (2000) Regional and cellular distribution of protein kinase C in rat cerebellar Purkinje cells. J Comp Neurol 427:235-254.

Barnes JA, Ebner BA, Duvick LA, Gao W, Chen G, Orr HT, Ebner TJ (2011) Abnormalities in the climbing fiber-Purkinje cell circuitry contribute to neuronal dysfunction in ATXN1[82Q] mice. J Neurosci 31:12778-12789.

Bastian AJ (1997) Mechanisms of ataxia. Phys Ther 77:672-675.

Bell CC, Grimm RJ (1969) Discharge properties of Purkinje cells recorded on single and double microelectrodes. J Neurophysiol 32:1044-1055.

Berridge CW (2008) Noradrenergic modulation of arousal. Brain Res Rev 58:1-17.

Bichet D, Cornet V, Geib S, Carlier E, Volsen S, Hoshi T, Mori Y, De WM (2000) The I-II loop of the Ca2+ channel alpha1 subunit contains an endoplasmic reticulum retention signal antagonized by the beta subunit. Neuron 25:177-190.

Bilak SR, Bilak MM, Morest DK (1995) NMDA receptor expression in the mouse cerebellar cortex. Synapse 20:257-268.

Bosman LW, Koekkoek SK, Shapiro J, Rijken BF, Zandstra F, van der EB, Owens CB, Potters JW, de G, Jr., Ruigrok TJ, De Zeeuw CI (2010) Encoding of whisker input by cerebellar Purkinje cells. J Physiol 588:3757-3783.

Bostan AC, Dum RP, Strick PL (2010) The basal ganglia communicate with the cerebellum. Proc Natl Acad Sci U S A 107:8452-8456.

Bostan AC, Dum RP, Strick PL (2013) Cerebellar networks with the cerebral cortex and basal ganglia. Trends Cogn Sci 17:241-254.

Bostan AC, Strick PL (2010) The cerebellum and basal ganglia are interconnected. Neuropsychol Rev 20:261-270.

Bourinet E, Soong TW, Sutton K, Slaymaker S, Mathews E, Monteil A, Zamponi GW, Nargeot J, Snutch TP (1999) Splicing of alpha 1A subunit gene generates phenotypic variants of P- and Q-type calcium channels. Nat Neurosci 2:407-415.

Bower JM (2002) The organization of cerebellar cortical circuitry revisited: implications for function. Ann NY Acad Sci 978:135-155.

Bower JM (2010) Model-founded explorations of the roles of molecular layer inhibition in regulating purkinje cell responses in cerebellar cortex: more trouble for the beam hypothesis. Front Cell Neurosci 4.

Bower JM, Kassel J (1990) Variability in tactile projection patterns to cerebellar folia crus IIA of the Norway rat. J Comp Neurol 302:768-778.

Bower JM, Woolston DC (1983) Congruence of spatial organization of tactile projections to granule cell and Purkinje cell layers of cerebellar hemispheres of the albino rat: vertical organization of cerebellar cortex. J Neurophysiol 49:745-766.

Braitenberg V (1961) Functional interpretation of cerebellar histology. Nature 190:539-540.

Braitenberg V, Atwood RP (1958) Morphological observations on the cerebellar cortex. J Comp Neurol 109:1-33.

Braitenberg V, Heck D, Sultan F (1997) The detection and generation of sequences as a key to cerebellar function: experiments and theory. Behav Brain Sci 20:229-245.

Brand S, Dahl AL, Mugnaini E (1976) The length of parallel fibers in the cat cerebellar cortex. An experimental light and electron microscopic study. Exp Brain Res 26:39-58.

Brasnjo G, Otis TS (2001) Neuronal glutamate transporters control activation of postsynaptic metabotropic glutamate receptors and influence cerebellar long-term depression. Neuron 31:607-616.

Brochu G, Maler L, Hawkes R (1990) Zebrin II: a polypeptide antigen expressed selectively by Purkinje cells reveals compartments in rat and fish cerebellum. J Comp Neurol 291:538-552.

Brodal A, Kawamura K (1980) Olivocerebellar projection: a review. Adv Anat Embryol Cell Biol 64:1-140.

Buisseret-Delmas C, Angaut P (1993) The cerebellar olivo-corticonuclear connections in the rat. Prog Neurobiol 40:63-87.

Burk K, Zuhlke C, Konig IR, Ziegler A, Schwinger E, Globas C, Dichgans J, Hellenbroich Y (2004) Spinocerebellar ataxia type 5: clinical and molecular genetic features of a German kindred. Neurology 62:327-329.

Buzsaki G, Wang XJ (2012) Mechanisms of gamma oscillations. Annu Rev Neurosci 35:203-225.

Caddick SJ, Wang C, Fletcher CF, Jenkins NA, Copeland NG, Hosford DA (1999) Excitatory but not inhibitory synaptic transmission is reduced in lethargic (Cacnb4(lh)) and tottering (Cacna1a(tg)) mouse thalami. J Neurophysiol 81:2066-2074.

Caddy KW, Biscoe TJ (1979) Structural and quantitative studies on the normal C3H and Lurcher mutant mouse. Philos Trans R Soc Lond B Biol Sci 287:167-201.

Calabrese V, Mancuso C, Calvani M, Rizzarelli E, Butterfield DA, Stella AM (2007) Nitric oxide in the central nervous system: neuroprotection versus neurotoxicity. Nat Rev Neurosci 8:766-775.

Calderon DP, Fremont R, Kraenzlin F, Khodakhah K (2011) The neural substrates of rapid-onset Dystonia-Parkinsonism. Nat Neurosci 14:357-365.

Campbell DB, Hess EJ (1999) L-type calcium channels contribute to the tottering mouse dystonic episodes. Mol Pharmacol 55:23-31.

Campbell DB, Hess EJ (1998) Cerebellar circuitry is activated during convulsive episodes in the tottering (tg/tg) mutant mouse. Neuroscience 85:773-783.

Campbell DB, North JB, Hess EJ (1999) Tottering mouse motor dysfunction is abolished on the Purkinje cell degeneration (pcd) mutant background. Exp Neurol 160:268-278.

Carabelli V, D'Ascenzo M, Carbone E, Grassi C (2002) Nitric oxide inhibits neuroendocrine Ca(V)1 L-channel gating via cGMP-dependent protein kinase in cell-attached patches of bovine chromaffin cells. J Physiol 541:351-366.

Carter AG, Regehr WG (2000) Prolonged synaptic currents and glutamate spillover at the parallel fiber to stellate cell synapse. J Neurosci 20:4423-4434.

Carter AG, Vogt KE, Foster KA, Regehr WG (2002) Assessing the role of calcium-induced calcium release in short-term presynaptic plasticity at excitatory central synapses. J Neurosci 22:21-28.

Catterall WA (1998) Structure and function of neuronal Ca2+ channels and their role in neurotransmitter release. Cell Calcium 24:307-323.

Chadderton P, Margrie TW, Hausser M (2004) Integration of quanta in cerebellar granule cells during sensory processing. Nature 428:856-860.

Chagnac-Amitai Y, Connors BW (1989) Horizontal spread of synchronized activity in neocortex and its control by GABA-mediated inhibition. J Neurophysiol 61:747-758.

Charcot J.M., Pitres A. (1877) Contribution a l'etude des localisations dans l'ecorse des hemispheres du cerveau. Revue mensuelle de medecine et de chirurgie 1:1-18, 113-123, 180-195, 357-376, 437-457.

Chaudhry FA, Lehre KP, van Lookeren CM, Ottersen OP, Danbolt NC, Storm-Mathisen J (1995) Glutamate transporters in glial plasma membranes: highly differentiated localizations revealed by quantitative ultrastructural immunocytochemistry. Neuron 15:711-720.

Chaudhuri D, Chang SY, DeMaria CD, Alvania RS, Soong TW, Yue DT (2004) Alternative splicing as a molecular switch for Ca2+/calmodulin-dependent facilitation of P/Q-type Ca2+ channels. J Neurosci 24:6334-6342.

Chaumont J, Guyon N, Valera AM, Dugue GP, Popa D, Marcaggi P, Gautheron V, Reibel-Foisset S, Dieudonne S, Stephan A, Barrot M, Cassel JC, Dupont JL, Doussau F, Poulain B, Selimi F, Lena C, Isope P (2013) Clusters of cerebellar Purkinje cells control their afferent climbing fiber discharge. Proc Natl Acad Sci U S A 110:16223-16228.

Chen C, Schofield GG (1995) Nitric oxide donors enhanced Ca2+ currents and blocked noradrenaline-induced Ca2+ current inhibition in rat sympathetic neurons. J Physiol 482 (Pt 3):521-531.

Chen G, Cramer SW, Ranum LPW, Swanson MS, Ebner TJ (2013) Autofluorescence optical imaging of the responses to intracortical stimulation in normal and mouse models of myotonic dystrophy. Soc Neurosci Abstr 530.09.

Chen G, Hanson CL, Ebner TJ (1996) Functional parasagittal compartments in the rat cerebellar cortex: an in vivo optical imaging study using neutral red. J Neurophysiol 76:4169-4174.

Chen G, Hanson CL, Ebner TJ (1998) Optical responses evoked by cerebellar surface stimulation *in vivo* using neutral red. Neuroscience 84:645-668.

Chen G, Popa LS, Wang X, Gao W, Barnes J, Hendrix CM, Hess EJ, Ebner TJ (2009) Low frequency oscillations in the cerebellar cortex of the tottering mouse. J Neurophysiol 101:234-245.

Chen J, Daggett H, De WM, Heinemann SH, Hoshi T (2002) Nitric oxide augments voltage-gated P/Q-type Ca(2+) channels constituting a putative positive feedback loop. Free Radic Biol Med 32:638-649.

Chen S, Hillman DE (1993) Compartmentation of the cerebellar cortex by protein kinase C delta. Neuroscience 56:177-188.

Chen X, Kovalchuk Y, Adelsberger H, Henning HA, Sausbier M, Wietzorrek G, Ruth P, Yarom Y, Konnerth A (2010) Disruption of the olivo-cerebellar circuit by Purkinje neuron-specific ablation of BK channels. Proc Natl Acad Sci U S A 107:12323-12328.

Chockkan V, Hawkes R (1994) Functional and antigenic maps in the rat cerebellum: zebrin compartmentation and vibrissal receptive fields in lobule IXa. J Comp Neurol 345:33-45.

Chung S, Zhang Y, Van Der HF, Hawkes R (2007) The anatomy of the cerebellar nuclei in the normal and scrambler mouse as revealed by the expression of the microtubule-associated protein kinesin light chain 3. Brain Res 1140:120-131.

Cohen D, Yarom Y (1998) Patches of synchronized activity in the cerebellar cortex evoked by mossy-fiber stimulation: questioning the role of parallel fibers. Proc Natl Acad Sci U S A 95:15032-15036.

Cohen D, Yarom Y (1999) Optical measurements of synchronized activity in isolated mammalian cerebellum. Neuroscience 94:859-866.

Coutinho V, Mutoh H, Knopfel T (2004) Functional topology of the mossy fibre-granule cell--Purkinje cell system revealed by imaging of intrinsic fluorescence in mouse cerebellum. Eur J Neurosci 20:740-748.

Cramer SW, Gao W, Chen G, Ebner TJ (2013) Reevaluation of the beam and radial hypotheses of parallel fiber action in the cerebellar cortex. J Neurosci 33:11412-11424.

Crepel F (2007) Developmental changes in retrograde messengers involved in depolarization-induced suppression of excitation at parallel fiber-Purkinje cell synapses in rodents. J Neurophysiol 97:824-836.

D'Angelo E, De FG, Rossi P, Taglietti V (1995) Synaptic excitation of individual rat cerebellar granule cells in situ: evidence for the role of NMDA receptors. J Physiol 484 (Pt 2):397-413.

D'Ascenzo M, Martinotti G, Azzena GB, Grassi C (2002) cGMP/protein kinase G-dependent inhibition of N-type Ca2+ channels induced by nitric oxide in human neuroblastoma IMR32 cells. J Neurosci 22:7485-7492.

D'Ascenzo M, Vairano M, Andreassi C, Navarra P, Azzena GB, Grassi C (2004) Electrophysiological and molecular evidence of L-(Cav1), N- (Cav2.2), and R-(Cav2.3) type Ca2+ channels in rat cortical astrocytes. Glia 45:354-363.

De Zeeuw CI, Koekkoek SK, Wylie DR, Simpson JI (1997) Association between dendritic lamellar bodies and complex spike synchrony in the olivocerebellar system. J Neurophysiol 77:1747-1758.

De PR, Sherman SM (2012) Modulatory effects of metabotropic glutamate receptors on local cortical circuits. J Neurosci 32:7364-7372.

De WM, Pragnell M, Campbell KP (1994) Ca2+ channel regulation by a conserved beta subunit domain. Neuron 13:495-503.

DeFelipe J, onso-Nanclares L, Arellano JI (2002) Microstructure of the neocortex: comparative aspects. J Neurocytol 31:299-316.

Dehnes Y, Chaudhry FA, Ullensvang K, Lehre KP, Storm-Mathisen J, Danbolt NC (1998) The glutamate transporter EAAT4 in rat cerebellar Purkinje cells: a glutamate-gated chloride channel concentrated near the synapse in parts of the dendritic membrane facing astroglia. J Neurosci 18:3606-3619.

Denier C, Ducros A, Vahedi K, Joutel A, Thierry P, Ritz A, Castelnovo G, Deonna T, Gerard P, Devoize JL, Gayou A, Perrouty B, Soisson T, Autret A, Warter JM, Vighetto A, van Bogaert P, Alamowitch S, Roullet E, Tournier-Lasserve E (1999) High prevalence of CACNA1A truncations and broader clinical spectrum in episodic ataxia type 2. Neurology 52:1816-1821.

Devonshire IM, Dommett EJ, Grandy TH, Halliday AC, Greenfield SA (2010) Environmental enrichment differentially modifies specific components of sensory-evoked activity in rat barrel cortex as revealed by simultaneous electrophysiological recordings and optical imaging in vivo. Neuroscience 170:662-669.

Dichter MA, Ayala GF (1987) Cellular mechanisms of epilepsy: a status report. Science 237:157-164.

Diener HC, Dichgans J (1992) Pathophysiology of cerebellar ataxia. Mov Disord 7:95-109.

Dizon MJ, Khodakhah K (2011) The role of interneurons in shaping Purkinje cell responses in the cerebellar cortex. J Neurosci 31:10463-10473.

Dow RS, Moruzzi G (1958) The physiology and pathology of the cerebellum. Minneapolis: University of Minnesota Press.

Drew PJ, Shih AY, Driscoll JD, Knutsen PM, Blinder P, Davalos D, Akassoglou K, Tsai PS, Kleinfeld D (2010) Chronic optical access through a polished and reinforced thinned skull. Nat Methods 7:981-984.

Drew PJ, Shih AY, Kleinfeld D (2011) Fluctuating and sensory-induced vasodynamics in rodent cortex extend arteriole capacity. Proc Natl Acad Sci U S A 108:8473-8478.

DU X, Wang J, Zhu H, Rinaldo L, Lamar KM, Palmenberg AC, Hansel C, Gomez CM (2013) Second cistron in CACNA1A gene encodes a transcription factor mediating cerebellar development and SCA6. Cell 154:118-133.

Duguid IC, Pankratov Y, Moss GW, Smart TG (2007) Somatodendritic release of glutamate regulates synaptic inhibition in cerebellar Purkinje cells via autocrine mGluR1 activation. J Neurosci 27:12464-12474.

Dzubay JA, Jahr CE (1999) The concentration of synaptically released glutamate outside of the climbing fiber-Purkinje cell synaptic cleft. J Neurosci 19:5265-5274.

Ebner BA, Ingram MA, Barnes JA, Duvick LA, Frisch JL, Clark HB, Zoghbi HY, Ebner TJ, Orr HT (2013) Purkinje cell ataxin-1 modulates climbing fiber synaptic input in developing and adult mouse cerebellum. J Neurosci in press.

Ebner TJ, Bloedel JR (1981) Temporal patterning in simple spike discharge of Purkinje cells and its relationship to climbing fiber activity. J Neurophysiol 45:933-947.

Ebner TJ, Chen G (2012) Tottering Mouse. In: Handbook of the Cerebellum and Cerebellar Disorders (Guol D, Koibuchi N, Manto M, Rossi F, Schmahmann JD, eds), New York: Springer.

Ebner TJ, Wang X, Gao W, Cramer SW, Chen G (2012) Parasagittal zones in the cerebellar cortex differ in excitability, information processing, and synaptic plasticity. Cerebellum 11:418-419.

ECCLES J, Llinas R, Sasaki K (1964) EXCITATION OF CEREBELLAR PURKINJE CELLS BY THE CLIMBING FIBRES. Nature 203:245-246.

Eccles JC, Ito M, Szentagothai J (1967) The Cerebellum as a Neuronal Machine. Berlin: Springer-Verlag.

Eccles JC, Llinas R, Sasaki K (1966b) The excitatory synaptic action of climbing fibres on the purkinje cells of the cerebellum. J Physiol 182:268-296.

Eccles JC, Llinas R, Sasaki K (1966a) Parallel fibre stimulation and the responses induced thereby in the Purkinje cells of the cerebellum. Exp Brain Res 1:17-39.

Ekerot CF, Jorntell H (2003) Parallel fiber receptive fields: a key to understanding cerebellar operation and learning. Cerebellum 2:101-109.

Ekerot CF, Jorntell H (2001) Parallel fibre receptive fields of Purkinje cells and interneurons are climbing fibre-specific. Eur J Neurosci 13:1303-1310.

Erickson MA, Haburcak M, Smukler L, Dunlap K (2007) Altered functional expression of Purkinje cell calcium channels precedes motor dysfunction in tottering mice. Neuroscience 150:547-555.

Evarts EV, Thach WT (1969) Motor mechanisms of the CNS: cerebrocerebellar interrelations. Annu Rev Physiol 31:451-498.

Fan X, Hughes KE, Jinnah HA, Hess EJ (2012) Selective and sustained alpha-amino-3-hydroxy-5-methyl-4-isoxazolepropionic acid receptor activation in cerebellum induces dystonia in mice. J Pharmacol Exp Ther 340:733-741.

Faraci FM (1992) Regulation of the cerebral circulation by endothelium. Pharmacol Ther 56:1-22.

Fenno L, Yizhar O, Deisseroth K (2011) The development and application of optogenetics. Annu Rev Neurosci 34:389-412.

Ferraguti F, Shigemoto R (2006) Metabotropic glutamate receptors. Cell Tissue Res 326:483-504.

Fletcher CF, Lutz CM, O'Sullivan TN, Shaughnessy JD, Jr., Hawkes R, Frankel WN, Copeland NG, Jenkins NA (1996) Absence epilepsy in tottering mutant mice is associated with calcium channel defects. Cell 87:607-617.

Fletcher CF, Tottene A, Lennon VA, Wilson SM, Dubel SJ, Paylor R, Hosford DA, Tessarollo L, McEnery MW, Pietrobon D, Copeland NG, Jenkins NA (2001) Dystonia and cerebellar atrophy in Cacna1a null mice lacking P/Q calcium channel activity. FASEB J 15:1288-1290.

Forti L, Pouzat C, Llano I (2000) Action potential-evoked Ca^{2+} signals and calcium channels in axons of developing rat cerebellar interneurones. J Physiol 527 Pt 1:33-48.

Fortier PA, Kalaska JF, Smith AM (1989) Cerebellar neuronal activity related to whole-arm reaching movements in the monkey. J Neurophysiol 62:198-211.

Frank-Cannon TC, Zeve DR, Abbott LC (2007) Developmental expression of neuronal nitric oxide synthase in P/Q-type voltage-gated calcium ion channel mutant mice, leaner and tottering. Brain Res 1140:96-104.

Fremont R, Khodakhah K (2012) Alternative approaches to modeling hereditary dystonias. Neurotherapeutics 9:315-322.

Fujita H, Aoki H, Ajioka I, Yamazaki M, Abe M, Oh-Nishi A, Sakimura K, Sugihara I (2014) Detailed expression pattern of aldolase C (Aldoc) in the cerebellum, retina and other areas of the CNS studied in Aldoc-Venus knock-in mice. PLoS ONE 9:e86679.

Fureman BE, Hess EJ (2005) Noradrenergic blockade prevents attacks in a model of episodic dysfunction caused by a channelopathy. Neurobiol Dis 20:227-232.

Fureman BE, Jinnah HA, Hess EJ (2002) Triggers of paroxysmal dyskinesia in the calcium channel mouse mutant tottering. Pharmacol Biochem Behav 73:631-637.

Gao W, Chen G, Reinert KC, Ebner TJ (2006) Cerebellar cortical molecular layer inhibition is organized in parasagittal zones. J Neurosci 26:8377-8387.

Gao W, Dunbar RL, Chen G, Reinert KC, Oberdick J, Ebner TJ (2003) Optical imaging of long-term depression in the mouse cerebellar cortex *in vivo*. J Neurosci 23:1859-1866.

Garwicz M, Andersson G (1992) Spread of synaptic activity along parallel fibres in cat cerebellar anterior lobe. Exp Brain Res 88:615-622.

Garwicz M, Jorntell H, Ekerot CF (1998) Cutaneous receptive fields and topography of mossy fibres and climbing fibres projecting to cat cerebellar C3 zone. J Physiol 512 (Pt 1):277-293.

Gincel D, Regan MR, Jin L, Watkins AM, Bergles DE, Rothstein JD (2007) Analysis of cerebellar Purkinje cells using EAAT4 glutamate transporter promoter reporter in mice generated via bacterial artificial chromosome-mediated transgenesis. Exp Neurol 203:205-212.

Glasauer S, Rossert C, Strupp M (2011) The role of regularity and synchrony of cerebellar Purkinje cells for pathological nystagmus. Ann N Y Acad Sci 1233:162-167.

Glickstein M, May JG, III, Mercier BE (1985) Corticopontine projection in the macaque: the distribution of labelled cortical cells after large injections of horseradish peroxidase in the pontine nuclei. J Comp Neurol 235:343-359.

Glynn D, Drew CJ, Reim K, Brose N, Morton AJ (2005) Profound ataxia in complexin I knockout mice masks a complex phenotype that includes exploratory and habituation deficits. Hum Mol Genet 14:2369-2385.

Green MC, Sidman RL (1962) Tottering--a neuromusclar mutation in the mouse and its linkage with oligosyndacylism. J Hered 53:233-237.

Griggs RC, Moxley RT, III, Lafrance RA, McQuillen J (1978) Hereditary paroxysmal ataxia: response to acetazolamide. Neurology 28:1259-1264.

Gundappa-Sulur G, De SE, Bower JM (1999) Ascending granule cell axon: an important component of cerebellar cortical circuitry. J Comp Neurol 408:580-596.

Haider B, Duque A, Hasenstaub AR, McCormick DA (2006) Neocortical network activity in vivo is generated through a dynamic balance of excitation and inhibition. J Neurosci 26:4535-4545.

Haines DE, Patrick GW, Saterlee P (1982) In: The Cerebellum-New Vista (Palsy SL, Chan-Palay V, eds), pp 320-367. New York: Springer-Verlag.

Hallem JS, Thompson JH, Gundappa-Sulur G, Hawkes R, Bjaalie JG, Bower JM (1999) Spatial correspondence between tactile projection patterns and the distribution of the antigenic purkinje cell markers anti-zebrin I and anti-zebrin II in the cerebellar folium crus IIa of the rat. Neuroscience 93:1083-1094.

Hansel C, Linden DJ, D'Angelo E (2001) Beyond parallel fiber LTD: the diversity of synaptic and non-synaptic plasticity in the cerebellum. Nat Neurosci 4:467-475.

Hartmann J, Konnerth A (2009) Mechanisms of metabotropic glutamate receptor-mediated synaptic signaling in cerebellar Purkinje cells. Acta Physiol 195:79-90.

Harvey RJ, Napper RM (1991) Quantitative studies on the mammalian cerebellum. Prog Neurobiol 36:437-463.

Hausser M, Clark BA (1997) Tonic synaptic inhibition modulates neuronal output pattern and spatiotemporal synaptic integration. Neuron 19:665-678.

Hausser M, Raman IM, Otis T, Smith SL, Nelson A, du LS, Loewenstein Y, Mahon S, Pennartz C, Cohen I, Yarom Y (2004) The beat goes on: spontaneous firing in mammalian neuronal microcircuits. J Neurosci 24:9215-9219.

Hawkes R, Colonnier M, Leclerc N (1985) Monoclonal antibodies reveal sagittal banding in the rodent cerebellar cortex. Brain Res 333:359-365.

Hawkes R, Herrup K (1995) Aldolase C/zebrin II and the regionalization of the cerebellum. J Mol Neurosci 6:147-158.

Hawkes R, Leclerc N (1987) Antigenic map of the rat cerebellar cortex: the distribution of parasagittal bands as revealed by monoclonal anti-Purkinje cell antibody mabQ113. J Comp Neurol 256:29-41.

Heck DH, Thach WT, Keating JG (2007) On-beam synchrony in the cerebellum as the mechanism for the timing and coordination of movement. Proc Natl Acad Sci U S A 104:7658-7663.

Heckroth JA, Abbott LC (1994) Purkinje cell loss from alternating sagittal zones in the cerebellum of leaner mutant mice. Brain Res 658:93-104.

Heiney SA, Kim J, Augustine GJ, Medina JF (2014) Precise control of movement kinematics by optogenetic inhibition of Purkinje cell activity. J Neurosci 34:2321-2330.

Heller AH, Dichter MA, Sidman RL (1983) Anticonvulsant sensitivity of absence seizures in the tottering mutant mouse. Epilepsia 24:25-34.

Helmich RC, Siebner HR, Giffin N, Bestmann S, Rothwell JC, Bloem BR (2010) The dynamic regulation of cortical excitability is altered in episodic ataxia type 2. Brain 133:3519-3529.

Hess EJ, Wilson MC (1991) Tottering and leaner mutations perturb transient developmental expression of tyrosine hydroxylase in embryologically distinct Purkinje cells. Neuron 6:123-132.

Hirono M, Obata K (2006) Alpha-adrenoceptive dual modulation of inhibitory GABAergic inputs to Purkinje cells in the mouse cerebellum. J Neurophysiol 95:700-708.

Hirooka K, Kourennyi DE, Barnes S (2000) Calcium channel activation facilitated by nitric oxide in retinal ganglion cells. J Neurophysiol 83:198-206.

Hishida R, Watanabe K, Kudoh M, Shibuki K (2011) Transcranial electrical stimulation of cortico-cortical connections in anesthetized mice. J Neurosci Methods 201:315-321.

Hobom M, Dai S, Marais E, Lacinova L, Hofmann F, Klugbauer N (2000) Neuronal distribution and functional characterization of the calcium channel alpha2delta-2 subunit. Eur J Neurosci 12:1217-1226.

Hoebeek FE, Khosrovani S, Witter L, De Zeeuw CI (2008) Purkinje cell input to cerebellar nuclei in tottering: ultrastructure and physiology. Cerebellum 7:547-558.

Hoebeek FE, Stahl JS, van Alphen AM, Schonewille M, Luo C, Rutteman M, van den Maagdenberg AM, Molenaar PC, Goossens HH, Frens MA, De Zeeuw CI (2005) Increased noise level of purkinje cell activities minimizes impact of their modulation during sensorimotor control. Neuron 45:953-965.

Hoffer BJ, Siggins GR, Oliver AP, Bloom FE (1973) Activation of the pathway from locus coeruleus to rat cerebellar Purkinje neurons: pharmacological evidence of noradrenergic central inhibition. J Pharmacol Exp Ther 184:553-569.

Holmes G (1939) The cerebellum of man. Brain 62:1-30.

Holmes G (1917) The symptoms of acute cerebellar injuries due to gunshot injuries. Brain 40:461-535.

Holtzman T, Rajapaksa T, Mostofi A, Edgley SA (2006) Different responses of rat cerebellar Purkinje cells and Golgi cells evoked by widespread convergent sensory inputs. J Physiol 574:491-507.

Horn KM, Deep A, Gibson AR (2013) Progressive limb ataxia following inferior olive lesions. J Physiol 591:5475-5489.

Hoshi E, Tremblay L, Feger J, Carras PL, Strick PL (2005) The cerebellum communicates with the basal ganglia. Nat Neurosci 8:1491-1493.

Houweling AR, Brecht M (2008) Behavioural report of single neuron stimulation in somatosensory cortex. Nature 451:65-68.

Huang CM, Miyamoto H, Huang RH (2006a) The mouse cerebellum from 1 to 34 months: parallel fibers. Neurobiol Aging 27:1715-1718.

Huang CM, Wang L, Huang RH (2006b) Cerebellar granule cell: ascending axon and parallel fiber. Eur J Neurosci 23:1731-1737.

Ikeda Y, Dick KA, Weatherspoon MR, Gincel D, Armbrust KR, Dalton JC, Stevanin G, Durr A, Zuhlke C, Burk K, Clark HB, Brice A, Rothstein JD, Schut LJ, Day JW, Ranum LP (2006) Spectrin mutations cause spinocerebellar ataxia type 5. Nat Genet 38:184-190.

Indriati DW, Kamasawa N, Matsui K, Meredith AL, Watanabe M, Shigemoto R (2013) Quantitative localization of Cav2.1 (P/Q-type) voltage-dependent calcium channels in Purkinje cells: somatodendritic gradient and distinct somatic coclustering with calcium-activated potassium channels. J Neurosci 33:3668-3678.

Isaacs KR, Abbott LC (1995) Cerebellar volume decreases in the tottering mouse are specific to the molecular layer. Brain Res Bull 36:309-314.

Isope P, Barbour B (2002) Properties of unitary granule cell-->Purkinje cell synapses in adult rat cerebellar slices. J Neurosci 22:9668-9678.

Isope P, Dieudonne S, Barbour B (2002) Temporal organization of activity in the cerebellar cortex: a manifesto for synchrony. Ann N Y Acad Sci 978:164-174.

Ito M (2006) Cerebellar circuitry as a neuronal machine. Prog Neurobiol 78:272-303.

Ito M (2002) Historical review of the significance of the cerebellum and the role of Purkinje cells in motor learning. Ann NY Acad Sci 978:273-288.

Ito M, Kano M (1982) Long-lasting depression of parallel fiber-Purkinje cell transmission induced by conjunctive stimulation of parallel fibers and climbing fibers in the cerebellar cortex. Neurosci Lett 33:253-258.

Ito M, Yoshida M, Obata K, Kawai N, Udo M (1970) Inhibitory control of intracerebellar nuclei by the purkinje cell axons. Exp Brain Res 10:64-80.

Iwasaki S, Momiyama A, Uchitel OD, Takahashi T (2000) Developmental changes in calcium channel types mediating central synaptic transmission. J Neurosci 20:59-65.

Jackman SL, Beneduce BM, Drew IR, Regehr WG (2014) Achieving high-frequency optical control of synaptic transmission. J Neurosci 34:7704-7714.

Jackson JH (1870) A study of convulsions. Transactions of the St Andrews Medical Graduates Association 3:162-204.

Jackson M, Song W, Liu MY, Jin L, Dykes-Hoberg M, Lin CI, Bowers WJ, Federoff HJ, Sternweis PC, Rothstein JD (2001) Modulation of the neuronal glutamate transporter EAAT4 by two interacting proteins. Nature 410:89-93.

Jaeger D, Bower JM (1994) Prolonged responses in rat cerebellar Purkinje cells following activation of the granule cell layer: an intracellular in vitro and in vivo investigation. Exp Brain Res 100:200-214.

Jen J, Kim GW, Baloh RW (2004) Clinical spectrum of episodic ataxia type 2. Neurology 62:17-22.

Jen J, Wan J, Graves M, Yu H, Mock AF, Coulin CJ, Kim G, Yue Q, Papazian DM, Baloh RW (2001) Loss-of-function EA2 mutations are associated with impaired neuromuscular transmission. Neurology 57:1843-1848.

Jen JC, Graves TD, Hess EJ, Hanna MG, Griggs RC, Baloh RW (2007) Primary episodic ataxias: diagnosis, pathogenesis and treatment. Brain 130:2484-2493.

Ji Z, Hawkes R (1994) Topography of Purkinje cell compartments and mossy fiber terminal fields in lobules II and III of the rat cerebellar cortex: spinocerebellar and cuneocerebellar projections. Neuroscience 61:935-954.

Jian K, Chen M, Cao X, Zhu XH, Fung ML, Gao TM (2007) Nitric oxide modulation of voltage-gated calcium current by S-nitrosylation and cGMP pathway in cultured rat hippocampal neurons. Biochem Biophys Res Commun 359:481-485.

Jorntell H, Ekerot CF (2002) Reciprocal bidirectional plasticity of parallel fiber receptive fields in cerebellar Purkinje cells and their afferent interneurons. Neuron 34:797-806.

Jörntell H, Ekerot CF (2002) Reciprocal bidirectional plasticity of parallel fiber receptive fields in cerebellar purkinje cells and their afferent interneurons. Neuron 34:797-806.

Jouvenceau A, Eunson LH, Spauschus A, Ramesh V, Zuberi SM, Kullmann DM, Hanna MG (2001) Human epilepsy associated with dysfunction of the brain P/Q-type calcium channel. Lancet 358:801-807.

Jung J, Testard H, Tournier-Lasserve E, Riant F, Vallet AE, Berroir S, Broussolle E (2010) Phenotypic variability of episodic ataxia type 2 mutations: a family study. Eur Neurol 64:114-116.

Kaja S, Hann V, Payne HL, Thompson CL (2007a) Aberrant cerebellar granule cell-specific GABA(A) receptor expression in the epileptic and ataxic mouse mutant, Tottering. Neuroscience 148:115-125.

Kaja S, van d, V, Broos LA, Frants RR, Ferrari MD, van den Maagdenberg AM, Plomp JJ (2007b) Characterization of acetylcholine release and the compensatory contribution of non-Ca(v)2.1 channels at motor nerve terminals of leaner Ca(v)2.1-mutant mice. Neuroscience 144:1278-1287.

Kano M, Garaschuk O, Verkhratsky A, Konnerth A (1995) Ryanodine receptor-mediated intracellular calcium release in rat cerebellar Purkinje neurones. J Physiol 487 (Pt 1):1-16.

Kanumilli S, Tringham EW, Payne CE, Dupere JR, Venkateswarlu K, Usowicz MM (2006) Alternative splicing generates a smaller assortment of CaV2.1 transcripts in cerebellar Purkinje cells than in the cerebellum. Physiol Genomics 24:86-96.

Kao CY (1966) Tetrodotoxin, saxitoxin and their significance in the study of excitation phenomena. Pharmacol Rev 18:997-1049.

Kaplan BJ, Seyfried TN, Glaser GH (1979) Spontaneous polyspike discharges in an epileptic mutant mouse (tottering). Exp Neurol 66:577-586.

Karavanova I, Vasudevan K, Cheng J, Buonanno A (2007) Novel regional and developmental NMDA receptor expression patterns uncovered in NR2C subunit-beta-galactosidase knock-in mice. Mol Cell Neurosci 34:468-480.

Kassel J (1980) Superior colliculus projections to tactile areas of rat cerebellar hemispheres. Brain Res 202:291-305.

Kassel J, Shambes GM, Welker W (1984) Fractured cutaneous projections to the granule cell layer of the posterior cerebellar hemisphere of the domestic cat. J Comp Neurol 225:458-468.

Keating JG, Thach WT (1995) Nonclock behavior of inferior olive neurons: interspike interval of Purkinje cell complex spike discharge in the awake behaving monkey is random. J Neurophysiol 73:1329-1340.

Khalilov I, Holmes GL, Ben-Ari Y (2003) In vitro formation of a secondary epileptogenic mirror focus by interhippocampal propagation of seizures. Nat Neurosci 6:1079-1085.

Kodama T, Itsukaichi-Nishida Y, Fukazawa Y, Wakamori M, Miyata M, Molnar E, Mori Y, Shigemoto R, Imoto K (2006) A CaV2.1 calcium channel mutation rocker reduces the number of postsynaptic AMPA receptors in parallel fiber-Purkinje cell synapses. Eur J Neurosci 24:2993-3007.

Kondo S, Marty A (1997) Protein kinase A-mediated enhancement of miniature IPSC frequency by noradrenaline in rat cerebellar stellate cells. J Physiol 498:165-176.

Korbo L, Andersen BB, Ladefoged O, Moller A (1993) Total numbers of various cell types in rat cerebellar cortex estimated using an unbiased stereological method. Brain Res 609:262-268.

Kostopoulos G, Veronikis DK, Efthimiou I (1987) Caffeine blocks absence seizures in the tottering mutant mouse. Epilepsia 28:415-420.

Kramer PL, Yue Q, Gancher ST, Nutt JG, Baloh R, Smith E, Browne D, Bussey K, Lovrien E, Nelson S, . (1995) A locus for the nystagmus-associated form of

episodic ataxia maps to an 11-cM region on chromosome 19p. Am J Hum Genet 57:182-185.

Kulik A, Haentzsch A, Luckermann M, Reichelt W, Ballanyi K (1999) Neuron-glia signaling via alpha(1) adrenoceptor-mediated $Ca^{(2+)}$ release in Bergmann glial cells in situ. J Neurosci 19:8401-8408.

Kulik A, Nakadate K, Hagiwara A, Fukazawa Y, Lujan R, Saito H, Suzuki N, Futatsugi A, Mikoshiba K, Frotscher M, Shigemoto R (2004) Immunocytochemical localization of the alpha 1A subunit of the P/Q-type calcium channel in the rat cerebellum. Eur J Neurosci 19:2169-2178.

Kullmann DM (2010) Neurological channelopathies. Annu Rev Neurosci 33:151-172.

Larouche M, Hawkes R (2006) From clusters to stripes: the developmental origins of adult cerebellar compartmentation. Cerebellum 5:77-88.

Latour I, Hamid J, Beedle AM, Zamponi GW, MacVicar BA (2003) Expression of voltage-gated Ca2+ channel subtypes in cultured astrocytes. Glia 41:347-353.

Leclerc N, Schwarting GA, Herrup K, Hawkes R, Yamamoto M (1992) Compartmentation in mammalian cerebellum: Zebrin II and P-path antibodies define three classes of sagittally organized bands of Purkinje cells. Proc Natl Acad Sci U S A 89:5006-5010.

Lee AK, Manns ID, Sakmann B, Brecht M (2006) Whole-cell recordings in freely moving rats. Neuron 51:399-407.

Lehre KP, Danbolt NC (1998) The number of glutamate transporter subtype molecules at glutamatergic synapses: chemical and stereological quantification in young adult rat brain. J Neurosci 18:8751-8757.

Lev-Ram V, Wong ST, Storm DR, Tsien RY (2002) A new form of cerebellar long-term potentiation is postsynaptic and depends on nitric oxide but not cAMP. Proc Natl Acad Sci U S A 99:8389-8393.

Levenes C, Daniel H, Crepel F (2001) Retrograde modulation of transmitter release by postsynaptic subtype 1 metabotropic glutamate receptors in the rat cerebellum. J Physiol 537:125-140.

Levitt P (1988) Normal pharmacological and morphometric parameters in the noradrenergic hyperinnervated mutant mouse, "tottering". Cell Tissue Res 252:175-180.

Levitt P, Lau C, Pylypiw A, Ross LL (1987) Central adrenergic receptor changes in the inherited noradrenergic hyperinnervated mutant mouse tottering. Brain Res 418:174-177.

Levitt P, Noebels JL (1981) Mutant mouse tottering: selective increase of locus ceruleus axons in a defined single-locus mutation. Proc Natl Acad Sci USA 78:4630-4634.

Liles WC, Taylor S, Finnell R, Lai H, Nathanson NM (1986) Decreased muscarinic acetylcholine receptor number in the central nervous system of the tottering (tg/tg) mouse. J Neurochem 46:977-982.

Liljelund P, Netzeband JG, Gruol DL (2000) L-Type calcium channels mediate calcium oscillations in early postnatal Purkinje neurons. J Neurosci 20:7394-7403.

Llano DA, Theyel BB, Mallik AK, Sherman SM, Issa NP (2009) Rapid and sensitive mapping of long-range connections in vitro using flavoprotein autofluorescence imaging combined with laser photostimulation. J Neurophysiol 101:3325-3340.

Llinas R, Sugimori M, Hillman DE, Cherksey B (1992) Distribution and functional significance of the P-type, voltage-dependent Ca2+ channels in the mammalian central nervous system. Trends Neurosci 15:351-355.

Llinas RR (1982) Radial connectivity in the cerebellar cortex: A novel view regarding the functional organization of the molecular layer. Exp Brain Res 6:189-194.

Llinas RR (1981) Electrophysiology of the cerebellar networks. In: Handbook of Physiology. Section 1. The nervous system. Vol. II. Motor control, Part 2 (Brookhart JM, Mountcastle VB, Brooks VB, Geiger SR, eds), pp 831-876. Bethesda, MD: American Physiol. Society.

Lohle M, Schrempf W, Wolz M, Reichmann H, Storch A (2008) Potassium channel blocker 4-aminopyridine is effective in interictal cerebellar symptoms in episodic ataxia type 2--a video case report. Mov Disord 23:1314-1316.

Lonchamp E, Gambino F, Dupont JL, Doussau F, Valera A, Poulain B, Bossu JL (2012) Pre and post synaptic NMDA effects targeting Purkinje cells in the mouse cerebellar cortex. PLoS ONE 7:e30180.

Lu H, Esquivel AV, Bower JM (2009) 3D electron microscopic reconstruction of segments of rat cerebellar Purkinje cell dendrites receiving ascending and parallel fiber granule cell synaptic inputs. J Comp Neurol 514:583-594.

Lundh H (1978) Effects of 4-aminopyridine on neuromuscular transmission. Brain Res 153:307-318.

Luvisetto S, Fellin T, Spagnolo M, Hivert B, Brust PF, Harpold MM, Stauderman KA, Williams ME, Pietrobon D (2004) Modal gating of human $Ca_V2.1$ (P/Q-type) calcium channels: I. The slow and the fast gating modes and their modulation by beta subunits. J Gen Physiol 124:445-461.

Maejima T, Wollenweber P, Teusner LU, Noebels JL, Herlitze S, Mark MD (2013) Postnatal loss of P/Q-type channels confined to rhombic-lip-derived neurons alters synaptic transmission at the parallel fiber to purkinje cell synapse and replicates genomic Cacna1a mutation phenotype of ataxia and seizures in mice. J Neurosci 33:5162-5174.

Maragakis N, Lin CG, Jin L, Dykes-Hoberg M, Rothstein JD (1997) Ataxia due to loss of the Purkinje-cell specific glutamate transporter EAAT4.

Marcaggi P, Attwell D (2005) Endocannabinoid signaling depends on the spatial pattern of synapse activation. Nat Neurosci 8:776-781.

Marr D (1969) A theory of cerebellar cortex. J Physiol 202:437-470.

Marsden J, Harris C (2011) Cerebellar ataxia: pathophysiology and rehabilitation. Clin Rehabil 25:195-216.

Marzban H, Khanzada U, Shabir S, Hawkes R, Langnaese K, Smalla KH, Bockers TM, Gundelfinger ED, Gordon-Weeks PR, Beesley PW (2003) Expression of the immunoglobulin superfamily neuroplastin adhesion molecules in adult and developing mouse cerebellum and their localisation to parasagittal stripes. J Comp Neurol 462:286-301.

Massaquoi SG (2012) Physiology of clinical dysfunction of the cerebellum. Handb Clin Neurol 103:37-62.

Mateos JM, Benitez R, Elezgarai I, Azkue JJ, Lazaro E, Osorio A, Bilbao A, Donate F, Sarria R, Conquet F, Ferraguti F, Kuhn R, Knopfel T, Grandes P (2000) Immunolocalization of the mGluR1b splice variant of the metabotropic glutamate receptor 1 at parallel fiber-Purkinje cell synapses in the rat cerebellar cortex. J Neurochem 74:1301-1309.

Mateos JM, Osorio A, Azkue J, Benitez R, Elezgaral I, Bilbao A, Diez J, Puente N, Kuhn R, Knopfel T, Hawkes R, Donate F, Grandes P (2001) Parasagittal compartmentalization of the metabotropic glutamate receptor mGluR1b in the cerebellar cortex. Eur J Anat 5:15-21.

Mathiesen C, Caesar K, Akgoren N, Lauritzen M (1998) Modification of activity-dependent increases of cerebral blood flow by excitatory synaptic activity and spikes in rat cerebellar cortex. J Physiol 512 (Pt 2):555-566.

Matsumoto M, Nakagawa T, Inoue T, Nagata E, Tanaka K, Takano H, Minowa O, Kuno J, Sakakibara S, Yamada M, Yoneshima H, Miyawaki A, Fukuuchi Y, Furuichi T, Okano H, Mikoshiba K, Noda T (1996) Ataxia and epileptic seizures in mice lacking type 1 inositol 1,4,5-trisphosphate receptor. Nature 379:168-171.

Matsushita K, Wakamori M, Rhyu IJ, Arii T, Oda S, Mori Y, Imoto K (2002) Bidirectional alterations in cerebellar synaptic transmission of tottering and rolling Ca^{2+} channel mutant mice. J Neurosci 22:4388-4398.

Meier H, MacPike AD (1971) Three syndromes produced by two mutant genes in the mouse. Clinical, pathological, and ultrastructural bases of tottering, leaner, and heterozygous mice. J Hered 62:297-302.

Mermelstein PG, Foehring RC, Tkatch T, Song WJ, Baranauskas G, Surmeier DJ (1999) Properties of Q-type calcium channels in neostriatal and cortical neurons are correlated with beta subunit expression. J Neurosci 19:7268-7277.

Mintz IM, Adams ME, Bean BP (1992) P-type calcium channels in rat central and peripheral neurons. Neuron 9:85-95.

Mintz IM, Sabatini BL, Regehr WG (1995) Calcium control of transmitter release at a cerebellar synapse. Neuron 15:675-688.

Molgo J, Lundh H, Thesleff S (1980) Potency of 3,4-diaminopyridine and 4-aminopyridine on mammalian neuromuscular transmission and the effect of pH changes. Eur J Pharmacol 61:25-34.

Moore PK, Handy RL (1997) Selective inhibitors of neuronal nitric oxide synthase--is no NOS really good NOS for the nervous system? Trends Pharmacol Sci 18:204-211.

Morton SM, Bastian AJ (2004) Cerebellar control of balance and locomotion. Neuroscientist 10:247-259.

Mugnaini E (1972) The histology and cytology of the cerebellar cortex. In: The Comparative Anatomy and Histology of the Cerebellum: The Human Cerebellum, Cerebellar Connections and Cerebellar Cortex (Larsell O, ed), pp 201-265. Minneapolis: University of Minnesota Press.

Murase S, Hayashi Y (1996) Expression pattern of integrin beta 1 subunit in Purkinje cells of rat and cerebellar mutant mice. J Comp Neurol 375:225-237.

Nachbauer W, Nocker M, Karner E, Stankovic I, Unterberger I, Eigentler A, Schneider R, Poewe W, Delazer M, Boesch S (2014) Episodic ataxia type 2: phenotype characteristics of a novel CACNA1A mutation and review of the literature. J Neurol 261:983-991.

Nagao S, Kwak S, Kanazawa I (1997) EAAT4, a glutamate transporter with properties of a chloride channel, is predominantly localized in Purkinje cell dendrites, and forms parasagittal compartments in rat cerebellum. Neuroscience 78:929-933.

Najafi F, Giovannucci A, Wang SS, Medina JF (2014) Sensory-driven enhancement of calcium signals in individual Purkinje cell dendrites of awake mice. Cell Rep 6:792-798.

Napper RM, Harvey RJ (1988) Number of parallel fiber synapses on an individual Purkinje cell in the cerebellum of the rat. J Comp Neurol 274:168-177.

Neufeld MY, Nisipeanu P, Chistik V, Korczyn AD (1996) The electroencephalogram in acetazolamide-responsive periodic ataxia. Mov Disord 11:283-288.

Neychev VK, Fan X, Mitev VI, Hess EJ, Jinnah HA (2008) The basal ganglia and cerebellum interact in the expression of dystonic movement. Brain 131:2499-2509.

Neychev VK, Gross RE, Lehericy S, Hess EJ, Jinnah HA (2011) The functional neuroanatomy of dystonia. Neurobiol Dis 42:185-201.

Nguyen-Vu TD, Kimpo RR, Rinaldi JM, Kohli A, Zeng H, Deisseroth K, Raymond JL (2013) Cerebellar Purkinje cell activity drives motor learning. Nat Neurosci 16:1734-1736.

Noebels JL (1984) A single gene error of noradrenergic axon growth synchronizes central neurones. Nature 310:409-411.

Noebels JL, Sidman RL (1979) Inherited epilepsy: spike-wave and focal motor seizures in the mutant mouse tottering. Science 204:1334-1336.

Odeh F, Ackerley R, Bjaalie JG, Apps R (2005) Pontine maps linking somatosensory and cerebellar cortices are in register with climbing fiber somatotopy. J Neurosci 25:5680-5690.

Ohkuma S, Katsura M, Hibino Y, Xu J, Shirotani K, Kuriyama K (1998) Multiple actions of nitric oxide on voltage-dependent Ca2+ channels in mouse cerebral cortical neurons. Brain Res Mol Brain Res 54:133-140.

Olson L, Fuxe K (1971) On the projections from locus coeruleus norepinephrine neurones: the cerebellar projections. Brain Res 28:165-171.

Ophoff RA, Terwindt GM, Vergouwe MN, van Eijk R, Oefner PJ, Hoffman SM, Lamerdin JE, Mohrenweiser HW, Bulman DE, Ferrari M, Haan J, Lindhout D, van Ommen GJ, Hofker MH, Ferrari MD, Frants RR (1996) Familial hemiplegic

migraine and episodic ataxia type-2 are caused by mutations in the Ca^{2+} channel gene CACNL1A4. Cell 87:543-552.

Otis TS, Brasnjo G, Dzubay JA, Pratap M (2004) Interactions between glutamate transporters and metabotropic glutamate receptors at excitatory synapses in the cerebellar cortex. Neurochem Int 45:537-544.

Ovsepian SV, Friel DD (2008) The leaner P/Q-type calcium channel mutation renders cerebellar Purkinje neurons hyper-excitable and eliminates Ca2+-Na+ spike bursts. Eur J Neurosci 27:93-103.

Oz G, Vollmers ML, Nelson CD, Shanley R, Eberly LE, Orr HT, Clark HB (2011) In vivo monitoring of recovery from neurodegeneration in conditional transgenic SCA1 mice. Exp Neurol 232:290-298.

Ozol K, Hayden JM, Oberdick J, Hawkes R (1999) Transverse zones in the vermis of the mouse cerebellum. J Comp Neurol 412:95-111.

Palay SL, Chan-Palay V (1974) Cerebellar Cortex: Cytology and Organization. New York: Springer-Verlag.

Pardo NE, Hajela RK, Atchison WD (2006) Acetylcholine release at neuromuscular junctions of adult tottering mice is controlled by N-(cav2.2) and R-type (cav2.3) but not L-type (cav1.2) Ca^{2+} channels. J Pharmacol Exp Ther 319:1009-1020.

Paukert M, Huang YH, Tanaka K, Rothstein JD, Bergles DE (2010) Zones of enhanced glutamate release from climbing fibers in the mammalian cerebellum. J Neurosci 30:7290-7299.

Pickel VM, Segal M, Bloom FE (1974) A radioautographic study of the efferent pathways of the nucleus locus coeruleus. J Comp Neurol 155:15-42.

Pietrobon D (2010) $Ca_V2.1$ channelopathies. Pflugers Arch 460:375-393.

Pijpers A, Apps R, Pardoe J, Voogd J, Ruigrok TJ (2006) Precise spatial relationships between mossy fibers and climbing fibers in rat cerebellar cortical zones. J Neurosci 26:12067-12080.

Pijpers A, Voogd J, Ruigrok TJ (2005) Topography of olivo-cortico-nuclear modules in the intermediate cerebellum of the rat. J Comp Neurol 492:193-213.

Piochon C, Irinopoulou T, Brusciano D, Bailly Y, Mariani J, Levenes C (2007) NMDA receptor contribution to the climbing fiber response in the adult mouse Purkinje cell. J Neurosci 27:10797-10809.

Piochon C, Levenes C, Ohtsuki G, Hansel C (2010) Purkinje cell NMDA receptors assume a key role in synaptic gain control in the mature cerebellum. J Neurosci 30:15330-15335.

Pizoli CE, Jinnah HA, Billingsley ML, Hess EJ (2002) Abnormal cerebellar signaling induces dystonia in mice. J Neurosci 22:7825-7833.

Plomp JJ, Vergouwe MN, van den Maagdenberg AM, Ferrari MD, Frants RR, Molenaar PC (2000) Abnormal transmitter release at neuromuscular junctions of mice carrying the tottering alpha(1A) Ca(2+) channel mutation. Brain 123 Pt 3:463-471.

Popa LS, Hewitt AL, Ebner TJ (2012) Predictive and feedback performance errors are signaled in the simple spike discharge of individual Purkinje cells. J Neurosci 32:15345-15358.

Qian J, Noebels JL (2000) Presynaptic Ca(2+) influx at a mouse central synapse with Ca(2+) channel subunit mutations. J Neurosci 20:163-170.

Qiu DL, Knopfel T (2007) An NMDA receptor/nitric oxide cascade in presynaptic parallel fiber-Purkinje neuron long-term potentiation. J Neurosci 27:3408-3415.

Raike RS, Pizoli CE, Weisz C, van den Maagdenberg AM, Jinnah HA, Hess EJ (2012) Limited regional cerebellar dysfunction induces focal dystonia in mice. Neurobiol Dis.

Raike RS, Weisz C, Hoebeek FE, Terzi MC, De Zeeuw CI, van den Maagdenberg AM, Jinnah HA, Hess EJ (2013) Stress, caffeine and ethanol trigger transient neurological dysfunction through shared mechanisms in a mouse calcium channelopathy. Neurobiol Dis 50:151-159.

Raiteri L, Raiteri M, Bonanno G (2002) Coexistence and function of different neurotransmitter transporters in the plasma membrane of CNS neurons. Prog Neurobiol 68:287-309.

Rajakulendran S, Graves TD, Labrum RW, Kotzadimitriou D, Eunson L, Davis MB, Davies R, Wood NW, Kullmann DM, Hanna MG, Schorge S (2010) Genetic and functional characterisation of the P/Q calcium channel in episodic ataxia with epilepsy. J Physiol 588:1905-1913.

Rajakulendran S, Kaski D, Hanna MG (2012) Neuronal P/Q-type calcium channel dysfunction in inherited disorders of the CNS. Nat Rev Neurol 8:86-96.

Raman IM, Bean BP (1999) Ionic currents underlying spontaneous action potentials in isolated cerebellar Purkinje neurons. J Neurosci 19:1663-1674.

Raman IM, Bean BP (1997) Resurgent sodium current and action potential formation in dissociated cerebellar Purkinje neurons. J Neurosci 17:4517-4526.

Ranck JB, Jr. (1975) Which elements are excited in electrical stimulation of mammalian central nervous system: a review. Brain Res 98:417-440.

Ranum LP, Schut LJ, Lundgren JK, Orr HT, Livingston DM (1994) Spinocerebellar ataxia type 5 in a family descended from the grandparents of President Lincoln maps to chromosome 11. Nat Genet 8:280-284.

Reeber SL, Otis TS, Sillitoe RV (2013) New roles for the cerebellum in health and disease. Front Syst Neurosci 7:83.

Reinert KC, Dunbar RL, Gao W, Chen G, Ebner TJ (2004) Flavoprotein autofluorescence imaging of neuronal activation in the cerebellar cortex *in vivo.* J Neurophysiol 92:199-211.

Reinert KC, Gao W, Chen G, Ebner TJ (2007) Flavoprotein autofluorescence imaging in the cerebellar cortex *in vivo*. J Neurosci Res 85:3221-3232.

Reinert KC, Gao W, Chen G, Wang X, Ebner TJ (2011) Cellular and metabolic origins of flavoprotein autofluorescence in the cerebellar cortex *in vivo*. Cerebellum 10:585-589.

Renzi M, Farrant M, Cull-Candy SG (2007) Climbing-fibre activation of NMDA receptors in Purkinje cells of adult mice. J Physiol 585:91-101.

Rhyu IJ, Abbott LC, Walker DB, Sotelo C (1999) An ultrastructural study of granule cell/Purkinje cell synapses in tottering (tg/tg), leaner (tg(la)/tg(la)) and compound heterozygous tottering/leaner (tg/tg(la)) mice. Neuroscience 90:717-728.

Rhyu IJ, Nahm SS, Hwang SJ, Kim H, Suh YS, Oda SI, Frank TC, Abbott LC (2003) Altered neuronal nitric oxide synthase expression in the cerebellum of calcium channel mutant mice. Brain Res 977:129-140.

Ribar TJ, Rodriguiz RM, Khiroug L, Wetsel WC, Augustine GJ, Means AR (2000) Cerebellar defects in Ca2+/calmodulin kinase IV-deficient mice. J Neurosci 20:RC107.

Rokni D, Llinas R, Yarom Y (2007) Stars and stripes in the cerebellar cortex: a voltage sensitive dye study. Front Syst Neurosci 1:1.

Rokni D, Llinas R, Yarom Y (2008) The morpho/functional discrepancy in the cerebellar cortex: looks alone are deceptive. Front Syst Neurosci 2:192-198.

Roth A, Hausser M (2001) Compartmental models of rat cerebellar Purkinje cells based on simultaneous somatic and dendritic patch-clamp recordings. J Physiol 535:445-472.

Rowland NC, Jaeger D (2005) Coding of tactile response properties in the rat deep cerebellar nuclei. J Neurophysiol 94:1236-1251.

Ryan DP, Ptacek LJ (2010) Episodic neurological channelopathies. Neuron 68:282-292.

Sachidhanandam S, Sreenivasan V, Kyriakatos A, Kremer Y, Petersen CC (2013) Membrane potential correlates of sensory perception in mouse barrel cortex. Nat Neurosci 16:1671-1677.

Saitow F, Satake S, Yamada J, Konishi S (2000) Beta-adrenergic receptor-mediated presynaptic facilitation of inhibitory GABAergic transmission at cerebellar interneuro-Purkinje cell synapses. J Neurophysiol 84:2016-2025.

Salin PA, Malenka RC, Nicoll RA (1996) Cyclic AMP mediates a presynaptic form of LTP at cerebellar parallel fiber synapses. Neuron 16:797-803.

Sandoz G, Bichet D, Cornet V, Mori Y, Felix R, De WM (2001) Distinct properties and differential beta subunit regulation of two C-terminal isoforms of the P/Q-type Ca(2+)-channel alpha(1A) subunit. Eur J Neurosci 14:987-997.

Santamaria F, Bower JM (2005) Background synaptic activity modulates the response of a modeled Purkinje cell to paired afferent input. J Neurophysiol 93:237-250.

Santamaria F, Jaeger D, de Schutter E, Bower JM (2002) Modulatory effects of parallel fiber and molecular layer interneuron synaptic activity on Purkinje cell responses to ascending segment input: a modeling study. J Comput Neurosci 13:217-235.

Santamaria F, Tripp PG, Bower JM (2007) Feedforward inhibition controls the spread of granule cell-induced Purkinje cell activity in the cerebellar cortex. J Neurophysiol 97:248-263.

Sarna JR, Hawkes R (2003) Patterned Purkinje cell death in the cerebellum. Prog Neurobiol 70:473-507.

Sarna JR, Larouche M, Marzban H, Sillitoe RV, Rancourt DE, Hawkes R (2003) Patterned Purkinje cell degeneration in mouse models of Niemann-Pick type C disease. J Comp Neurol 456:279-291.

Sarna JR, Marzban H, Watanabe M, Hawkes R (2006) Complementary stripes of phospholipase Cbeta3 and Cbeta4 expression by Purkinje cell subsets in the mouse cerebellum. J Comp Neurol 496:303-313.

Sasaki K, Bower JM, Llinas R (1989) Multiple Purkinje cell recording in rodent cerebellar cortex. Eur J Neurosci 1:572-586.

Sasaki S, Huda K, Inoue T, Miyata M, Imoto K (2006) Impaired feedforward inhibition of the thalamocortical projection in epileptic Ca2+ channel mutant mice, tottering. J Neurosci 26:3056-3065.

Sato T, Miura M, Yamada M, Yoshida T, Wood JD, Yazawa I, Masuda M, Suzuki T, Shin RM, Yau HJ, Liu FC, Shimohata T, Onodera O, Ross CA, Katsuki M, Takahashi H, Kano M, Aosaki T, Tsuji S (2009) Severe neurological phenotypes of Q129 DRPLA transgenic mice serendipitously created by en masse expansion of CAG repeats in Q76 DRPLA mice. Hum Mol Genet 18:723-736.

Sawada K, Kalam AA, Sakata-Haga H, Lee NS, Jeong YG, Fukui Y (2009) Striking pattern of Purkinje cell loss in cerebellum of an ataxic mutant mouse, tottering. Acta Neurobiol Exp (Wars) 69:138-145.

Schmolesky MT, Weber JT, De Zeeuw CI, Hansel C (2002) The making of a complex spike: ionic composition and plasticity. Ann N Y Acad Sci 978:359-390.

Scholle HC, Jinnah HA, Arnold D, Biedermann FH, Faenger B, Grassme R, Hess EJ, Schumann NP (2010) Kinematic and electromyographic tools for characterizing movement disorders in mice. Mov Disord 25:265-274.

Schuchmann S, Albrecht D, Heinemann U, von Bohlen und HO (2002) Nitric oxide modulates low-Mg2+-induced epileptiform activity in rat hippocampal-entorhinal cortex slices. Neurobiol Dis 11:96-105.

Serinagaoglu Y, Zhang R, Zhang Y, Zhang L, Hartt G, Young AP, Oberdick J (2007) A promoter element with enhancer properties, and the orphan nuclear receptor RORalpha, are required for Purkinje cell-specific expression of a Gi/o modulator. Mol Cell Neurosci 34:324-342.

Seyfried TN, Glaser GH (1985) A review of mouse mutants as genetic models of epilepsy. Epilepsia 26:143-150.

Sghirlanzoni A, Pareyson D, Lauria G (2005) Sensory neuron diseases. Lancet Neurol 4:349-361.

Shambes GM, Beermann DH, Welker W (1978a)
Multiple tactile areas in cerebellar cortex: another patchy cutaneous projection to granule cell columns in rats. Brain Res 157:123-128.

Shambes GM, Gibson JM, Welker W (1978b) Fractured somatotopy in granule cell tactile areas of rat cerebellar hemispheres revealed by micromapping. Brain Behav Evol 15:94-140.

Sherman SM, Guillery RW (2011) Distinct functions for direct and transthalamic corticocortical connections. J Neurophysiol 106:1068-1077.

Shimamoto K, Lebrun B, Yasuda-Kamatani Y, Sakaitani M, Shigeri Y, Yumoto N, Nakajima T (1998) DL-threo-beta-benzyloxyaspartate, a potent blocker of excitatory amino acid transporters. Mol Pharmacol 53:195-201.

Shin JH, Kim YS, Linden DJ (2008) Dendritic glutamate release produces autocrine activation of mGluR1 in cerebellar Purkinje cells. Proc Natl Acad Sci USA 105:746-750.

Shin JH, Linden DJ (2005) An NMDA receptor/nitric oxide cascade is involved in cerebellar LTD but is not localized to the parallel fiber terminal. J Neurophysiol 94:4281-4289.

Shin SL, De Schutter E. (2006) Dynamic synchronization of Purkinje cell simple spikes. J Neurophysiol 96:3485-3491.

Shinoda Y, Sugiuchi Y, Futami T (1987) Excitatory inputs to cerebellar dentate nucleus neurons from the cerebral cortex in the cat. Exp Brain Res 67:299-315.

Sillitoe RV, Hulliger M, Dyck R, Hawkes R (2003) Antigenic compartmentation of the cat cerebellar cortex. Brain Res 977:1-15.

Sillitoe RV, Joyner AL (2007) Morphology, molecular codes, and circuitry produce the three-dimensional complexity of the cerebellum. Annu Rev Cell Dev Biol 23:549-577.

Sillitoe RV, Marzban H, Larouche M, Zahedi S, Affanni J, Hawkes R (2005) Conservation of the architecture of the anterior lobe vermis of the cerebellum across mammalian species. Prog Brain Res 148:283-297.

Sillitoe RV, Stephen D, Lao Z, Joyner AL (2008) Engrailed homeobox genes determine the organization of Purkinje cell sagittal stripe gene expression in the adult cerebellum. J Neurosci 28:12150-12162.

Sims RE, Hartell NA (2006) Differential susceptibility to synaptic plasticity reveals a functional specialization of ascending axon and parallel fiber synapses to cerebellar Purkinje cells. J Neurosci 26:5153-5159.

Sims RE, Hartell NA (2005) Differences in transmission properties and susceptibility to long-term depression reveal functional specialization of ascending axon and parallel fiber synapses to Purkinje cells. J Neurosci 25:3246-3257.

Smith KJ, Felts PA, John GR (2000) Effects of 4-aminopyridine on demyelinated axons, synapses and muscle tension. Brain 123 (Pt 1):171-184.

Soong TW, DeMaria CD, Alvania RS, Zweifel LS, Liang MC, Mittman S, Agnew WS, Yue DT (2002) Systematic identification of splice variants in human P/Q-type channel alpha1(2.1) subunits: implications for current density and Ca2+-dependent inactivation. J Neurosci 22:10142-10152.

Spacey S (1993) Episodic Ataxia Type 2.

Spacey SD, Hildebrand ME, Materek LA, Bird TD, Snutch TP (2004) Functional implications of a novel EA2 mutation in the P/Q-type calcium channel. Ann Neurol 56:213-220.

Spinazzi M, Angelini C, Patrini C (2010) Subacute sensory ataxia and optic neuropathy with thiamine deficiency. Nat Rev Neurol 6:288-293.

Stahl JS, James RA, Oommen BS, Hoebeek FE, De Zeeuw CI (2006) Eye movements of the murine P/Q calcium channel mutant tottering, and the impact of aging. J Neurophysiol 95:1588-1607.

Stahl JS, Thumser ZC (2014) Flocculus Purkinje Cell Signals in Mouse Cacna1a Calcium Channel Mutants of Escalating Severity; An Investigation of the Role of Firing Irregularity in Ataxia. J Neurophysiol.

Stahl JS, Thumser ZC (2013) 4-aminopyridine does not enhance flocculus function in tottering, a mouse model of vestibulocerebellar dysfunction and ataxia. PLoS ONE 8:e57895.

Stephens GJ, Morris NP, Fyffe RE, Robertson B (2001) The Cav2.1/alpha1A (P/Q-type) voltage-dependent calcium channel mediates inhibitory neurotransmission onto mouse cerebellar Purkinje cells. Eur J Neurosci 13:1902-1912.

Stosiek C, Garaschuk O, Holthoff K, Konnerth A (2003) In vivo two-photon calcium imaging of neuronal networks. Proc Natl Acad Sci U S A 100:7319-7324.

Strick PL, Dum RP, Fiez JA (2009) Cerebellum and nonmotor function. Annu Rev Neurosci 32:413-434.

Strupp M, Kalla R, Dichgans M, Freilinger T, Glasauer S, Brandt T (2004) Treatment of episodic ataxia type 2 with the potassium channel blocker 4-aminopyridine. Neurology 62:1623-1625.

Sugihara I (2011) Compartmentalization of the deep cerebellar nuclei based on afferent projections and aldolase C expression. Cerebellum 10:449-463.

Sugihara I, Fujita H, Na J, Quy PN, Li BY, Ikeda D (2009) Projection of reconstructed single Purkinje cell axons in relation to the cortical and nuclear aldolase C compartments of the rat cerebellum. J Comp Neurol 512:282-304.

Sugihara I, Shinoda Y (2004) Molecular, topographic, and functional organization of the cerebellar cortex: a study with combined aldolase C and olivocerebellar labeling. J Neurosci 24:8771-8785.

Sullivan MR, Nimmerjahn A, Sarkisov DV, Helmchen F, Wang SS (2005) In vivo calcium imaging of circuit activity in cerebellar cortex. J Neurophysiol 94:1636-1644.

Sved AF, Cano G, Passerin AM, Rabin BS (2002) The locus coeruleus, Barrington's nucleus, and neural circuits of stress. Physiol Behav 77:737-742.

Syapin PJ (1983) Inhibition of pentylenetetrazol induced genetically-determined stereotypic convulsions in tottering mutant mice by diazepam. Pharmacol Biochem Behav 18:389-394.

Syapin PJ (1982) Effects of the tottering mutation in the mouse: multiple neurologic changes. Exp Neurol 76:566-573.

Szentagothai J (1965) THE USE OF DEGENERATION METHODS IN THE INVESTIGATION OF SHORT NEURONAL CONNEXIONS. Prog Brain Res 14:1-32.

Takahashi M, Kovalchuk Y, Attwell D (1995) Pre- and postsynaptic determinants of EPSC waveform at cerebellar climbing fiber and parallel fiber to Purkinje cell synapses. J Neurosci 15:5693-5702.

Takayasu Y, Iino M, Ozawa S (2004) Roles of glutamate transporters in shaping excitatory synaptic currents in cerebellar Purkinje cells. Eur J Neurosci 19:1285-1295.

Takayasu Y, Iino M, Takatsuru Y, Tanaka K, Ozawa S (2009) Functions of glutamate transporters in cerebellar Purkinje cell synapses. Acta Physiol (Oxf) 197:1-12.

Tanaka J, Matsuzaki M, Tarusawa E, Momiyama A, Molnar E, Kasai H, Shigemoto R (2005) Number and density of AMPA receptors in single synapses in immature cerebellum. J Neurosci 25:799-807.

Tanaka K, Watase K, Manabe T, Yamada K, Watanabe M, Takahashi K, Iwama H, Nishikawa T, Ichihara N, Kikuchi T, Okuyama S, Kawashima N, Hori S, Takimoto M, Wada K (1997) Epilepsy and exacerbation of brain injury in mice lacking the glutamate transporter GLT-1. Science 276:1699-1702.

Tehrani MH, Barnes EM, Jr. (1995) Reduced function of gamma-aminobutyric acidA receptors in tottering mouse brain: role of cAMP-dependent protein kinase. Epilepsy Res 22:13-21.

Tehrani MH, Barnes EM, Jr. (1990) Basal and drug-induced cAMP levels in cortical slices from the tottering mouse. Epilepsy Res 7:205-209.

Tehrani MH, Baumgartner BJ, Liu SC, Barnes EM, Jr. (1997) Aberrant expression of GABAA receptor subunits in the tottering mouse: an animal model for absence seizures. Epilepsy Res 28:213-223.

Terada N, Banno Y, Ohno N, Fujii Y, Murate T, Sarna JR, Hawkes R, Zea Z, Baba T, Ohno S (2004) Compartmentation of the mouse cerebellar cortex by sphingosine kinase. J Comp Neurol 469:119-127.

Teramoto T, Kuwada M, Niidome T, Sawada K, Nishizawa Y, Katayama K (1993) A novel peptide from funnel web spider venom, omega-Aga-TK, selectively blocks, P-type calcium channels. Biochem Biophys Res Commun 196:134-140.

Thach WT (1978) Correlation of neural discharge with pattern and force of muscular activity, joint position, and direction of intended next movement in motor cortex and cerebellum. J Neurophysiol 41:654-676.

Thach WT, Jr. (1967) Somatosensory receptive fields of single units in cat cerebellar cortex. J Neurophysiol 30:675-696.

Thach WT (1968) Discharge of Purkinje and cerebellar nuclear neurons during rapidly alternating arm movements in the monkey. J Neurophysiol 31:785-797.

Thach WT, Goodkin HP, Keating JG (1992) The cerebellum and the adaptive coordination of movement. Annu Rev Neurosci 15:403-442.

Tian L, Akerboom J, Schreiter ER, Looger LL (2012) Neural activity imaging with genetically encoded calcium indicators. Prog Brain Res 196:79-94.

Todorov B, Kros L, Shyti R, Plak P, Haasdijk ED, Raike RS, Frants RR, Hess EJ, Hoebeek FE, De Zeeuw CI, van den Maagdenberg AM (2012) Purkinje cell-specific ablation of Ca(V)2.1 channels is sufficient to cause cerebellar ataxia in mice. Cerebellum 11:246-258.

Tottene A, Fellin T, Pagnutti S, Luvisetto S, Striessnig J, Fletcher C, Pietrobon D (2002) Familial hemiplegic migraine mutations increase Ca(2+) influx through single human CaV2.1 channels and decrease maximal CaV2.1 current density in neurons. Proc Natl Acad Sci U S A 99:13284-13289.

Tsai MC, Tanaka K, Overstreet-Wadiche L, Wadiche JI (2012) Neuronal glutamate transporters regulate glial excitatory transmission. J Neurosci 32:1528-1535.

Usowicz MM, Sugimori M, Cherksey B, Llinas R (1992) P-type calcium channels in the somata and dendrites of adult cerebellar Purkinje cells. Neuron 9:1185-1199.

Valle MS, Eian J, Bosco G, Poppele RE (2008) Cerebellar cortical activity in the cat anterior lobe during hindlimb stepping. Exp Brain Res 187:359-372.

Van BP, Szliwowski HB (1996) EEG findings in acetazolamide-responsive hereditary paroxysmal ataxia. Neurophysiol Clin 26:335-340.

Vane JR (1971) Inhibition of prostaglandin synthesis as a mechanism of action for aspirin-like drugs. Nat New Biol 231:232-235.

Vetter P, Roth A, Hausser M (2001) Propagation of action potentials in dendrites depends on dendritic morphology. J Neurophysiol 85:926-937.

Voogd J (1967) Comparative aspects of the structure and fibre connexions of the mammalian cerebellum. Prog Brain Res 25:94-134.

Voogd J (1969) The importance of fiber connections in the comparative anatomy of the mammalian cerebellum. In: Neurobiology of Cerebellar Evolution and Development (Llinas R, ed), pp 493-514. Chicago: A.M.A.-E.R.F. Institute for Biomedical Research.

Voogd J, Bigare F (1980) Topographical distribution of olivary and corticonuclear fibers in the cerebellum. A review. In: The Inferior Olivary Nucleus (Courville J, deMontigny C, Lamarre Y, eds), pp 207-234. New York: Raven.

Voogd J, Pardoe J, Ruigrok TJH, Apps R (2003) The distribution of climbing and mossy fiber collateral branches from the copula pyramidis and the paramedian lobule: Congruence of climbing fiber cortical zones and the pattern of zebrin banding within the rat cerebellum. J Neurosci 23:4645-4656.

Voogd J, Ruigrok TJ (1997) Traverse and longitudinal patterns in the mammalian cerebellum. In: Progress in Brain Research (De Zeeuw CI, Strata P, Voogd J, eds), Elsevier Science.

Voogd J, Ruigrok TJ (2004) The organization of the corticonuclear and olivocerebellar climbing fiber projections to the rat cerebellar vermis: the congruence of projection zones and the zebrin pattern. J Neurocytol 33:5-21.

Wadiche JI, Jahr CE (2005) Patterned expression of Purkinje cell glutamate transporters controls synaptic plasticity. Nat Neurosci 8:1329-1334.

Wakamori M, Yamazaki K, Matsunodaira H, Teramoto T, Tanaka I, Niidome T, Sawada K, Nishizawa Y, Sekiguchi N, Mori E, Mori Y, Imoto K (1998) Single tottering mutations responsible for the neuropathic phenotype of the P-type calcium channel. J Biol Chem 273:34857-34867.

Walker D, De WM (1998) Subunit interaction sites in voltage-dependent Ca2+ channels: role in channel function. Trends Neurosci 21:148-154.

Walter JT, Alvina K, Womack MD, Chevez C, Khodakhah K (2006) Decreases in the precision of Purkinje cell pacemaking cause cerebellar dysfunction and ataxia. Nat Neurosci 9:389-397.

Walter JT, Dizon MJ, Khodakhah K (2009) The functional equivalence of ascending and parallel fiber inputs in cerebellar computation. J Neurosci 29:8462-8473.

Walter JT, Khodakhah K (2009) The advantages of linear information processing for cerebellar computation. Proc Natl Acad Sci USA 106:4471-4476.

Wang X, Chen G, Gao W, Ebner TJ (2011) Parasagittally aligned, mGluR1-dependent patches are evoked at long latencies by parallel fiber stimulation in the mouse cerebellar cortex *in vivo*. J Neurophysiol 105:1732-1746.

Wang X, Chen G, Gao W, Ebner TJ (2009) Long-term potentiation of the responses to parallel fiber stimulation in mouse cerebellar cortex *in vivo*. Neurosci 162:713-722.

Wang XJ (2010) Neurophysiological and computational principles of cortical rhythms in cognition. Physiol Rev 90:1195-1268.

Wappl E, Koschak A, Poteser M, Sinnegger MJ, Walter D, Eberhart A, Groschner K, Glossmann H, Kraus RL, Grabner M, Striessnig J (2002) Functional consequences of P/Q-type Ca^{2+} channel Cav2.1 missense mutations associated with episodic ataxia type 2 and progressive ataxia. J Biol Chem 277:6960-6966.

Welsh JP, Yuen G, Placantonakis DG, Vu TQ, Haiss F, O'Hearn E, Molliver ME, Aicher SA (2002) Why do Purkinje cells die so easily after global brain ischemia? Aldolase C, EAAT4, and the cerebellar contribution to posthypoxic myoclonus. Adv Neurol 89:331-359.

Westenbroek RE, Sakurai T, Elliott EM, Hell JW, Starr TV, Snutch TP, Catterall WA (1995) Immunochemical identification and subcellular distribution of the alpha 1A subunits of brain calcium channels. J Neurosci 15:6403-6418.

Wise AK, Cerminara NL, Marple-Horvat DE, Apps R (2010) Mechanisms of synchronous activity in cerebellar Purkinje cells. J Physiol 588:2373-2390.

Witter L, Canto CB, Hoogland TM, de G, Jr., De Zeeuw CI (2013) Strength and timing of motor responses mediated by rebound firing in the cerebellar nuclei after Purkinje cell activation. Front Neural Circuits 7:133.

Womack MD, Hoang C, Khodakhah K (2009) Large conductance calcium-activated potassium channels affect both spontaneous firing and intracellular calcium concentration in cerebellar Purkinje neurons. Neuroscience 162:989-1000.

Womack MD, Khodakhah K (2003) Somatic and dendritic small-conductance calcium-activated potassium channels regulate the output of cerebellar purkinje neurons. J Neurosci 23:2600-2607.

Womack MD, Khodakhah K (2002) Characterization of large conductance Ca^{2+}-activated K^{+} channels in cerebellar Purkinje neurons. Eur J Neurosci 16:1214-1222.

Woodward DJ, Moises HC, Waterhouse BD, Hoffer BJ, Freedman R (1979) Modulatory actions of norepinephrine in the central nervous system. Fed Proc 38:2109-2116.

Wu HS, Sugihara I, Shinoda Y (1999) Projection patterns of single mossy fibers originating from the lateral reticular nucleus in the rat cerebellar cortex and nuclei. J Comp Neurol 411:97-118.

Wykes RC, Bauer CS, Khan SU, Weiss JL, Seward EP (2007) Differential regulation of endogenous N- and P/Q-type Ca2+ channel inactivation by Ca2+/calmodulin impacts on their ability to support exocytosis in chromaffin cells. J Neurosci 27:5236-5248.

Yaginuma H, Matsushita M (1987) Spinocerebellar projections from the thoracic cord in the cat, as studied by anterograde transport of wheat germ agglutinin-horseradish peroxidase. J Comp Neurol 258:1-27.

Yang G, Chen G, Ebner TJ, Iadecola C (1999) Nitric oxide is the predominant mediator of cerebellar hyperemia during somatosensory activation in rats. Am J Physiol 277:R1760-R1770.

Yang G, Pan F, Parkhurst CN, Grutzendler J, Gan WB (2010) Thinned-skull cranial window technique for long-term imaging of the cortex in live mice. Nat Protoc 5:201-208.

Yang Y, Lisberger SG (2014) Purkinje-cell plasticity and cerebellar motor learning are graded by complex-spike duration. Nature.

Yartsev MM, Givon-Mayo R, Maller M, Donchin O (2009) Pausing purkinje cells in the cerebellum of the awake cat. Front Syst Neurosci 3:2.

Yoshimura N, Seki S, de Groat WC (2001) Nitric oxide modulates Ca(2+) channels in dorsal root ganglion neurons innervating rat urinary bladder. J Neurophysiol 86:304-311.

Yu QX, Ebner TJ, Bloedel JR (1985) Electrophysiological study of the corticonuclear projection in the cat cerebellum. Brain Res 327:121-134.

Zariwala HA, Borghuis BG, Hoogland TM, Madisen L, Tian L, De Zeeuw CI, Zeng H, Looger LL, Svoboda K, Chen TW (2012) A Cre-dependent GCaMP3 reporter mouse for neuronal imaging in vivo. J Neurosci 32:3131-3141.

Zasorin NL, Baloh RW, Myers LB (1983) Acetazolamide-responsive episodic ataxia syndrome. Neurology 33:1212-1214.

Zhou YD, Turner TJ, Dunlap K (2003) Enhanced G protein-dependent modulation of excitatory synaptic transmission in the cerebellum of the Ca^{2+} channel-mutant mouse, tottering. J Physiol 547:497-507.